Unraveling Ovarian Cancer Stem Cell Dependencies on miRNA and Epigenetic Regulation Utilizing Enhanced 3D Culture Models

by

Deren Demirel Yavuz

A Dissertation Submitted to the
Graduate School of Health Sciences in Partial
Fulfillment of the Requirements for the Degree of

Doctor of Philosophy
in
Cellular and Molecular Medicine

KOÇ ÜNİVERSİTESİ

September 19, 2025

Unraveling Ovarian Cancer Stem Cell Dependencies on miRNA and Epigenetic Regulation Utilizing Enhanced 3D Culture Models

Koc University

Graduate School of Health Sciences

This is to certify that I have examined this copy of a doctoral dissertation by

Deren Demirel Yavuz

and have found that it is complete and satisfactory in all respects,
and that any and all revisions required by the final
examining committee have been made.

Committee Members:

Assist. Prof. İrem Durmaz Şahin (Advisor)

Prof. Tuğba Bağcı Önder

Prof. Özgür Öktem

Prof. Ayşe Elif Erson Bensan

Assist. Prof. Zeynep Tokçaer Keskin

Date: 19 September 2025

I dedicate this thesis to my dear family.

ABSTRACT

Unraveling Ovarian Cancer Stem Cell Dependencies on miRNA and Epigenetic Regulation Utilizing Enhanced 3D Culture Models

Deren Demirel Yavuz

Doctor of Philosophy in Cellular and Molecular Medicine

September 19, 2025

High-grade serous ovarian cancer (HGSOC) is the deadliest gynecologic malignancy, largely due to therapy-resistant cancer stem cells (CSCs) that drive recurrence and poor clinical outcomes. This thesis aimed to establish reliable CSC models, uncover novel regulators of stemness, and investigate their mechanistic roles to inform therapeutic strategies.

Two 3D culture methods—ultra-low attachment (ULA) spheroids and gelatin methacrylate photomask (GelMA-Pm) encapsulation—were optimized with OVCAR-3 and OVSAHO cell lines and validated in patient-derived samples. OVCAR-3 cells cultured in ULA formed compartmentalized spheroids with enriched CSC and epithelial-to-mesenchymal transition (EMT) traits and multidrug resistance, making this the most robust system.

Small RNA sequencing of spheroids identified hsa-miR-548ah-3p as a consistently downregulated and underexplored miRNA. Functional rescue with miRNA mimics reversed CSC characteristics, reduced drug resistance, and impaired migration and invasion. RNA-seq profiling under prolonged mimic treatment highlighted “rescue genes,” including VIM, CXCR4, and KIT, integrating with miRNA target predictions. Parallel analyses revealed global 3′UTR lengthening in CSC spheroids, a dormancy-like program that remained responsive to miR-548ah-3p restoration.

Complementing these findings, a CRISPR-Cas9 dropout screen with the EPI-KOL epigenetic library identified essential regulators of spheroid survival. Top dependencies converged on DNA damage response (ATM, BRCA1), polycomb and chromatin remodeling (SUZ12, EPC2, EP400, PBRM1), and RNA metabolism (SNRPF, SYNCRIP, PARG).

In summary, this thesis integrates 3D culture modeling, miRNA functional studies, APA profiling, and CRISPR screening to reveal that HGSOC CSCs rely on a DNA damage–chromatin–APA axis. Restoration of miR-548ah-3p effectively counteracts CSC traits and drug resistance, nominating it—together with epigenetic regulators—as promising therapeutic entry points. These findings establish optimized 3D culture systems for CSC modeling and uncover mechanistic vulnerabilities that may guide future strategies to overcome resistance in HGSOC.

ÖZETÇE

Over Kanser Kök Hücrelerinin miRNA ve Epigenetik Düzenlemelere Bağımlılıklarının Geliştirilmiş 3D Kültür Modelleri ile Açığa Çıkarılması

Deren Demirel Yavuz

Hücresel Moleküler Tıp, Doktora

Eylül 19, 2025

Yüksek dereceli seröz over kanseri (HGSOC), en ölümcül jinekolojik malignitedir ve bunun başlıca nedeni tedaviye dirençli kanser kök hücrelerinin (CSC) tümör nüksü ve kötü klinik sonuçları yönlendirmesidir. Bu tezde amaç güvenilir CSC modelleri kurmak, kök hücreselliği düzenleyen yeni unsurları belirlemek ve mekanistik rollerini aydınlatarak olası tedavi stratejilerine ışık tutmaktır.

İki farklı 3D kültür yöntemi—ultra-düşük yapışma (ULA) sferoidleri ve jelatin metakrilat fotomask (GelMA-Pm) enkapsülasyonu—OVCAR-3 ve OVSAHO hücre serileri ile optimize edilmiş ve hasta kaynaklı örneklerde doğrulanmıştır. ULA ortamında kültüre edilen OVCAR-3 hücreleri, zengin CSC özellikleri, epitel-mezenkimal geçiş (EMT) belirteçleri ve çoklu ilaç direnci sergileyen bölümlenmiş sferoidler oluşturmuş ve en güvenilir model olarak belirlenmiştir.

Küçük RNA dizilemesi, sferoidlerde hsa-miR-548ah-3p'nin anlamlı biçimde baskılandığını göstermiştir. Bu miRNA'nın mimik ile geri kazandırılması CSC özelliklerini tersine çevirmiş, ilaç direncini azaltmış ve göç/invazyon yeteneklerini zayıflatmıştır. Uzun süreli mimik uygulaması sonrası RNA-seq analizleri, VIM, CXCR4 ve KIT gibi "kurtarıcı genler"i ortaya çıkarmış ve miRNA hedef tahminleriyle uyumlu bulunmuştur. Paralel analizler CSC sferoidlerinde global 3′UTR uzamalarını, yani dormansi benzeri bir programı göstermiş; ancak bu desen miR-548ah-3p geri kazandırılması ile geri döndürülebilmiştir.

Bulguları tamamlayıcı olarak, EPI-KOL epigenetik kütüphanesi kullanılarak gerçekleştirilen CRISPR-Cas9 taraması sferoidlerin yaşaması için gerekli düzenleyicileri ortaya koymuştur. En kritik bağımlılıklar DNA hasar yanıtı (ATM, BRCA1), polikomb/ kromatin yeniden şekillenmesi (SUZ12, EPC2, EP400, PBRM1) ve RNA metabolizması (SNRPF, SYNCRIP, PARG) üzerine yoğunlaşmıştır.

Sonuç olarak bu tez, 3D kültür modellemeyi, miRNA fonksiyonel analizlerini, APA profilini ve CRISPR taramasını entegre ederek HGSOC kök hücrelerinin DNA hasarı–kromatin–APA eksenine bağımlı olduğunu ortaya koymaktadır. miR-548ah-3p'nin geri kazandırılması CSC özelliklerini ve ilaç direncini etkili biçimde tersine çevirmekte olup, epigenetik düzenleyicilerle birlikte umut verici terapötik hedefler olarak öne çıkmaktadır. Bu bulgular CSC modellemesinde optimize edilmiş 3D sistemler sunmakta ve direnç mekanizmalarını aşmaya yönelik stratejiler için yeni bir temel sağlamaktadır.

ACKNOWLEDMENTS

I would like to sincerely thank my advisor, İrem Durmaz Şahin, whose guidance and expertise have been invaluable throughout my doctoral studies. Her constructive feedback and constant support greatly shaped the direction of this work and helped me grow as a researcher.

I am equally thankful to my thesis committee members, Tuğba Bağcı Önder and Özgür Öktem and for generously sharing their time and insights. Their thoughtful suggestions and critical perspectives provided clarity and depth that significantly strengthened this dissertation. I want to give my special thanks to Tuğba Bağcı Önder and Gözde Korkmaz for being a guidance multiple times throughout my PhD education.

My appreciation also goes to my colleagues and friends in the IDS laboratory: Elif Merve Aydın, İdil Su Canıtez and Gizem Yılmaz Demir with their long-lasting companionship and my newer lab mates, Büşra Demirkan and Arya Akdağ with their friendship and their vision they brought to my research. Their technical assistance and relaxing coffee breaks together, made life in the lab both productive and enjoyable. I want to thank friends Arda Işıklar and Ecem Metin for their high spirits and mood-boosting friendships. All the other colleagues who provided scientific insights, I am forever in their debt.

I gratefully acknowledge the institutional and financial support from Koç University as well as funding and resources provided by L'oreal Women In Science Program, TÜSEB and KUTTAM Laboratories. Their contribution made it possible to pursue the research presented in this thesis.

I want to thank Meltem Türkyılmaz for encouraging me and inspiring me throughout my academic career.

Beyond the academic sphere, I am deeply thankful to my friends who stood by me and celebrated each milestone with me. Güneş İkbal and Anıl Küçükbabuccu provided brain blooming conversations, endless understanding and extracurricular work supports which made my stressful days much brighter. Special thanks to my dear friend Hüma Varıcı, who listened to my anxious thoughts in sleepless nights without complaining. Hakan and Emine Azman also relentlessly listened and offered solutions to my troubles, and we shared the scientist's concerns with each other. To my crew and wise friends, who lifted my spirits in difficult times Batuhan Tozkoparan, Emrullah Özdemir, Sena Nur Bayram, Ali Çimen, Azra Akdeniz, Diren Güner, Marjin Arven, Yasin Sapmaz and Yunus Gürpınar. I also received so much support from my social media community, "The Unicorns" as we sometimes called each other. Countless direct messages and comments made hardest times bearable and hopeful.

Honorable mentions I have are my cats Rimbaud and Bruno for providing the cutest support, Sevda Çınar for always believing in me, Uygar Tanrıkulu and Övünç Sarp Özdemir for all the fun and extra-curricular activities we shared, Kurzgesagt YouTube channel for all the science and hope and Mihaela Zavolan for the expertise, support and trust she provided for my future career. All the great researchers out there, some of which are cited in this

thesis I express my gratitude toward each of them, for their work contributed so much insight to my own.

I want to take a brief commemoration to honor my friends I lost during my PhD. Evgeny, Faruk Özkan and Cemre Uçaryılmaz Metin, your loss changed so much. To my friends that I never get to sunbath lying on the grass anymore, I wish you could be here to celebrate with me.

My loving, caring and selfless husband, my life-long friend whom I walk every single rocky road with, Yasin Yavuz. There are no words in this universe to express my gratitude towards you, my love. This thesis or where I stand would not be possible without you. Thank you for all the help with housework and kind offerings you provided on my most tiring and busy days.

Most importantly, I owe profound gratitude to my family. Their patience, unconditional love, and belief in me have been the foundation of my strength and perseverance. Without them, this achievement would not have been possible. Their financial and emotional support surpassed everything I could ever imagine. Thank you, Dad cheering for your little girl's big dreams and supporting her in every step. Mom, thank you for countless times you expressed your proudness to me and calling me your future Nobel Prize winner. I am so proud of you for listening to my experiments and lab life, remembering tiny details and even providing help. Last but not least, my sister, you initially encouraged me to choose the job of my dreams, I would not be here without your support and love.

This thesis is dedicated with love and gratitude to all of them.

TABLE OF CONTENTS

LIST OF TABLES

LIST OF FIGURES

ABBREVIATIONS

3′UTR	3′ untranslated region
ACTB	β-actin (housekeeping control gene)
ADM	Adrenomedullin
AKT3	AKT serine/threonine kinase 3
ALDH1A1	Aldehyde dehydrogenase 1 family member A1
APA	Alternative polyadenylation
ATM	Ataxia telangiectasia mutated
BCA	Bicinchoninic acid assay
BRCA1/2	Breast cancer gene 1/2
CD117	KIT receptor tyrosine kinase (CSC marker).
CD133	Prominin-1 (CSC marker).
CD44	Cluster of differentiation 44 (CSC marker).
CDK2	Cyclin-dependent kinase 2.
CSC	Cancer stem cell
CXCR4	C-X-C motif chemokine receptor 4
DAPI	4′,6-diamidino-2-phenylindole
DDR	DNA damage response
DESeq2	Differential Expression Sequencing 2 (R package)
DNA	Deoxyribonucleic acid

dNTP	Deoxynucleotide triphosphate
ECM	Extracellular matrix
EMT	Epithelial-to-mesenchymal transition
EPI-KOL	Epigenetic knockout library
EP400	E1A binding protein p400 (NuA4 complex component)
FFPE	Formalin-fixed paraffin-embedded
FGF	Fibroblast growth factor
FRZB	Frizzled-related protein B
GelMA-Pm	Gelatin methacryloyl encapsulation with photomasks
gDNA	Genomic DNA
GO	Gene ontology
HGSOC	High-grade serous ovarian cancer
HR	Homologous recombination
HRD	Homologous recombination deficiency
IC_{50}	Half-maximal inhibitory concentration
IFN	Interferon
LOH	Loss of heterozygosity
MAGeCK	Model-based Analysis of Genome-wide CRISPR-Cas9 Knockout
MBTD1	MBT domain-containing protein 1
miRNA	MicroRNA

mRNA	Messenger RNA
MTT	3-(4,5-dimethylthiazol-2-yl)-2,5-diphenyltetrazolium bromide assay
NC	Negative control
NCI-SRB	National Cancer Institute sulforhodamine B assay
OCT-4	Octamer-binding transcription factor 4 (POU5F1)
OVCAR-3	Human ovarian carcinoma cell line (BRCA-WT)
OVSAHO	Human ovarian carcinoma cell line (BRCA1/2-deficient)
PARG	Poly(ADP-ribose) glycohydrolase
PARylation	Poly(ADP-ribosyl)ation
PBS	Phosphate-buffered saline
PDGFA	Platelet-derived growth factor subunit A
PCR	Polymerase chain reaction
PMEPA1	Prostate transmembrane protein, androgen-induced 1
PRC2	Polycomb repressive complex 2
qPCR	Quantitative polymerase chain reaction
RBP	RNA-binding protein
RNA	Ribonucleic acid
RNA-seq	RNA sequencing
RNP	Ribonucleoprotein complex
RT-qPCR	Reverse transcription quantitative PCR

SC	Stem cell
sgRNA	Single-guide RNA
SMM	Sphere medium monolayer.
SOX2	SRY-box transcription factor 2
SRB	Sulforhodamine B assay
SUZ12	Suppressor of zeste 12 (PRC2 subunit)
TGFBI	Transforming growth factor-beta induced protein
TLR	Toll-like receptor
ULA	Ultra-low attachment
UV	Ultraviolet.
VIM	Vimentin
WT	Wild-type
ZBTB7C	Zinc finger and BTB domain containing 7C

CHAPTER 1:

INTRODUCTION

1.1 Cancer Disease: A Health Burden and a Global Challenge

Cancer continues to stand as one of the foremost causes of disease and death across the globe. Its overall incidence has been rising steadily, driven by the natural consequence of aging populations and widespread lifestyle changes -involving more “carcinogen” exposure- and the growing reach of modern diagnostic tools, which make detection more frequent and databases broader. Global health authorities such as GLOBOCAN and the World Health Organization estimate that many millions of individuals receive a cancer diagnosis each year, with the disease contributing to roughly one in every six deaths worldwide (Bray et al., 2024). In fact, according to ACS, US expects 2 million new cancer cases and 618,000 deaths among them in 2025, excluding non-melanoma skin cancers (American Cancer Society, 2025). Although the past few decades have brought substantial progress in areas such as early diagnosis, the development of targeted molecular drugs, and the clinical success of immunotherapy, cancer as a whole remains an immense challenge. Its biological complexity, the diversity of its subtypes, and its notorious tendency to relapse continue to limit the long-term effectiveness of current treatment strategies.

Beyond the biological and clinical aspects, cancer also places a heavy socio-economic strain on societies. The financial costs of managing the disease are escalating sharply, particularly in wealthier nations where advanced therapies are widely adopted(Mariotto et al., 2020). At the same time, low- and middle-income regions frequently lack the infrastructure and resources needed to provide some of the most basic diagnostic tests or standard treatments, leaving many patients without adequate care. This imbalance highlights the pressing importance of not only advancing preventive approaches but also ensuring that effective therapies can be made accessible and affordable on a global scale, which primarily requires for cancer researches to prevail being conducted (Atun et al., 2020).

1.1.1 The Biological Basis of Cancer

The Hallmarks of Cancer

Cancer is not a uniform condition but rather a broad spectrum of diseases that share certain defining features, most notably the loss of normal growth control and the capacity of abnormal cells to invade surrounding tissues and eventually spread to distant organs. The biological principles underlying this transformation have been studied for decades, and one of the most enduring frameworks is the "hallmarks of cancer" first articulated by Hanahan and Weinberg and subsequently expanded in later revisions (Hanahan & Weinberg, 2000). These hallmarks outline the fundamental biological capabilities acquired during tumorigenesis:

- sustaining proliferative signaling,
- evading growth suppressors,
- resisting programmed cell death,
- enabling limitless replicative potential,
- inducing angiogenesis to secure a blood supply,
- activating mechanisms for invasion and metastasis (Hanahan & Weinberg, 2011).

In updated versions, additional dimensions have been incorporated, including deregulation of cellular energetics, avoidance of immune destruction, and, more recently, phenotypic plasticity and epigenetic reprogramming as critical contributors to malignant progression. Together, these features provide a conceptual map of how cancers arise and evolve (Hanahan, 2022). The hallmarks of cancer wheel was represented, adapted with highlighting of the crucial mechanisms that this thesis addresses in detail, in Figure 1.1.

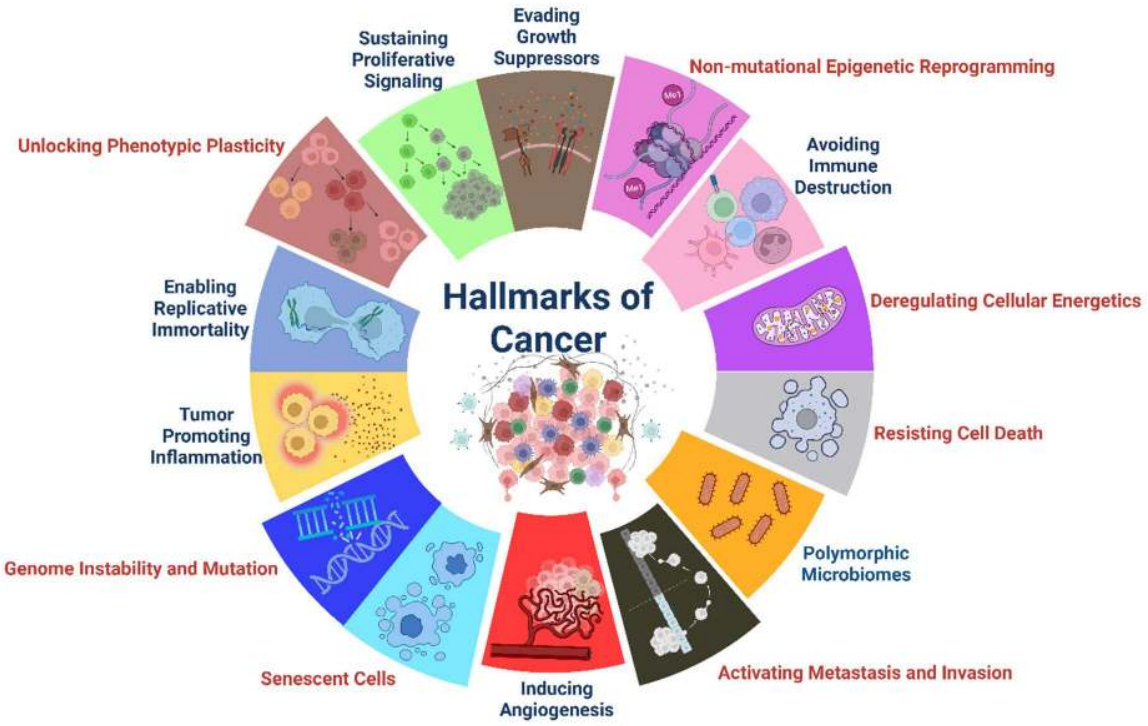

Figure 1.1: *Hallmarks of Cancer with Emphasis on CSC related and Epigenetic/Post-transcriptional Regulation Dimensions*. The highlighted traits — phenotypic plasticity, epigenetic reprogramming, deregulated metabolism, genome instability, and resistance to cell death — are particularly relevant to high-grade serous ovarian cancer stem cells and form the conceptual foundation of this thesis. (Figure Adapted from "Hallmarks of Cancer: New Dimensions", Hanahan, 2022.)

Together, these hallmarks provide a conceptual map of how cancers arise and progress, but they do not capture the full dynamics of how tumors evolve over time. This has led to the development of complementary models of tumor evolution, discussed below.

Models of Tumor Evolution

Two major paradigms have shaped our understanding of tumor development and heterogeneity.

Clonal Evolution Theory: Tumors evolve through a Darwinian process in which genetic alterations confer growth advantages to particular clones, leading to selection, expansion, and intratumoral heterogeneity (Nowell, 1976), (Greaves & Maley, 2012).

Cancer Stem Cell Theory: Tumors are hierarchically organized, with a subpopulation of stem-like cells that self-renew and generate diverse progeny, driving tumor maintenance and relapse (Batlle & Clevers, 2017).

Integration of Models: Increasing evidence indicates that these models are not mutually exclusive. CSCs themselves can undergo clonal evolution, and plasticity between CSC and non-CSC states suggests that tumor progression reflects both genetic diversification and functional hierarchy (Kreso & Dick, 2014) .

These models provide complementary insights into tumor biology, and together they help explain why cancers are so heterogeneous and difficult to eradicate.

Tumor Heterogeneity

Cancer progression is rarely linear or uniform across patients. It is a dynamic, context-dependent process shaped by the interplay of multiple hallmarks, the evolutionary trajectories of tumor clones, and the functional hierarchy of CSCs. Such interwoven processes, combined with inherited and acquired mutations and the rapid microevolution of tumor cell populations, help explain why cancers frequently develop resistance and why treatments that initially show promise often lose effectiveness over time.

Recognizing this complexity has shifted the field toward integrative therapeutic strategies that aim to target not an isolated hallmark but rather combinations of interdependent molecular mechanisms. In recent years, zooming in on these signaling pathways and cellular processes has yielded promising alternatives to conventional therapeutic approaches (Dagogo-Jack & Shaw, 2018).

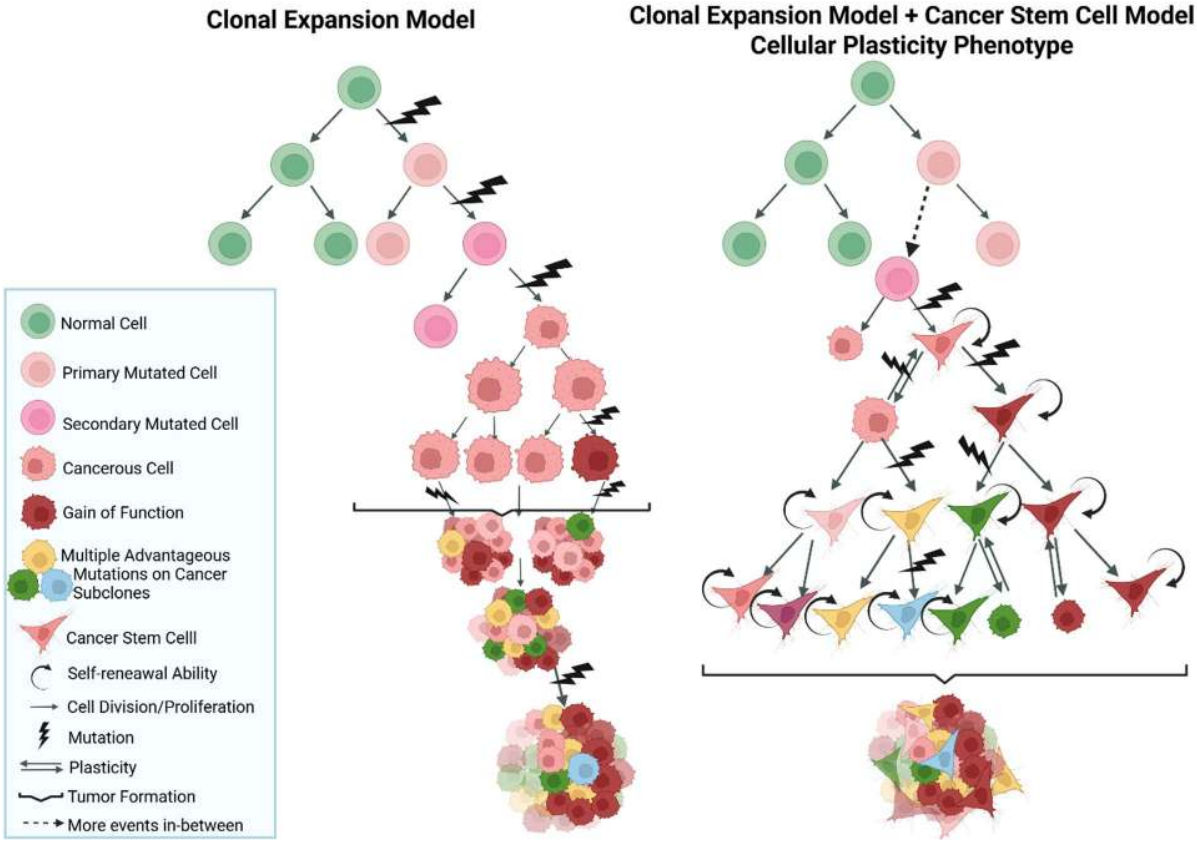

Figure 1.2: *Tumor Evolution Models Explaining Tumor Heterogeneity.* Figure was adapted and re-designed from multiple sources defining clonal expansion, CSC model, and integrative plasticity model (Laks et al., 2010).

Therapeutic Resistance

Resistance arises through a variety of mechanisms, many of which are shared across different tumor types. Among the most well-characterized are:

- *Drug efflux and multidrug resistance (MDR)*: Overexpression of ATP-binding cassette (ABC) transporters enables tumor cells to actively expel chemotherapeutic agents, reducing their intracellular concentration.

- *Enhanced DNA damage repair*: Upregulated repair pathways, including homologous recombination and non-homologous end joining, allow cancer cells to survive genotoxic therapies.
- *Altered apoptotic signaling*: Dysregulation of pro- and anti-apoptotic proteins (e.g., p53, BCL-2 family) renders cells less responsive to death signals induced by treatment.
- *Epithelial-to-mesenchymal transition (EMT)*: Acquisition of mesenchymal traits confers migratory potential and therapy tolerance.
- *Metabolic reprogramming and quiescence*: Tumor cells can adapt their energy requirements, shift between oxidative phosphorylation and glycolysis, or enter a quiescent state to withstand therapeutic stress (Al-Dimassi et al., 2014) (Mansoori et al., 2017).

Importantly, many of these resistance mechanisms converge on or are enriched within cancer stem cell (CSC) populations. CSCs exhibit high expression of drug efflux transporters, increased DNA repair proficiency, a propensity for cell cycle quiescence, and remarkable metabolic adaptability. These traits enable CSCs to survive conventional chemotherapy and radiotherapy, ultimately reconstituting the tumor and driving disease relapse (Prieto-Vila et al., 2017). This close link between CSC biology and therapeutic resistance positions CSCs as a critical driver of recurrence and underscores their importance as a focal point in modern cancer research.

Cancer Stem Cells

The concept of cancer stem cells (CSCs) emerged from the recognition that tumors are not homogeneous masses of identical cells, but rather hierarchically organized structures in which a small subpopulation possesses the unique ability to both self-renew and generate the diverse progeny that comprise the bulk of the tumor. First demonstrated in leukemia and later extended to solid tumors, CSCs are defined by their capacity to initiate tumors in xenograft models at limiting dilution and to sustain long-term tumor growth in a manner analogous to normal tissue stem cells (Bonnet & Dick, 1997) (Reya et al., 2001).

CSCs are endowed with several attributes that distinguish them from the bulk tumor population and that critically influence tumor behavior:

- *Self-renewal and differentiation*: CSCs maintain their own pool while producing differentiated progeny that constitute the majority of the tumor mass.
- *Therapy resistance*: CSCs evade cytotoxic treatments through high expression of efflux pumps, enhanced DNA repair mechanisms, reduced apoptotic sensitivity, and frequent adoption of quiescent or slow-cycling states.
- *Senescence evasion*: CSCs display mechanisms that circumvent replicative exhaustion, allowing indefinite propagation.
- *Metabolic flexibility*: CSCs can dynamically reprogram their metabolism, shifting between oxidative phosphorylation and glycolysis, which supports survival in diverse microenvironments and under treatment stress.
- *Cell cycle deregulation*: CSCs often exhibit altered checkpoint control, enabling persistence and regrowth after therapy-induced damage.

The presence of cancer stem cells (CSCs) carries far-reaching consequences for how tumors develop and how patients respond to treatment. Unlike the bulk of tumor cells that are often eliminated by surgery, chemotherapy, or radiotherapy, CSCs tend to endure these standard approaches. Their persistence allows them to repopulate the tumor, to act as seeds for relapse, and to play a central role in both metastatic spread and acquired resistance to therapy. Observations across a wide range of malignancies—including breast, colorectal, pancreatic, and ovarian cancers—show that higher levels of CSC markers generally correlate with worse clinical outcomes, such as poorer prognosis and shortened survival.

What complicates matters even further is that CSCs are not necessarily a stable or rigid subpopulation. A growing body of evidence suggests that so-called “non-CSCs” can under certain pressures, such as treatment stress or signals from the tumor microenvironment, revert or dedifferentiate back into a stem-like state. This plasticity means that eliminating CSCs alone may not be sufficient, since new ones can emerge from more differentiated tumor cells, adding another layer of difficulty to therapeutic design and long-term disease control (R. J. Jones, 2009).

Together, these characteristics position CSCs as central players in cancer biology, functioning both as the engines of tumor initiation and as reservoirs of therapeutic resistance. Their study has therefore become a major focus of modern oncology, with the goal of identifying vulnerabilities that could be exploited to achieve more durable clinical responses.

1.2 Ovarian Cancer

1.2.1 Epidemiology and Clinical Burden

Ovarian cancer remains one of the most lethal gynecological malignancies worldwide. Despite ranking below cervical and endometrial cancers in incidence, it accounts for the highest mortality among cancers of the female reproductive system. According to the most recent global estimates (GLOBOCAN, WHO), hundreds of thousands of women are newly diagnosed each year, with a nearly equivalent number of deaths annually, underscoring the aggressive nature of the disease. The overall five-year survival rate remains dismal, often ranging between 30% and 45%, largely due to late-stage diagnosis when peritoneal dissemination and distant metastases have already occurred (Torre et al., 2018).

The disease typically presents with vague, nonspecific symptoms such as bloating, abdominal discomfort, or early satiety, which often leads to delays in diagnosis. As a result, more than two-thirds of patients are diagnosed at advanced stages (FIGO stage III or IV), when the therapeutic options are limited and prognosis is poor. While improvements in surgical techniques and chemotherapy regimens have modestly extended progression-free survival, recurrence rates remain alarmingly high, with the majority of patients eventually relapsing after first-line treatment (Reid et al., 2017).

From a public health perspective, ovarian cancer imposes a substantial socio-economic burden. The high cost of advanced chemotherapeutics and biologic agents, coupled with the need for long-term surveillance and repeated interventions, strains healthcare systems. Moreover, the disease exerts significant psychological and physical tolls on patients and families, highlighting the urgent need for better early detection strategies and more durable therapeutic approaches (Cress et al., 2015).

1.2.2 Histopathological Subtypes of Ovarian Cancer

Ovarian cancer is not a single disease but rather a heterogeneous collection of tumors that differ in their histopathological subtypes, molecular alterations, clinical behavior, and response to therapy. In very general terms, ovarian tumors are usually divided into three groups: epithelial tumors, which account for roughly 90% of cases; germ cell tumors, which make up about 5%; and sex cord–stromal tumors, which comprise another 5%. Among these, epithelial ovarian cancers are by far the most important from a clinical perspective, both because of their high frequency and because they are responsible for the majority of deaths related to ovarian cancer (Lheureux et al., 2019).

Within this epithelial group, at least four major histological subtypes are commonly recognized: serous, endometrioid, clear cell, and mucinous carcinomas. Of these, high-grade serous ovarian carcinoma (HGSOC) stands out as the most prevalent, representing close to 70% of cases and the overwhelming majority of advanced-stage diagnoses (Torre et al., 2018). In contrast, low-grade serous carcinomas are comparatively rare and display a rather different profile, often showing slower progression and carrying a much lower frequency of TP53 mutations than their high-grade counterparts.

It is also worth noting that pathologists frequently classify epithelial ovarian cancers into two broader categories, referred to as Type I and Type II tumors. Type I tumors, which include low-grade serous, endometrioid, clear cell, and mucinous subtypes, tend to develop from relatively well-defined precursor lesions, follow a stepwise evolutionary path, and are genetically more stable. These tumors are, in many cases, detected at earlier stages and usually progress in a more indolent manner. Type II tumors, with HGSOC as the dominant form, are quite different. They are characterized by pronounced genomic instability, near-universal TP53 mutations, frequent homologous recombination deficiency, and very rapid progression. Unsurprisingly, these cancers are most often diagnosed at advanced stages and are the major contributors to the overall poor survival outcomes seen in ovarian cancer (Kurman & Shih, 2016).

Taken together, this biological and clinical heterogeneity highlights the importance of considering subtype-specific features when designing research and clinical approaches. Nevertheless, because of its sheer prevalence, aggressive biology, and central role in ovarian

cancer mortality, HGSOC has, perhaps inevitably, become the main focus of ongoing investigations and remains the subtype most intensively studied.

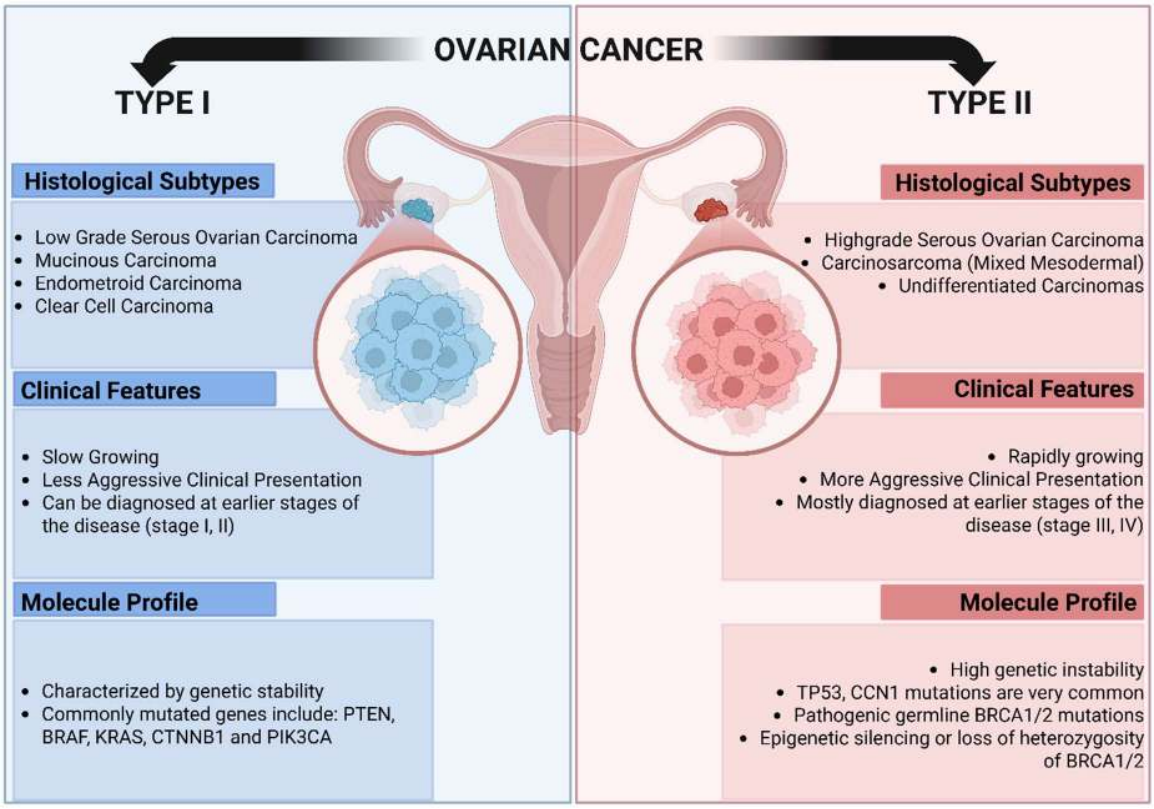

Figure 1.3: *Summary of Histological Subtypes of Ovarian Cancer and their characterization.* Figure was adapted from (Zhu et al., 2022)

1.2.3 High Grade Serous Ovarian Cancer (HGSOC)

High-grade serous ovarian carcinoma (HGSOC) is by far the most frequent and clinically aggressive form of ovarian cancer. It accounts for around 70% of epithelial ovarian cancers and the great majority of advanced-stage diagnoses, making it the dominant driver of ovarian cancer mortality worldwide. Clinically, HGSOC is marked by rapid progression, widespread peritoneal dissemination, and a strong tendency to recur after treatment(Matulonis et al., 2016).

Pathogenesis and Molecular Features

HGSOC is almost universally associated with TP53 mutations, found in more than 95% of cases, and these mutations are closely linked to its pronounced genomic instability and heterogeneity (Bell et al., 2011). Roughly half of HGSOCs also carry defects in homologous recombination repair (HRR). This is most often due to inherited or somatic mutations in BRCA1 or BRCA2, although epigenetic silencing of other HRR-related genes can also play a role. Homologous recombination deficiency (HRD) not only drives genomic instability but also creates a therapeutic vulnerability that can be targeted with PARP inhibitors(Moore et al., 2018). Beyond HRD, HGSOC typically shows widespread copy number changes, structural rearrangements, and significant dysregulation of pathways controlling the cell cycle and DNA damage response — all of which feed into its aggressive clinical course.

Cell of Origin

For many years, HGSOC was thought to originate from the ovarian surface epithelium. However, evidence now strongly supports the fallopian tube, particularly the secretory epithelial cells of the fimbriae, as the primary site of origin. The identification of serous tubal intraepithelial carcinoma (STIC) lesions in risk-reducing salpingo-oophorectomy specimens from BRCA mutation carriers provided critical support for this revised model (Vaughan et al., 2011). This shift in perspective has not only clarified some of the earliest events in HGSOC development but has also influenced prevention strategies, such as the adoption of salpingectomy in women at high genetic risk.

Clinical Presentation and Diagnosis

HGSOC usually presents with vague and nonspecific symptoms — bloating, abdominal pain, changes in appetite or satiety — that are easily overlooked. Because of this, more than two-thirds of patients are diagnosed only when the disease has already reached an advanced stage (FIGO stage III–IV). By this point, the cancer has typically spread throughout the peritoneal cavity and is frequently accompanied by malignant ascites. Although serum CA-125 and imaging are widely used in diagnosis and monitoring, their limited sensitivity and specificity prevent them from being reliable tools for early detection (Fader et al., 2014).

Standard Treatment Approaches

The frontline treatment of HGSOC continues to rely on maximal cytoreductive surgery (Pomel et al., 2007) followed by platinum- and taxane-based chemotherapy (Verschraegen et al., 2015). Many patients initially respond well to platinum, but unfortunately relapse is common, and in most cases expected. In recent years, the use of targeted therapies has changed the management of this disease. PARP inhibitors such as olaparib, niraparib, and rucaparib provide significant benefit for patients with BRCA mutations or HRD-positive tumors, improving progression-free survival. Anti-angiogenic therapy with bevacizumab has also shown value in specific patient groups. Nevertheless, resistance to both chemotherapy and targeted agents remains the greatest challenge to achieving durable remission (Pujade-Lauraine et al., 2017).

Challenges and Prognosis

Overall prognosis in HGSOC is still poor. The majority of patients experience multiple relapses, even with newer therapeutic options. Platinum-resistant disease, which is defined as recurrence within six months of completing platinum-based chemotherapy, is particularly problematic and leaves clinicians with very few effective treatments. Moreover, even in the setting of PARP inhibitor therapy, resistance can emerge through several mechanisms, including secondary BRCA mutations, stabilization of replication forks, and rewiring of DNA repair pathways. Because of this, survival gains have been modest, and HGSOC remains an area of urgent need for better mechanistic insights into therapy resistance and recurrence biology (Q. Wang et al., 2021).

1.2.4 Cancer Stem Cells in Ovarian Cancer

Mounting evidence indicates that cancer stem cells (CSCs) play a central role in the biology of ovarian cancer, particularly in the high-grade serous subtype. CSCs have been identified in ovarian tumors and ascites using markers such as CD44, CD117 (c-Kit), CD133, ALDH1, SOX2, NANOG, and OCT4, many of which are shared with normal stem cells (S. Zhang et al., 2008) (Baba et al., 2009). These cells demonstrate the classical CSC properties of self-renewal, differentiation, and tumor-initiating capacity in xenograft models, confirming their functional role in disease maintenance.

CSC enrichment in spheroids and ascites

A key clinical feature of HGSOC is the accumulation of malignant ascites and widespread dissemination within the peritoneal cavity. In this context, tumor cells often form multicellular spheroids, which are enriched for CSC-like populations. These spheroids not only facilitate survival in the ascitic fluid but also enhance metastatic colonization at secondary sites. Importantly, spheroid cultures derived from patient samples and established cell lines consistently demonstrate increased expression of stemness markers and greater tumor-initiating capacity compared to adherent counterparts (Latifi et al., 2011) (J. Zhang et al., 2012).

CSC-mediated therapy resistance

Ovarian CSCs are implicated in resistance to both platinum-based chemotherapy and emerging targeted agents. Their high expression of ABC transporters, efficient DNA repair mechanisms, and ability to remain quiescent or adopt alternative metabolic states confer substantial survival advantages during treatment (Steg et al., 2012) (Abubaker et al., 2013). As a result, conventional therapies effectively debulk the tumor mass but leave behind CSC populations that eventually drive relapse. Elevated CSC marker expression has been correlated with shorter progression-free survival and poor overall outcomes in clinical cohorts, reinforcing their relevance to patient prognosis.

Plasticity and clinical implications

Beyond being a static subpopulation, ovarian CSCs exhibit plasticity, whereby non-stem tumor cells can dedifferentiate into CSC-like states under environmental or therapeutic pressures. This dynamic interconversion complicates therapeutic strategies and underscores the need for interventions that can disrupt CSC maintenance pathways. Several signaling cascades — including WNT, NOTCH, Hedgehog, and PI3K/AKT — have been implicated in ovarian CSC regulation, making them attractive but challenging therapeutic targets (Kumar et al., 2021).

Together, these findings position CSCs as critical drivers of disease progression, therapy resistance, and recurrence in ovarian cancer. Their enrichment in patient-derived spheroids

and ascites directly links CSC biology to the clinical behavior of HGSOC, highlighting the importance of developing models and tools that faithfully recapitulate CSC dynamics for both mechanistic studies and translational applications.

1.2.5 Limitations of Conventional Models and the Need for Advanced Systems

Despite the significant advances that have been made in understanding ovarian cancer biology, the models most commonly used to study this disease still have important shortcomings when it comes to reflecting its true complexity. Two-dimensional (2D) monolayer cultures, which remain the standard experimental system, are popular because they are easy to handle and highly reproducible. Yet, they fail to recreate the three-dimensional structure, the cellular diversity, and the microenvironmental cues that strongly influence tumor behavior in vivo. Cells grown on flat plastic surfaces often lose many of their stem-like features, display altered patterns of gene expression, and show drug sensitivities that differ markedly from those observed in patients (Edmondson et al., 2014) (Nath & Devi, 2016). As a result, it is not unusual for compounds that look effective in 2D assays to show little or no benefit in clinical trials.

Animal models such as patient-derived xenografts (PDXs) and genetically engineered mouse models (GEMMs) offer a step closer to physiological relevance by recreating at least some of the interactions between tumor and host. At the same time, they are resource-demanding, require long timelines, and are not easily scalable for high-throughput studies. Moreover, PDX models in particular may fail to preserve the dynamic cancer stem cell (CSC) populations and the transcriptomic complexity present in human tumors, which limits their utility for studying stemness-related mechanisms (Thoma et al., 2014).

In recent years, three-dimensional (3D) culture systems have gained traction as a useful “middle ground” between oversimplified 2D systems and costly animal models. Approaches such as ultra-low attachment (ULA) spheroid culture and hydrogel-based matrices allow tumor cells to self-organize into spheroid structures that more closely mimic in vivo growth. These models enable CSC enrichment, reproduce several forms of therapy resistance, and provide a controlled setting for studying transcriptomic and epigenetic features(Liao et al.,

2014). Importantly, they are also relatively cost-effective, scalable, and versatile, making them attractive for translational applications.

For ovarian cancer in particular, 3D spheroid cultures are highly relevant. Malignant ascites from patients with high-grade serous ovarian carcinoma (HGSOC) frequently contain multicellular spheroids enriched for CSCs, which are thought to drive both metastasis and recurrence (Shield et al., 2009). Reproducing this phenomenon in vitro therefore creates models with direct clinical relevance. Even so, not all 3D systems perform equally well in capturing CSC dynamics or achieving translational fidelity. Comparative analyses remain essential for determining which models best represent patient tumors and which can serve as the most reliable platforms for mechanistic and therapeutic studies (Kenny et al., 2015).

With these points in mind, the present thesis begins by evaluating multiple 3D culture approaches in ovarian cancer, with a particular focus on ultra-low attachment spheroid systems and hydrogel-based photomasking using GelMA. By comparing two representative HGSOC cell lines alongside patient-derived material, the first part of this work aims to identify which model is most effective at enriching CSC traits and, at the same time, holds the greatest potential for translationally relevant insights.

1.3 Post-transcriptional Regulation in Cancer

RNA-based regulation has emerged as a critical layer of cancer biology, complementing genetic and epigenetic mechanisms. The following subsections outline the key modes of post-transcriptional regulations and epitranscriptomic control and their relevance to tumor progression.

1.3.1 Overview of Post-Transcriptional & Epitranscriptomic Regulation

In addition to the more familiar layers of genetic mutations and epigenetic changes, cancer cells are also profoundly influenced by disruptions in RNA metabolism. This area, refers to the dynamic set of processes occurring post-transcriptionally and modifications to RNAs that regulate their fate beyond the underlying nucleotide sequence. It encompasses the activity of, the roles of non-coding RNAs, RNA-binding proteins and chemical modifications directly on RNA molecules themselves (Barbieri & Kouzarides, 2020). Taken together, these

mechanisms act to fine-tune the stability, localization, translation, and eventual degradation of transcripts, thereby exerting broad control over gene expression programs and the plasticity of the cancer cell state (Wu et al., 2025).

Aberrant regulation at this post-transcriptional level has increasingly been recognized as a hallmark of tumor development and progression. For instance, altered activity of RNA-binding proteins can profoundly change splicing choices or affect the stability of oncogenic transcripts. Likewise, microRNAs (miRNAs) can suppress tumor suppressor genes or, when lost, permit the unchecked expression of oncogenes. Alternative polyadenylation (APA) reshapes the length and regulatory content of 3′ untranslated regions (3′UTRs), influencing how transcripts interact with microRNAs and RNA-binding proteins. Chemical modifications such as N^6-methyladenosine (m^6A) introduce yet another layer of control, adding subtle but powerful regulatory effects. In combination, these processes provide cancer cells with a kind of transcriptomic flexibility, allowing them to adapt quickly to changes in their environment and to withstand therapeutic pressures (Roundtree et al., 2017).

It is worth noting that post-transcriptional control has a particularly strong connection to cancer stem cell (CSC) biology. CSC populations frequently maintain specialized RNA regulatory networks that support states of quiescence, survival under genotoxic or metabolic stress, and shifts in energy utilization (Hao et al., 2023). These adaptations not only preserve the tumor-initiating potential of CSCs but also strengthen their resistance to therapy. For this reason, mapping and understanding the RNA regulatory landscape has become an increasingly important goal, since it may reveal points of vulnerability that could be exploited to interfere with CSC maintenance and, ultimately, to improve treatment outcomes.

1.3.2 MicroRNAs in Cancer & CSC Biology

MicroRNAs (miRNAs) are a class of short, non-coding RNA molecules, generally ranging between 19 and 25 nucleotides, that fine-tune gene expression at the post-transcriptional level. They exert their regulatory role mainly by binding to complementary sequences within the 3′ untranslated regions (3′UTRs) of messenger RNAs, which can lead either to transcript degradation or to inhibition of translation. In this way, miRNAs act as modulators of protein output rather than as simple on/off switches. Since their discovery at the beginning of the 21st

century, they have been established as key regulators of fundamental processes such as differentiation, proliferation, and apoptosis, and their misregulation has been strongly tied to cancer initiation and progression (Croce, 2009) (Rupaimoole & Slack, 2017)

miRNAs in cancer development

Dysregulated expression of miRNAs has been observed in almost every form of cancer studied to date. Oncogenic miRNAs, often referred to as "oncomiRs," can drive tumorigenesis by silencing critical tumor suppressor pathways, while tumor-suppressive miRNAs are frequently lost or downregulated, allowing unchecked oncogenic signaling. The miR-17~92 cluster provides a well-known example of an oncomiR group with potent tumor-promoting activity. In contrast, tumor-suppressive miRNAs such as the let-7 family or miR-34a are often absent in aggressive tumors, which contributes to disease progression. The shifting balance between these tumor-promoting and tumor-suppressing networks plays a major role in shaping tumor heterogeneity and the adaptive capacity of malignant cells (Svoronos et al., 2016).

miRNAs in CSC biology

An increasing body of work has shown that cancer stem cells (CSCs) rely on unique miRNA networks to sustain their stem-like features and to withstand therapy. Tumor-suppressive miRNAs, including members of the let-7 family, are known to limit self-renewal pathways and counteract differentiation blocks. On the other hand, oncomiRs such as miR-21 and miR-155 have been reported to reinforce stemness programs, resistance to cell death, and the metastatic potential of CSCs (Shimono et al., 2009) (C. Liu et al., 2011). Specific miRNAs also act by regulating the core transcription factors associated with stemness—NANOG, OCT4, SOX2, and c-MYC—creating feedback loops that stabilize the CSC state and make these cells particularly resilient.

miRNAs, therapy resistance, and plasticity

Beyond their role in tumor initiation and maintenance, miRNAs are also implicated in shaping how CSCs respond to treatment. They regulate multiple resistance-associated mechanisms, including drug efflux transporters, DNA repair genes, and apoptosis regulators. The miR-200

family, for instance, is closely linked to the control of epithelial-to-mesenchymal transition (EMT), a process associated with CSC plasticity and with the acquisition of chemoresistance (Koutsaki et al., 2017). By adjusting their miRNA expression profiles in response to therapeutic pressures, CSCs can shift between stem-like and more differentiated states, further complicating efforts to eliminate them.

Overall significance

Collectively, these observations place miRNAs at the center of cancer biology—not only as regulators of tumor growth and survival but also as orchestrators of CSC plasticity and resilience. Their ability to function either as oncogenes or as tumor suppressors highlights their dual potential: on one hand, as biomarkers that may improve diagnosis and prognosis, and on the other, as promising therapeutic targets in the context of precision oncology.

1.3.3 Alternative Polyadnylation (APA) and 3'UTR Dynamics

Messenger RNA (mRNA) molecules are processed at their 3′ ends through cleavage and polyadenylation, and many genes use this step to generate isoforms with different 3′ untranslated region (3′UTR) lengths. This mechanism, termed alternative polyadenylation (APA), is thought to affect more than 70% of human genes (Tian & Manley, 2016) (Xu & Zhang, 2020). Both experimental studies and computational surveys have catalogued this widespread diversity, showing how APA is shaped by the interplay of core 3′-end processing factors and various RNA-binding proteins (Gruber & Zavolan, 2019). Shortening of 3′UTRs can remove binding sites for microRNAs or RBPs, often resulting in more stable transcripts and increased translation, whereas extension of 3′UTRs can introduce additional regulatory sequences that influence localization or dampen expression. In this way, APA provides flexibility in post-transcriptional regulation and has been closely linked to the large-scale reprogramming of gene expression in cancer. Some studies give particular emphasis to how cis-elements within the 3′UTR, and their interactions with RBPs and miRNAs, contribute to these regulatory shifts (Erson-Bensan, 2016).

Functional implications of APA

Changes in polyadenylation site usage can therefore be highly consequential. Shortened 3′UTRs typically lose important cis-regulatory elements, such as recognition sites for miRNAs or RBPs, which increases mRNA stability and enhances protein production. In contrast, transcripts with longer 3′UTRs acquire additional motifs that can change RNA localization or introduce further regulatory checkpoints.

APA in cancer biology

Across many tumor types, APA patterns are frequently remodeled. A widely observed trend is global 3′UTR shortening, which enables oncogenes to escape microRNA-mediated repression and boosts their expression (Sandberg et al., 2008). At the same time, selective lengthening events have been described, particularly involving tumor suppressor transcripts, underlining APA's context-dependent role (Xia et al., 2014). A 2019 review by Gruber and Zavolan thoroughly discuss both the mechanistic regulation of APA and its broader implications in human disease.

Connections to CSC biology and therapy resistance

Emerging work suggests that cancer stem cells (CSCs) make strategic use of APA to remodel their transcriptomes. Shortening of 3′UTRs helps maintain expression of stemness-related transcription factors by bypassing tumor-suppressive miRNAs, collective evidence points out that while lengthened isoforms of metabolic or stress-response genes appear to give CSCs the flexibility to survive under therapeutic and environmental pressures. Such rewiring of RNA regulatory networks not only contributes to CSC resilience but may also offer opportunities for biomarker discovery and targeted intervention (Erson-Bensan & Can, 2016).

1.3.4 Other RNA Modifications & RBPs

Beyond microRNAs and alternative polyadenylation, the scope of RNA regulation extends to a wide variety of chemical RNA modifications and the actions of RNA-binding proteins (RBPs). Together, these regulatory layers add further complexity to post-transcriptional control and are now understood to have major influences on cancer development and progression.

RNA modifications

Among the more than 170 chemical modifications identified on RNA so far, N^6-methyladenosine (m^6A) is by far the most thoroughly investigated. This modification is not static but is written, erased, and interpreted by distinct protein groups. The "writers" (such as METTL3, METTL14, and WTAP) install the mark, "erasers" (FTO, ALKBH5) remove it, and "readers" (including the YTHDF proteins and IGF2BP family) recognize and act upon it (S. Wang et al., 2022). In the context of cancer, dysregulation of this system has been shown to stabilize oncogenic transcripts, boost the translation of growth-promoting genes, and reinforce stemness-associated pathways. METTL3-driven methylation, for instance, has been connected to epithelial–mesenchymal transition (EMT) and invasive behavior, whereas ALKBH5 has been implicated in maintaining CSC traits by demethylating key transcripts such as NANOG (Shen et al., 2020). Other modifications, including 5-methylcytosine (m^5C) and pseudouridine (Ψ), are also beginning to draw attention for their roles in transcript stability and translational regulation, although their contributions to tumor biology are still being uncovered (Mao et al., 2025) (Zhao & He, 2015).

RNA-binding proteins (RBPs)

RBPs play essential roles across RNA metabolism, controlling processes such as splicing, stability, localization, and translation. Several have been identified with clear oncogenic or tumor-suppressive potential.

- *The IGF2BP family* (IGF2BP1, 2, and 3) is a notable example, stabilizing m^6A-modified transcripts of oncogenes like MYC, thereby promoting cell proliferation and invasion (Huang et al., 2018).
- *HuR (ELAVL1)*, a broadly expressed RBP, binds AU-rich motifs in 3′UTRs to stabilize mRNAs tied to survival and proliferation, and is often elevated in tumors where it has been linked to chemoresistance(Cai et al., 2022).
- *LIN28A and LIN28B* act differently by blocking the maturation of the let-7 miRNA family, which normally functions in tumor suppression, thereby helping cancer cells preserve stemness and pluripotency programs (Ma et al., 2021).

Convergence with CSC biology

Taken together, RNA modifications and RBPs are deeply integrated into the regulation of cancer stem cells. Modifications such as m^6A and m^5C influence the stability and translation of transcripts central to stemness, while RBPs including LIN28, HuR, and the IGF2BPs generate reinforcing feedback loops that secure CSC-related transcriptional networks. These combined layers of regulation provide CSCs with a high degree of adaptability and survival capacity under therapeutic pressure. Because of this, both RNA modifications and RBPs are now being investigated as promising therapeutic entry points, with the goal of undermining CSC resilience and improving patient outcomes (L. Yang et al., 2024).

1.3.5 miRNAs, APA and Other Epitranscriptomic Regulators in Ovarian Cancer

RNA regulation has increasingly come into focus as an essential layer of control in ovarian cancer (OC), with particular significance in the high-grade serous subtype (HGSOC). A wide range of mechanisms—including microRNAs (miRNAs), alternative polyadenylation (APA), chemical RNA modifications such as N^6-methyladenosine (m^6A) and 5-methylcytosine (m^5C), A-to-I RNA editing, and the activity of RNA-binding proteins (RBPs)—have all been implicated in tumor initiation, progression, therapy resistance, and, perhaps most importantly, the maintenance of cancer stem cell (CSC) populations.

MicroRNAs in ovarian cancer

Dysregulated miRNA expression is pervasive across ovarian cancers and influences several of the classical hallmarks of malignancy.

- *EMT and metastasis*: Loss of the tumor-suppressive miR-200 family removes repression of ZEB1/2, thereby driving epithelial–mesenchymal transition (EMT) (Bendoraite et al., 2010). In contrast, oncogenic miR-181a strengthens TGF-β-mediated EMT by inhibiting SMAD7, with higher levels of this miRNA correlating with recurrence and worse outcomes in HGSOC (Parikh et al., 2014). miR-9 also contributes by directly targeting E-cadherin and promoting EMT (Zhou et al., 2017).
- *Stemness and CSC traits:* Downregulation of let-7 family members and miR-34a allows derepression of stemness-related transcription factors such as LIN28 (Ma et

al., 2021), SOX2, NANOG, and MYC, thereby supporting self-renewal and resistance to therapy (Chirshev et al., 2021). In contrast, oncogenic miR-20a has been shown to enhance CSC-like phenotypes (Flores et al., 2017).

- *Apoptosis and proliferation*: miR-21, one of the most consistently upregulated miRNAs in OC, promotes proliferation and survival by suppressing PTEN and PDCD4 (Jiang et al., 2023). On the other hand, tumor-suppressive miRNAs such as miR-125b and miR-34a inhibit Bcl-2, thus promoting apoptosis (Saburi et al., 2022) (Guan et al., 2011).
- *Therapy resistance*: Numerous miRNAs modulate drug response. In HGSOC, miR-622 mediates resistance to both platinum and PARP inhibitors by targeting Ku70/80 and restoring homologous recombination (Choi et al., 2016). Cisplatin resistance has been associated with reduced expression of miR-486-3p (J. Wang & Wu, 2024) and miR-30a (Nayak et al., 2025), while paclitaxel resistance involves the downregulation of miR-194-5p and miR-522-3p (Miyamoto et al., 2020).
- *Autophagy and metabolism:* Autophagy-related resistance is shaped by miRNAs such as miR-30a, which blocks Beclin-1–dependent autophagy (Y. Ding et al., 2024). More recently, miR-937-5p was reported to promote autophagy and proliferation in HGSOC through stabilization of ULK1 (Z. Zhang et al., 2024).

Alternative polyadenylation (APA) in Ovarian Canvcer

Remodeling of polyadenylation has also been tied to ovarian cancer. In single-cell OC datasets, IGF2BP3 was found to cooperate with NUDT21 to regulate APA of SPTBN1, thereby enhancing invasion and metastasis (Luo et al., 2025). Because APA alters the availability of microRNA binding sites, this mechanism provides a direct point of intersection between APA and miRNA-mediated control.

m⁶A RNA methylation in Ovarian Cancer

Several components of the m⁶A machinery are deregulated in ovarian tumors. METTL3, often upregulated, drives invasion and EMT by enhancing translation of AXL (Hua et al., 2018). YTHDF1, which is amplified in OC, increases translation of oncogenic targets such as EIF3C, promoting tumor growth, metastasis, and cisplatin resistance (T. Liu et al., 2021). Conversely,

the “eraser” ALKBH5, activated by NF-κB/TLR4 signaling, maintains CSC programs by demethylating transcripts such as NANOG (L. L. Chang et al., 2021). The IGF2BP family, especially IGF2BP2 and IGF2BP3, is also upregulated in HGSOC and stabilizes m^{6}A-modified oncogenic transcripts, reinforcing both stemness and invasive traits (Huang et al., 2018).

m^{5}C RNA methylation in Ovarian Cancer

The m^{5}C methyltransferase NSUN2 has been shown to promote ovarian tumorigenesis through a positive feedback loop involving NSUN2–m^{5}C–E2F1. Moreover, altered m^{5}C modification signatures have been associated with prognosis in ovarian cancer cohorts (X. Liu et al., 2024).

A-to-I RNA editing in Ovarian Cancer

Dysregulation of ADAR1 alters the RNA editing landscape in ovarian cancer, contributing to growth and immune evasion. These findings are consistent with broader pan-cancer data that link ADAR1 to interferon signaling modulation and therapeutic resistance (Rehwinkel & Mehdipour, 2025) (Y. Wang et al., 2024).

RNA-binding proteins (RBPs) in Ovarian Cancer

A number of RBPs play central roles in ovarian cancer post-transcriptional control. HuR (ELAVL1) is frequently overexpressed and stabilizes mRNAs that promote survival and proliferation, contributing to drug resistance (Cai et al., 2022). IGF2BP1 promotes invasion through SRC/MAPK signaling while LIN28A and LIN28B block maturation of let-7 miRNAs, thereby maintaining CSC programs (Bley et al., 2021).

Overall significance

Collectively, these findings emphasize the wide-ranging influence of RNA regulation in ovarian cancer. By altering pathways linked to EMT, stemness, apoptosis, drug response, autophagy, and immune evasion, miRNAs, APA, RNA modifications, and RBPs act in concert to drive the aggressive biology of HGSOC. Many of these mechanisms ultimately converge

on CSCs, directly connecting RNA regulatory mechanisms' deregulation to recurrence and poor patient outcomes.

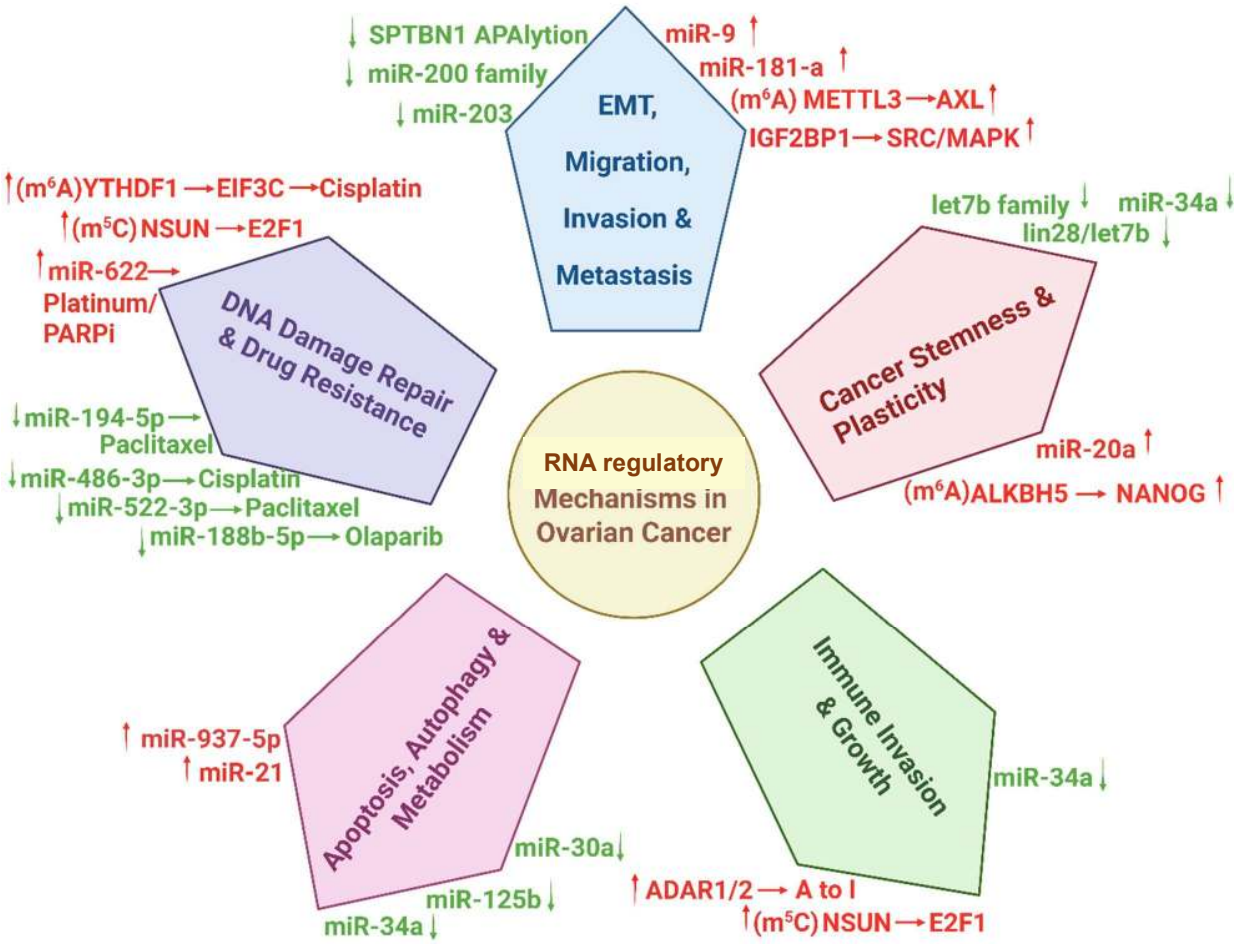

Figure 1.4: *RNA Regulatory Mechanisms in Ovarian Cancer.* This schematic was inspired from (L. Ding et al., 2019) about miRNAs in triple negative breast cancer. All the resources used to illustrate the figure is cited in 1.4.5.

1.3.6 Clinical Applications of miRNAs

The realization that microRNAs (miRNAs) act as broad regulators of gene expression has fueled strong interest in their use as therapeutic agents. Broadly, two main approaches have been developed: the first seeks to restore the activity of tumor-suppressive miRNAs through synthetic mimics, while the second focuses on silencing oncogenic miRNAs using anti-miRs (antagomiRs) or locked nucleic acid (LNA)–modified inhibitors.

Therapeutic strategies

A well-known clinical effort in this area was MRX34, a liposomal mimic of the tumor-suppressive miR-34a. This compound progressed into Phase I testing in patients with advanced solid tumors and initially showed signs of antitumor activity. However, the trial had to be stopped early because of serious immune-related toxicities, including severe cytokine release syndromes and other immune-mediated side effects (Beg et al., 2017). Another notable example is miravirsen, an LNA-based inhibitor of miR-122, which provided proof of concept for the feasibility of targeting miRNAs. In Phase II trials for hepatitis C virus infection, it demonstrated biological activity (Janssen et al., 2013). Still, the findings also revealed potential problems, including off-target effects and metabolic disturbances, which raise concerns for applications in oncology.

Challenges and limitations

Bringing miRNA-based therapeutics into the clinic has proven challenging, and several barriers remain:

- *Delivery and specificity:* Stable, tumor-directed delivery without unwanted distribution to other tissues is still a major hurdle.
- *Stability and degradation:* Naked miRNAs degrade rapidly in circulation, requiring protective carriers such as lipid nanoparticles or exosomes.
- *Immune activation:* One of the most serious obstacles is the unwanted activation of innate immunity. Synthetic RNA molecules can be detected by toll-like receptors (TLRs) and RIG-I-like receptors, setting off interferon-driven signaling cascades. This problem was highlighted in the MRX34 trial, where patients experienced severe immune and allergic reactions, ultimately forcing early termination of the study (Hong et al., 2020).
- *Tumor heterogeneity:* Because the activity of a given miRNA can differ depending on cellular or tumor context, a molecule may act as a suppressor in one setting but play a different role in another, complicating predictions of therapeutic outcome.

Clinical outlook

Despite these difficulties, the promise of miRNA-based therapeutics has not diminished. Advances in nanoparticle formulations, tissue-specific delivery strategies, and exosome-mediated transfer are being actively developed to improve safety and efficacy. At the same time, miRNAs are also gaining attention as diagnostic and prognostic biomarkers, since they are relatively stable in blood and display disease-specific signatures. Particularly relevant to ovarian cancer and CSC biology, manipulating miRNAs that regulate stemness programs may provide new opportunities to reduce therapy resistance and lower the risk of relapse.

Taken together, these findings indicate that RNA-level regulation—particularly post-transcriptional mechanisms such as microRNAs, alternative polyadenylation (APA), and RNA-binding proteins, alongside chemical RNA modifications—can act as central drivers of ovarian cancer biology. Through these routes, cancer cells remodel their transcriptomes to sustain proliferation, evade apoptosis, reprogram metabolism, and preserve CSC populations under therapeutic pressure. Several of these processes are already entering clinical exploration, underscoring both the promise and the challenges of targeting RNA-based regulation. In HGSOC, where relapse and resistance are common, delineating RNA-level control reveals opportunities to identify vulnerabilities not accounted for by genetic or chromatin alterations alone.

Building on this perspective, the next section turns to epigenetic regulation, another dynamic and reversible layer that intersects closely with RNA-mediated processes. Epigenetic regulators—including DNA methylation, histone modifications, and chromatin remodelers—cooperate with miRNA- and APA-driven programs, as well as RNA-modification pathways, to shape CSC identity and influence therapeutic resistance. Together, these interdependent layers motivate the integrative approach taken in this thesis.

1.4 Epigenetic Regulation in Cancer

1.4.1 Overview of Epigenetic Mechanisms

Epigenetics describes heritable changes in gene expression that take place without altering the DNA sequence itself. These changes act as an additional regulatory layer, one that is both dynamic and reversible, and allow the genome to integrate signals from development, the environment, and cellular stress. In the context of cancer, disruption of this regulatory balance

has been linked to nearly every stage of tumorigenesis—from the earliest steps of initiation through progression and metastasis, and eventually to the emergence of therapy resistance (P. A. Jones & Baylin, 2007) (Feinberg et al., 2016)

The main categories of epigenetic regulation can be broadly grouped as follows (Dawson & Kouzarides, 2012):

- *DNA methylation*: The attachment of methyl groups to cytosines, most often at CpG dinucleotides, is carried out by DNA methyltransferases (DNMTs). Aberrant methylation patterns are common in cancer: hypermethylation of CpG islands in promoters can silence tumor-suppressor genes, while genome-wide hypomethylation tends to destabilize the genome and activate oncogenic elements (B. Jin & Robertson, 2013).
- *Histone modifications*: Histones undergo a range of post-translational modifications—including acetylation, methylation, phosphorylation, and ubiquitination—that alter chromatin accessibility and transcriptional activity. In general, acetylation mediated by histone acetyltransferases (HATs) promotes transcriptional activation, while removal of these marks by histone deacetylases (HDACs) leads to repression. When misregulated, histone modifications disrupt programs controlling cell proliferation, lineage differentiation, and DNA repair (Chi et al., 2010).
- *Chromatin remodeling complexes*: Large ATP-dependent complexes, such as SWI/SNF, ISWI, and polycomb repressive complexes (PRC1/2), actively reorganize nucleosomes and higher-order chromatin structure. Alterations in these complexes are often observed in tumors and can suppress differentiation pathways while preserving stem-like transcriptional programs (Parreno et al., 2022).
- *Non-coding RNAs*: Already addressed in RNA-level regulations, several long non-coding RNAs (lncRNAs) and small RNAs are considered among the epigenetic regulators, since they also act by changing the expression levels without changing the gene dosage. They can also act by recruiting chromatin-modifying proteins to defined genomic regions (Mattick et al., 2023).

Together, these mechanisms shape what is often described as the "epigenetic landscape," a framework that determines when and where genes are expressed. The plasticity of this landscape is particularly relevant in cancer, since tumor cells frequently exploit epigenetic reprogramming to adapt to therapy and environmental stress. At the same time, because epigenetic changes are in principle reversible, they present attractive therapeutic opportunities. This is illustrated by the clinical success of DNMT inhibitors and HDAC inhibitors in hematological cancers, while efforts to extend such approaches to solid tumors—and to target cancer stem cell regulation in particular—remain an active and rapidly evolving area of research

1.4.2 Epigenetics and CSC Maintenance

A growing body of evidence suggests that epigenetic control is central to the maintenance of cancer stem cell (CSC) populations in many tumor types, including ovarian cancer. Epigenetic mechanisms regulate the delicate balance between self-renewal and differentiation, protect stemness programs under conditions of stress, and support the plasticity that enables CSCs to survive therapy and adapt to their microenvironment (Easwaran et al., 2014).

DNA methylation and CSC identity

Aberrant patterns of DNA methylation play a decisive role in sustaining CSC traits. Promoter hypermethylation can silence genes that normally promote differentiation, thereby maintaining cells in an undifferentiated state. At the same time, demethylation at key pluripotency loci allows persistent expression of transcription factors such as OCT4, SOX2, and NANOG. DNA methyltransferases—including DNMT1, DNMT3A, and DNMT3B—are frequently upregulated in CSCs, and inhibition of these enzymes has been shown to diminish stem-like characteristics and increase chemosensitivity (Muñoz et al., 2012).

Histone modifications and polycomb regulation

CSC gene expression programs are also shaped by histone modifications, particularly methylation and acetylation. Polycomb repressive complexes (PRC1/2) introduce H3K27me3 marks that silence differentiation genes while sustaining transcriptional networks associated with stemness (Margueron & Reinberg, 2011). Overexpression of EZH2, the catalytic subunit

of PRC2, has been correlated with enhanced self-renewal, increased tumor-initiating potential, and poor patient outcomes in a number of cancers, ovarian carcinoma among them (C. J. Chang & Hung, 2012). On the other hand, acetylation of histones at promoters of pluripotency genes promotes CSC maintenance, whereas histone deacetylases (HDACs) repress tumor suppressor activity and are frequently linked to therapy resistance (Haberland et al., 2009).

Chromatin remodeling and plasticity

ATP-dependent remodeling complexes provide another dimension of control by modulating chromatin accessibility at regulatory regions important for CSC identity. Mutations or functional alterations in SWI/SNF family members can weaken differentiation programs while encouraging lineage plasticity. This remodeling capacity supports the ability of CSCs to shift between stem-like and more differentiated states, depending on cues from the tumor environment or therapeutic stress (Wainwright & Scaffidi, 2017).

CSC resistance phenotypes

Collectively, these layers of regulation equip CSCs with a broad set of survival strategies: they can avoid apoptosis, remain dormant in a quiescent state, rewire metabolic programs, and repair DNA more efficiently than the bulk tumor cell population. These properties underpin the ability of CSCs to withstand conventional therapies and explain their central role in recurrence and disease persistence (Shibue & Weinberg, 2017).

In summary, epigenetic reprogramming is not only characteristic of CSC biology but also a critical driver of resistance to therapy. The reversible nature of epigenetic modifications has therefore attracted considerable interest as a therapeutic target, with the hope that disrupting these regulatory systems could impair CSC maintenance and improve long-term outcomes (Flavahan et al., 2017).

1.4.3 CRISPR-Based Functional Screens in Epigenetic Discovery

Unbiased functional genomics approaches have greatly expanded our ability to dissect the complexities of cancer biology. Among these, CRISPR/Cas9-based screening has emerged as

one of the most powerful strategies to identify essential genes and pathways. Unlike candidate-driven experiments, genome-wide or pathway-focused CRISPR libraries enable systematic interrogation of gene function across thousands of loci at once by introducing targeted loss-of-function perturbations in a given cellular model (Shalem et al., 2014) (T. Wang et al., 2014).

Epigenetic regulators as screening targets

Epigenetic regulators lend themselves particularly well to these kinds of functional screens. Because of their broad impact on transcriptional networks, they often represent critical nodes that support tumor survival, differentiation programs, and resistance mechanisms. Indeed, CRISPR-based studies have repeatedly pointed to DNA methyltransferases (DNMTs), histone-modifying enzymes such as EZH2 (the catalytic subunit of PRC2), and ATP-dependent chromatin remodelers as being indispensable for CSC maintenance and for sustaining tumor growth (Shi et al., 2015). In addition, screening efforts frequently reveal synthetic lethal interactions—for instance, the dependence of EZH2 activity in tumors harboring mutations in SWI/SNF components—illustrating why these regulators are of such therapeutic interest (Kim & Roberts, 2016).

CRISPR screens in CSC-enriched models

When CRISPR libraries are applied in settings that enrich for CSCs, they can uncover dependencies that would otherwise remain hidden in bulk tumor cell populations. Sphere-formation assays and 3D culture models, for example, generate contexts where stemness-associated requirements become much more apparent than in conventional two-dimensional cultures. Using such conditions, CRISPR-based screens have identified DNA damage repair factors, polycomb proteins, and chromatin remodelers as crucial for preserving CSC features and tumor-initiating capacity (B. Wang et al., 2019) (Toledo et al., 2015).

Advantages over earlier approaches

Compared to RNAi knockdown methods, CRISPR screening offers clear advantages. RNAi approaches often suffered from incomplete silencing and off-target effects, which clouded interpretation. In contrast, CRISPR generates true gene knockouts, producing stronger signals

and a higher level of reliability in identifying essential regulators. Beyond this, pooled CRISPR screens are scalable, making them suitable for unbiased discovery even in complex culture models.

Application in this thesis

In the present work, a customized CRISPR library called EPIKOL by (Yedier-Bayram et al., 2022) designed to target epigenetic regulators was employed in both monolayer and spheroid culture systems. This approach made it possible to identify factors selectively required for CSC enrichment and maintenance. By providing an unbiased functional link between epigenetic control and ovarian CSC biology, these screens complemented transcriptomic analyses and highlighted pathways that converge on stemness and therapy resistance.

1.4.4 Epigenetics and Ovarian Cancer

Ovarian cancer, and especially its high-grade serous subtype (HGSOC), is strongly influenced by widespread epigenetic deregulation. A range of studies have shown that DNA methylation, histone modifications, and chromatin remodeling work together to promote tumor growth, therapy resistance, and the persistence of cancer stem cell (CSC) populations.

DNA methylation

Aberrant DNA methylation is one of the defining epigenetic alterations in HGSOC. Promoter hypermethylation at CpG islands frequently silences well-known tumor suppressors such as BRCA1, RASSF1A, and MLH1, while global hypomethylation destabilizes the genome and can activate oncogenes (Wei et al., 2003) (Widschwendter et al., 2004). Changes in DNA methyltransferase (DNMT) activity have also been tied to chemoresistance, and preclinical studies show that DNMT inhibitors may restore platinum sensitivity (Liang & Weisenberger, 2017). CSCs, in particular, often carry distinct methylation signatures that keep pluripotency-related transcription factors active, thereby reinforcing stemness and survival under stress.

Histone modifications and polycomb regulation

Alterations in histone marks are also commonly observed in ovarian cancer. The catalytic PRC2 subunit EZH2 is frequently overexpressed, leading to accumulation of the repressive

H3K27me3 mark. This silences differentiation pathways and promotes self-renewal programs, with high EZH2 expression correlating with poor outcomes and therapy resistance (C. J. Chang & Hung, 2012) (Yi et al., 2017). At the same time, reduced histone acetylation at tumor suppressor promoters contributes to silencing, while HDAC overexpression drives proliferation and stem-like states. Notably, treatment with HDAC inhibitors has been shown to reduce CSC features and can enhance the effects of chemotherapy (Takai & Narahara, 2010).

Chromatin remodeling

Defects in chromatin remodeling complexes have also been described in ovarian tumors. Loss-of-function mutations or functional alterations in SWI/SNF components, which are relatively frequent in gynecologic cancers, make cells dependent on EZH2 activity, creating synthetic lethal vulnerabilities (Wilson & Roberts, 2011) (Kim & Roberts, 2016). Such remodeling changes appear to enhance cellular plasticity and support CSC maintenance, allowing tumor cells to shift between states depending on environmental or therapeutic pressures.

CSC persistence and resistance

In HGSOC, epigenetic deregulation is closely connected to CSC survival and therapy resistance. Epigenetic silencing of apoptotic genes, activation of DNA repair pathways, and reprogramming of cell-cycle regulators collectively allow CSCs to tolerate genotoxic stress and drive relapse by regenerating the tumor after therapy. This interplay between epigenetic plasticity and CSC biology helps explain the high recurrence rate of HGSOC and underscores why epigenetic regulators are attractive therapeutic targets.

Altogether, these findings demonstrate that ovarian cancer is not shaped by genetics alone, but also by a complex and dynamic epigenetic layer. By maintaining CSC states, enhancing adaptability, and enabling drug resistance, epigenetic regulators play a central role in disease progression. Understanding these processes is key to designing effective therapies that address not only the genetic mutations but also the epigenetic circuits sustaining CSCs in HGSOC.

1.5 Crosstalk between Post-transcriptional and Epigenetic Regulators

Recent studies have emphasized that epigenetic mechanisms including RNA-level regulation, rarely function in isolation. Instead, they operate as interconnected layers of gene regulation that reinforce one another to shape cancer cell fate. Epigenetic regulators, such as histone modifiers and chromatin remodelers, influence the transcription of RNA-modifying enzymes and non-coding RNAs, while epitranscriptomic marks such as m^{6}A can modulate the stability and translation of transcripts encoding chromatin regulators. This bidirectional interplay creates feedback loops that sustain malignant transcriptional programs and provide tumor cells with rapid adaptability under stress conditions. In ovarian cancer, such crosstalk is likely to underpin the persistence of CSC populations, as both epigenetic and RNA-based regulators converge on networks controlling stemness, plasticity, and therapeutic resistance (Kan et al., 2022).

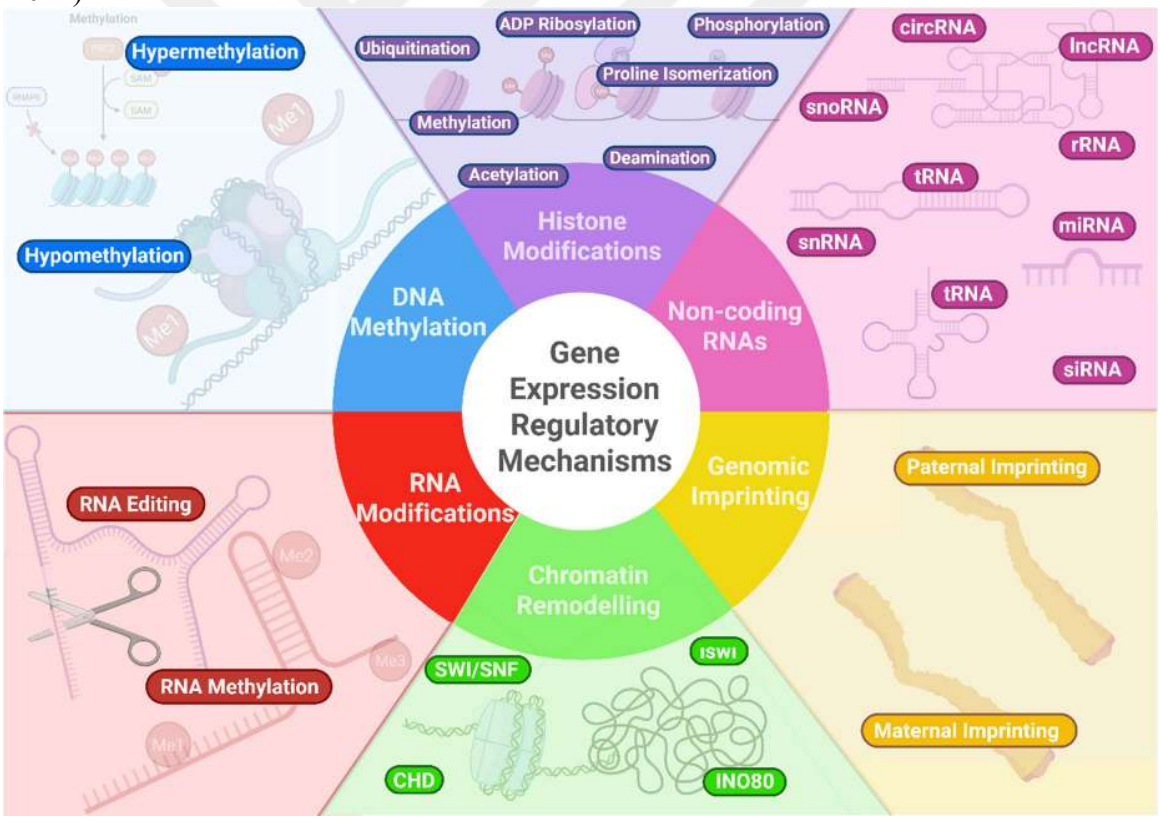

Figure 1.5: *Summary of Mechanisms Regulating Gene Expression.* Figure represents the mentioned ovarian cancer epigenetic and post-transcriptional regulations combined. Adapted from (Xie et al., 2021)

1.6 Rationale and Scope of the Thesis

1.6.1 Knowledge Gaps in Ovarian Cancer Stem Cell Biology

High-grade serous ovarian carcinoma (HGSOC) remains the most lethal gynecologic malignancy due to late diagnosis, frequent relapse, and the near-universal emergence of chemoresistance. Cancer stem-like cells (CSCs/OCSCs) are increasingly implicated in these features. Despite advances in marker discovery and phenotypic characterization, key gaps persist:

- *Modeling limitations:* Conventional 2D culture lacks the 3D architecture, microenvironmental cues, and spheroid biology relevant to OCSCs in ascites. Improved in vitro models are required to study OCSC enrichment and therapeutic vulnerabilities.
- *Incomplete view of post-transcriptional regulation:* While miRNAs, 3′UTR isoform selection via APA, and RNA regulatory networks are shown to influence CSC traits in different cancer types , their coordinated contributions to OCSCs and HGSOC progression and therapy response remain underexplored.
- *Unmapped epigenetic dependencies:* Epigenetic reprogramming is a hallmark of CSC biology, yet systematic functional studies that identify which chromatin regulators are essential for OCSC maintenance are limited.

1.6.2 Aims and Experimental Strategy

To address these gaps, this thesis implements an integrative strategy that combines physiologically relevant 3D culture models, transcriptome and post-transcriptional profiling (miRNA and APA), and CRISPR-based functional genomics.

Overall Aim. To identify actionable regulators that sustain OCSC phenotypes across chromatin and post-transcriptional layers in 3D models of HGSOC.

Central Hypothesis. OCSC traits are stabilized by the convergent control of chromatin-based programs and post-transcriptional outputs (miRNA targeting and APA-mediated 3′UTR

remodeling); perturbing nodal epigenetic factors will elicit predictable changes in isoform usage and gene expression that are measurable in 3D systems.

Specific Aims

Establish and benchmark 3D culture systems for OCSC enrichment. Systematically evaluate ultra-low-attachment (ULA) spheroids and GelMA-based photomasked hydrogels in OVCAR-3 and OVSAHO, alongside patient-derived samples, to define a robust and translationally relevant OCSC model framework.

Dissect post-transcriptional regulation of OCSC traits. Profile miRNA and mRNA expression and quantify APA (QAPA-based 3′UTR isoform usage) in 3D conditions; assess how sustained miRNA mimic exposure reshapes isoform usage and transcript abundance, and explore predicted interactions with APA-impacted genes and RBPs.

Identify essential epigenetic regulators via CRISPR screening. Perform a targeted loss-of-function screen of chromatin regulators in monolayer vs spheroid settings to uncover dependencies that contribute to OCSC maintenance, and integrate findings with Aim 2 to prioritize convergent regulatory nodes.

1.6.3 Outline of Thesis Structure

The thesis is organized into three experimental parts aligned with these aims:

Part I: Modeling OCSCs in 3D. Development and benchmarking of ULA vs GelMA systems and validation with patient-derived cells.

Part II: Post-transcriptional regulation of OCSC traits. miRNA/mRNA profiling and APA dynamics in 3D, including the impact of prolonged miRNA exposure on 3′UTR isoform usage.

Part III: Epigenetic vulnerabilities revealed by CRISPR screening. Systematic interrogation of chromatin regulators across monolayer and spheroid conditions, with integrative analysis across Parts I–II to highlight actionable nodes.

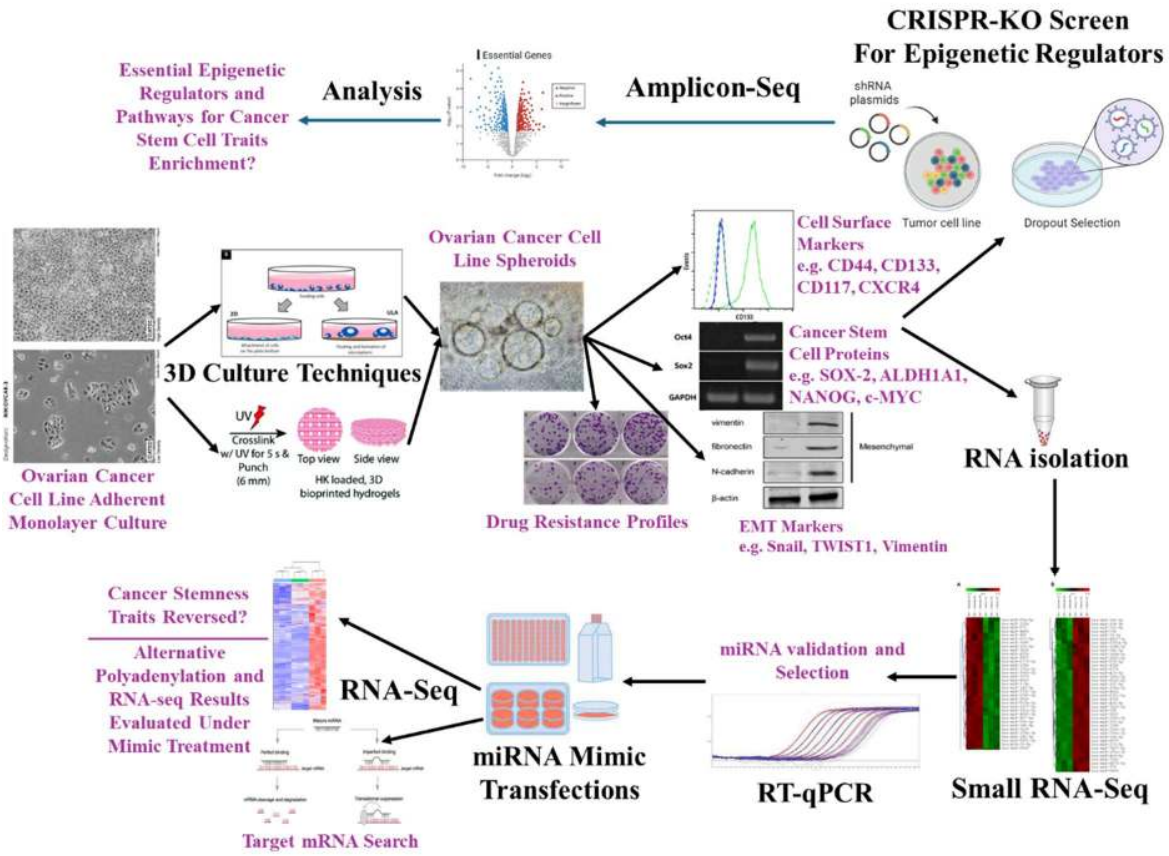

Figure 1.6: *Summary of Experimental Strategies Applied in This Thesis*. Methodologies are written in bold black and legends are written in purple.

CHAPTER 2

2. MATERIALS AND METHODS

2.1 Materials

2.1.1 Cell lines & biological samples

- OVCAR-3 (ATCC)
- OVSAHO (ATCC)
- Primary HGSOC tumor tissues (with IRB approval 2019.257.IRB2.079)
- Patient ascites samples (same IRB as above)
- HEK293T (ATCC) (for lentiviral production)

2.1.2 Basal media & supplements

- DMEM/F12 (Biowest L0095-500 or Multicell 319-094 or Equivalent)
- HBSS (1× and 10×; Gibco or Equivalent, L0611-500)
- DPBS / PBS (1×) (Biowest L0615-500 or Equivalent)
- Amphotericin B (fungizone), 0.1% in media where noted (Biowest or Equivalent)
- Fetal Bovine Serum (FBS) (Biowest S1810-500 or Equivalent)
- Penicillin/Streptomycin (P/S) (100×) (Biowest L0022-100 or Equivalent)
- L-glutamine (200 mM stock) (Biowest X0550-100 or Equivalent)

2.1.3 Spheroid/3D culture supplements

- EGF (5 ng/mL working) (Sigma, SRP3027-500UG)
- FGF (10 ng/mL working) (Sigma, F3685-25UG)

- Insulin (5 µg/mL working) (Sigma, I9278-5ML)
- Ultra-Low Attachment (ULA) plates (Costar® 6-well Clear Flat Bottom Ultra-Low Attachment (CLS3471))
- Gelatin-Methacrylate (GelMA)
    - Bovine skin gelatin (Sigma)
    - Methacrylic anhydride (MA) (Sigma)
    - Carbonate–bicarbonate buffer (0.25 M, pH 9)
    - Dialysis tubing (12–14 kDa MWCO)
    - Lyophilizer (for GelMA prep)
    - Irgacure 2959 (2-Hydroxy-4′-(2-hydroxyethoxy)-2-methylpropiophenone), photoinitiator; 1% (w/v) in DPBS
    - UV curing system (OmniCure S2000 or equivalent; 6.25 W/cm²)
    - Custom photomasks (designed in CorelDRAW; printed locally)
    - Glass slides and 0.3 mm spacers
    - Glass-bottom dishes (for imaging)

2.1.4 Enzymes & dissociation reagents

- Trypsin-EDTA 0.25% (for routine passaging) (Multicell, 325-043)
- Trypsin-EDTA 0.05% (gentler dissociation) (Multicell, 325-052)
- Accutase (Biowest, L0950-100)
- Collagenase/Dispase (Roche; 3 mg/mL total; ~2.4 U/mL dispase + 0.3 U/mL collagenase)

- Collagenase Type II (Gibco; 1 mg/mL for GelMA digestion)
- Rotor–stator homogenizer (for tissues)

2.1.5 Fixatives, permeabilization & blocking

- Paraformaldehyde (PFA) 4% (fixation) (Electron Microscopy Sciences)
- Triton X-100 (0.1% in PBS, permeabilization) (Sigma)
- SuperBlock (Thermo) or equivalent blocking buffer
- CellO-IF (Cellorama) blocking/staining solution
- VectaShield with DAPI (mounting medium with nuclear stain)

2.1.6 Antibodies (IF / Flow / WB)

- α-Tubulin (rabbit mAb) (Cell Signaling (11H10) Rabbit mAb #2125; IF 1:50)
- β-Actin (rabbit mAb) (Cell Signaling β-Actin (13E5) Rabbit mAb #4970; Western: 1:1000)
- Vinculin (mouse mAb) (Cell Signaling (E1E9V) XP® Rabbit mAb; Western: 1:1000)
- Calnexin (rabbit mAb) (Cell Signaling (C5C9) Rabbit mAb; Western: 1:1000)
- GAPDH (rabbit mAb) (Cell Signaling (14C10) Rabbit mAb; Western: 1:1000)
- SOX-2 (rabbit mAb) (Cell Signaling (D6D9) XP® Rabbit mAb #3579; Western: 1:500)
- OCT-4 (rabbit mAb) (Cell Signaling (V241); Western: 1:500)
- NANOG (rabbit mAb) (Cell Signaling (D73G4) XP® Rabbit mAb #4903; Western: 1:500)
- ALDH1A1 (rabbit mAb) (Abcam (ab9883); Western: 1:500)

- c-MYC (rabbit mAb) (Cell Signaling (D84C12) Rabbit mAb; Western: 1:500)
- Slug (rabbit mAb) (Cell Signaling (C19G7) Rabbit mAb #9585; Western: 1:500)
- Snail (rabbit mAb) (Cell Signaling (C15D3) Rabbit mAb #3879; Western: 1:500)
- TWIST1 (rabbit mAb) (Cell Signaling (E5G9Y) Rabbit mAb #90445; Western: 1:250)
- Vimentin (rabbit mAb) (Cell Signaling (D21H3) XP® Rabbit mAb #5741; Western: 1:500)
- Cyclin D1 (rabbit mAb) (Cell Signaling (92G2) Rabbit mAb; Western: 1:500)
- Alexa Fluor 488 anti-rabbit/anti-mouse secondary (IF 1:50–1:200) (Invitrogen)
- Alexa Fluor 594 anti-rabbit/anti-mouse secondary (IF 1:50-1:200) (Invitrogen)
- CD133-PE (conjugated) (Miltenyi Biotec 130-110-962/CD133-1-PE/100tests200ul/Miltenyi 130-112-195/CD133-2-PE/100tests200ul/Miltenyi; IF/flow, 1:50)
- CD117-PE (conjugated) (Miltenyi Biotec 130-116-730; IF/flow, 1:50)
- CD44-FITC (conjugated) (Miltenyi Biotec 130-113-903; IF/flow, 1:50)
- CXCR4-FITC (conjugated) (Miltenyi Biotec 130-117-519; IF/flow, 1:50)
- (WB) HRP-conjugated secondary antibodies (1:2000) (Abcam)
- Blotting-grade blocker (3-5% milk in TBST) and BSA (for blocking and antibody diluent)

2.1.7 Western blot reagents & membranes

- RIPA lysis buffer (+ protease inhibitor 10% v/v and phosphatase inhibitor 1% v/v cocktails)

- BCA Protein Assay Kit (Thermo, e.g., #23225)
- Laemmli sample buffer (4×) + β-mercaptoethanol (Bio-Rad)
- SDS-PAGE gels (4–15% gradient, 12-well, 10-well; Bio-Rad)
- PVDF membranes (Bio-Rad)
- TBST (TBS + 0.1–0.2% Tween-20) (E-Lab-Sciences, Sigma)
- Chemiluminescent substrate (Immobilon Forte, Millipore /Thermo ECL/ Thermo Femto)
- Transfer system (semi-dry) (Bio-Rad)

2.1.8 Flow cytometry

- CytoFLEX flow cytometer (Beckman Coulter)
- FACS buffer: PBS + 1% FBS + 2 mM EDTA
- Conjugated antibodies (Miltenyi Biotec; as above)
- 4% PFA (fixation)

2.1.9 Nucleic acid extraction & cDNA/qPCR

- NucleoSpin RNA kit (Macherey-Nagel)
- NucleoSpin Tissue Kit (Macherey-Nagel) (For CRISPR-KO Screen library prep)
- Gel and PCR Clean-up Kit (Macherey-Nagel) (For CRISPR-KO Screen library prep)
- Quick-RNA Miniprep Plus kit (Zymo Research) – for tissues and miRNAs
- TRIzol reagent (Qiagen or Invitrogen) – for GelMA-released cells
- Chloroform

- DNA/RNA Shield™ (Zymo)
- RNAlater (Invitrogen)
- M-MLV Reverse Transcriptase (Promega)
- Phusion Polymerase Kit (NEB)
- Q5 High Fidelity Polymerase Kit (NEB)
- SYBR Green qPCR Master Mix (Roche)
- miRNA stem-loop RT primers (for hsa-miR-548ah-3p, hsa-miR-146a-5p, hsa-miR-151a-3p, hsa-miR-619-5p, hsa-miR-146b-5p, hsa-let-7b-5p) (Macrogen)
- U6 snoRNA primers (endogenous control) (Macrogen)
- Nuclease-free water, qPCR plates, optical seals

2.1.10 Transfection & treatments

- Lipofectamine 3000 (Invitrogen)
- miRNA mimics (miR-548ah-3p cat.no: 4464067/ assay ID: MC22814; w/ negative control)
- Opti-MEM (Gibco)

2.1.11 Sequencing (library prep & QC; performed by service provider)

- TruSeq Small RNA Library Kit (Illumina)*
- TruSeq Stranded mRNA Library Kit (Illumina)*
- HiSeq/NovaSeq sequencing (outsourced)
- FastQC, Cutadapt, STAR, Salmon, DESeq2, PAQR2 (software—see below)

2.1.12 CRISPR/Cas9 screening

- Cas9-Blast lentiviral vector (blasticidin resistance)
- EPI-KOL custom sgRNA library (epigenetic regulators)
- GFP reporter vector (for Cas9 activity check)
- PEI (polyethylenimine) transfection reagent (for HEK293T)
- PEG solution (for viral precipitation/concentration)
- 0.45 μm filters
- Blasticidin and Puromycin (selection antibiotics)
- Genomic DNA extraction kit (high-molecular-weight gDNA from large cell pellets)
- PCR reagents for sgRNA cassette amplification (high-fidelity polymerase, primers)
- Agarose, DNA ladders, gel extraction kit
- NGS service for sgRNA amplicons
- MAGeCK / MAGeCK-Flute (analysis software)

2.1.13 Viability & migration assays

- TCA 10% (v/v) for fixation (ice-cold)
- Cold Methanol
- Sulforhodamine B (SRB) 0.4% (m/v) in 1% acetic acid
- Crystal Violet
- Hoechst 33342 (Thermo)
- Acetic acid 1% (wash)
- Tris base 10 mM (SRB elution)

- 96-well plates
- Phase-contrast microscope
- Fluorescent Microscope
- Pipette tips
- Drugs used in assays:
    - Olaparib (Selleckchem)
    - Niraparib (Selleckchem)
    - Carboplatin (Clinical Grade)
    - Cisplatin (Selleckchem)
    - Paclitaxel (Selleckchem)
    - Doxorubicin (Selleckchem)
    - Sunitinib (Selleckchem)

2.1.14 General buffers & chemicals

- Carbonate–bicarbonate buffer (0.25 M, pH 9; for GelMA synthesis)
- DPBS/PBS (1×)
- EDTA (for PBS/EDTA FACS buffer)
- Ethanol, ddH_2O
- NaCl, Tris, Tween-20, BSA, Milk powder

2.1.15 Plasticware & consumables

- T-flasks (T-25, T-75)

- 6-well ULA plates (Corning)
- 96-well plates
- 100 mm dishes
- 15/50 mL conical tubes
- 1.5/2 mL microcentrifuge tubes
- Glass slides / coverslips, spacers (0.3 mm)
- Trans-well Inserts (0.8 μm, 12-Well)
- Serological pipettes, filter tips

2.1.16 Instruments & equipment

- CO_2 incubators (37 °C, 5% CO_2)
- Biological safety cabinet (BSC)
- Benchtop centrifuges (with 15/50 mL and microcentrifuge rotors; capable up to 13,000 × g)
- Lyophilizer (for GelMA)
- UV curing lamp/system (OmniCure S2000 or equivalent)
- Brightfield microscope
- Leica confocal microscope (10×, 20×, 63× objectives; 405/488/594 nm lasers; PMT & HyD detectors)
- Plate reader (515 nm capability for SRB)
- Western blot system (power supply, gel apparatus, semi-dry transfer)
- Odyssey Fc (LI-COR) or equivalent chemiluminescence imager

- Flow cytometer (CytoFLEX, Beckman Coulter)
- Thermocyclers (PCR & qPCR LightCycler 480)
- Freezers (–20 °C, –80 °C)
- Water bath / heating blocks

2.1.17 Software & analysis

- Microscopy: Leica software
- Flow cytometry: CytoFLEX software
- Image analysis: ImageJ
- Statistics/plots: GraphPad Prism, RStudio (ggplot2, pheatmap)
- RNA-seq: FastQC, Cutadapt, STAR, Salmon, DESeq2
- APA: PAQR2 (plus custom scripts)
- CRISPR screen: MAGeCK, MAGeCK-Flute
- HPC/remote: MobaXterm or Linux Based PC setup

2.2 Methods

2.2.1 Cell Culture and Patient-Derived Samples

2.2.1.1 Cell lines and conventional 2D culture

Human ovarian carcinoma cell lines OVCAR-3 and OVSAHO (ATCC, USA) were maintained in DMEM/F12 (Biowest) supplemented with 10% fetal bovine serum (FBS; Sigma), 1% penicillin–streptomycin (Biowest), and 1% L-glutamine (Biowest). Cells were cultured in T-75 flasks (Corning) at 37 °C, 5% CO_2 in a humidified incubator and passaged at approximately 70% confluence using 0.25% trypsin–EDTA (Multicell). Routine

mycoplasma testing was performed; experiments were conducted within consistent passage ranges.

2.2.1.2 Ultra-low attachment (ULA) 3D cultures

Spheroids were generated from OVCAR-3, OVSAHO, or primary ovarian cancer cells after enzymatic dissociation to single cells (trypsinization followed by gentle trituration). (1–3) × 10^5 cells were seeded per well in 6-well ULA plates (Corning) in 3–6 mL "spheroid medium" (DMEM/F12 [Multicell] containing 0.5% FBS, 1% penicillin–streptomycin, 1% L-glutamine, 10 ng/mL FGF [Sigma], 10 ng/mL EGF [Sigma], and 5 µg/mL insulin [Sigma]). Cultures were maintained at 37 °C, 5% CO_2. Spheroid aggregates became visible by day 14; thereafter, half-medium changes were performed by gently adding 3–5 mL fresh spheroid medium without disturbing aggregates. Between day 14–28, mature spheroids exhibited compartmentalization (OVCAR-3) and cancer stem-like cell (CSC) enrichment. For passaging, spheroids were collected by centrifugation (200 × g, 2 min), resuspended, and, if required, partially dissociated with Accutase (Innovative Cell Technologies) or 0.05% trypsin–EDTA. Spheroids were passaged up to three times; later generations (P2–P3) typically formed larger spheroids more rapidly, whereas P4–P5 cultures accumulated more debris.

2.2.1.3 Gelatin-methacrylate (GelMA) hydrogel cultures with photomasking

GelMA was prepared as previously described. Briefly, 10 g gelatin (bovine skin; Sigma) was dissolved in 100 mL 0.25 M carbonate–bicarbonate buffer (pH 9) at 50 °C. Methacrylic anhydride (Sigma) was added dropwise at 50 °C with stirring; after 1 h, the reaction mixture was neutralized to pH 7.4, dialyzed against distilled water for 7 days at 40 °C (12–14 kDa cutoff), lyophilized, and stored at –20 °C. For encapsulation, lyophilized GelMA (ZetaMatrix) was dissolved to 5% (w/v) in DPBS containing 1% (w/v) Irgacure 2959 (Sigma) and warmed to 37 °C with vortexing until fully dissolved. Cell suspensions were generated by trypsinization, pelleted (300 × g, 5 min), and resuspended in 5% GelMA to 4 × 10^6 cells/mL. 100 µL aliquots were cast between glass slides separated by 0.3 mm spacers. Photopatterning was performed by overlaying custom photomasks (CorelDRAW design, printed in İzmir, Turkey) and irradiating with UV (6.25 W/cm², 50 s) using an OmniCure S2000 curing system.

Crosslinked hydrogels were rinsed in DPBS and transferred to glass-bottom dishes containing spheroid medium, then maintained at 37 °C, 5% CO_2 for 14 days with periodic bright-field imaging.

2.2.1.4 Isolation of epithelial cells from primary tumor tissues and ascites

High-grade serous ovarian carcinoma (HGSOC) tumor tissues were collected intraoperatively into ice-cold DPBS or HBSS. Tissues were minced with sterile scalpels and digested in 3 mg/mL Collagenase/Dispase (Roche) at 37 °C for 1 h with gentle agitation, filtered through 100 µm strainers, washed with warm DPBS, and centrifuged (400 × g, 5 min). Pellets were resuspended in DMEM/F12 supplemented with 20% FBS, 1% penicillin–streptomycin, and 0.1% Amphotericin B and plated in 100 mm dishes; medium was refreshed every 4–5 days until ~80% confluence for downstream use.

Ascites fluid was processed within 1 h of collection. Samples were centrifuged (500 × g, 5 min), washed 2–3× with HBSS to remove erythrocytes and debris, and resuspended in complete DMEM/F12 (20% FBS, 1% penicillin–streptomycin, 0.1% Amphotericin B), then plated in T-25 flasks at 37 °C, 5% CO_2. Patient-derived materials were collected with written informed consent and used under Research Ethics Committee approval 2019.257.IRB2.079.

2.2.2 CSC Characterization

2.2.2.1 Immunofluorescence staining of spheroids

ULA spheroids. Spheroids were pelleted (200 × g), fixed in 4% PFA for 20 min at 4 °C, washed in PBS, and incubated in CellO-IF blocking/permeabilization solution (Cellorama). Primary antibody anti-α-tubulin (Cell Signaling; 1:50) was applied overnight at 4 °C, followed by Alexa Fluor 488-conjugated anti-rabbit secondary (1:50, 2 h, RT). CD133-PE (Miltenyi; 1:50) was incubated for 20 min at 4 °C. Nuclei were counterstained with DAPI (VectaShield mounting medium). Imaging was performed on a Leica confocal microscope using 10× and 63× objectives.

GelMA constructs. Hydrogels were washed, fixed in 4% PFA (1 h, 4 °C), permeabilized with 0.1% Triton X-100, blocked with SuperBlock (Thermo), and stained as above (α-tubulin →

Alexa 488; CD133-PE; DAPI). Images were acquired on Leica confocal systems using 10× and 20× objectives.

2.2.2.2 Flow cytometry for cell-surface markers

Cells were dissociated to single-cell suspensions, washed in PBS containing 1% FBS and 2 mM EDTA, and fixed in 4% PFA. Blocking was performed with SuperBlock or 5% BSA in PBS. Conjugated antibodies (Miltenyi; 2 µL in 100 µL PBS/1% FBS) were incubated for 10 min at 4 °C, followed by three PBS washes. Data were acquired on a CytoFLEX (Beckman Coulter); standard gating (singlets, live cells) and fluorescence-minus-one controls were applied where appropriate.

2.2.2.3 Western blotting

Cell pellets (≥ 5×10^5 cells) were lysed in RIPA buffer (BioRad) supplemented with protease inhibitors (10%) and phosphatase inhibitors (1%) (Thermo). Lysates were incubated on ice for 45 min with intermittent vortexing and clarified by centrifugation (13,000 × g, 15 min, 4 °C). Protein concentration was determined by BCA assay (Thermo). Equal protein amounts (20-30 µg) were denatured in Laemmli buffer (BioRad) with β-mercaptoethanol (95 °C, 7 min), separated on 4–15% gradient (10-12 or 15 well gels) SDS-PAGE (Bio-Rad), and transferred to PVDF membranes (Bio-Rad) with semi-dry transfer system of BioRad in Standard MW transfer (30 minutes, 25V, varying Ampers). Membranes were blocked in 5% milk/TBST (overnight, 4 °C), incubated with primary antibodies (1:500–1:1000, 1 h, RT or overnight at 4 °C), washed, and probed with HRP-conjugated secondary antibodies (1:2000, 1 h, RT). Signal was developed with ECL/Femto/Immobilon Forte substrates (Thermo, Millipore) and imaged on a LI-COR Odyssey Fc.

2.2.3 RNA Isolation and Molecular Analyses

2.2.3.1 RNA extraction from cell lines and spheroids

For 2D cultures, cells were harvested by 0.25% trypsin–EDTA (Multicell) and pelleted (300 × g, 5 min). ULA spheroids were collected directly, pelleted (300 × g, 5 min), and washed in PBS. Pellets were stored at –80 °C until extraction. Total RNA was isolated using NucleoSpin

RNA (Macherey-Nagel) or Zymo Quick-RNA Miniprep with on-column DNase treatment, following the manufacturer's instructions. RNA concentration and purity were assessed by NanoDrop (Thermo Fisher).

2.2.3.2 RNA extraction from GelMA encapsulates

GelMA constructs were digested with Collagenase II (Gibco; 1 mg/mL, 15 min, 37 °C) to release cells. After centrifugation (300 × g, 5 min), pellets were resuspended in TRIzol (Qiagen) and stored overnight at –20 °C. Chloroform (200 µL) was added, samples were centrifuged (12,000 × g, 15 min, 4 °C), and the aqueous phase was processed using NucleoSpin RNA for column clean-up. RNA concentration and integrity were evaluated by NanoDrop and agarose gel electrophoresis.

2.2.3.3 RNA extraction from patient tissues

RNAlater-preserved tissues (Invitrogen) were transferred to 2 mL tubes and homogenized in 300 µL DNA/RNA Shield™ (Zymo Research) using a rotor–stator homogenizer (15–20 s pulses). Lysates were clarified (12,000 × g, 10 min, 4 °C), and total RNA was purified with Zymo Quick-RNA Miniprep Plus according to the manufacturer's protocol.

2.2.3.4 cDNA synthesis and quantitative PCR (qPCR)

For mRNA targets, 500 ng total RNA was reverse-transcribed using M-MLV reverse transcriptase (Promega) with gene-specific primers or random hexamers (37 °C, 90 min; inactivation 65 °C, 5 min). For miRNAs (e.g., hsa-miR-548ah-3p, hsa-miR-146b-5p, hsa-let-7b-5p), stem-loop RT primers were used; U6 snoRNA served as endogenous control. cDNA was stored at –20 °C. qPCR reactions (20 µL) contained 10 µL SYBR Green Master Mix (Roche), 2 µL cDNA, 1 µL primer mix, and nuclease-free water. Amplification was performed on a LightCycler 480 (Roche) with 50 cycles followed by a melt curve (start 65 °C). Relative expression was analyzed by the ΔΔCt method with appropriate calibrators and biological replicate averaging.

2.2.3.5 miRNA reverse transcription (stem-loop cDNA)

Total RNA from cell lines, spheroids, or primary samples was reverse-transcribed using stem-loop RT primers specific to each mature miRNA. Unless noted otherwise, 100–500 ng total RNA served as input per reaction. Reverse transcription was performed with M-MLV Reverse Transcriptase (Promega) according to the manufacturer's instructions, with the following composition for a 15 µL reaction:

- Total RNA in nuclease-free water to 7.5 µL
- 5× First-Strand Buffer, 3.0 µL (1× final)
- dNTP mix (10 mM each), 0.5 µL (≈0.33 mM each final)
- RNase inhibitor (40 U/µL), 0.5 µL (20 U final)
- Stem-loop RT primer (1 µM), 1.0 µL (target-specific; sequences listed in Table 2.1)
- M-MLV Reverse Transcriptase (200 U/µL), 0.75 µL (150 U final)
- DTT (0.1 M), add to 1–5 mM final (per kit; adjust water accordingly)

Thermal program (adapted from the canonical stem-loop protocol): 16 °C 30 min, 42 °C 30 min, 85 °C 5 min, hold 4 °C. No-template (NTC) and no-RT controls were included for each primer set. For targets spanning multiple miRNAs, separate RT reactions were performed per miRNA. Resulting cDNA was diluted 1:5 in nuclease-free water before qPCR unless noted.

Primer design. Stem-loop RT primers were designed to be complementary to the 3′ six nucleotides of the mature miRNA at the primer's 3′ end, appended to a hairpin/universal sequence that enables use of a universal reverse primer in qPCR (sequences in Table 2.1). This design enhances specificity for mature miRNAs over precursors.

2.2.3.6 miRNA quantitative PCR (qPCR; SYBR, stem-loop)

miRNA abundance was quantified by SYBR-based qPCR using a miRNA-specific forward primer and a universal reverse primer complementary to the stem-loop cDNA tail. Reactions (final volume 20 µL) contained:

- 2× SYBR Green Master Mix (Roche), 10.0 µL
- Forward primer (10 µM), 0.6 µL (0.3 µM final; miRNA-specific)
- Universal reverse primer (10 µM), 0.6 µL (0.3 µM final)
- Diluted cDNA, 2.0 µL (from Section 1.2.3.5)

- Nuclease-free water, 6.8 µL

Amplification was performed on a LightCycler 480 (Roche) with the following cycling: 95 °C 2 min (enzyme activation), then 40 cycles of 95 °C 15 s, 60 °C 60 s with single-point acquisition. A melt-curve (e.g., 65–95 °C, 0.2–0.5 °C/step) verified single-product amplification. All reactions were run in technical triplicate; U6 snRNA (RNU6-1) served as endogenous control unless otherwise specified. Relative expression was calculated by the ΔΔCt method using NC (control) spheroids as the calibrator. Primer efficiencies (90–110%) were verified on five-point dilution series, and assays failing specificity (multiple peaks) or efficiency were excluded or redesigned.

Controls and reporting. Each plate included NTC and no-RT controls for every primer pair. Assays with Ct > 35 were considered low-confidence and interpreted cautiously. Primer sequences (miRNA-specific forward, universal reverse) and stem-loop RT primers are provided in Supplementary Table [Sx], with amplicon lengths and efficiency values.

Primers List

Table 2.1: *Sequences of primers used in this thesis.*

Gene	**Forward Primer**	**Reverse Primer**
β-Actin	CACCATTGGCAATGAGCGGTTC	AGGTCTTTGCGGATGTCCACGT
SOX-2	AACCAGCGCATGGACAGTTA	GACTTGACCACCGAACCCAT
ALDH1A1	CTGTGTTCCAGGAGCCGAAT	AGCATCCATAGTACGCCACG
NANOG	TGATTTGTGGGCCTGAAGAAA	TGGTGGTAGGAAGAGTAAAG
MYC	CGTCCTCGGATTCTCTGCTC	GCTGGTGCATTTTCGGTTGT

548ah-RT-Stem-loop Primer	GTCGTATCCAGTGCAGGGTCCGAGGTATTCGCACTGGATACGACGCAAAA	
151a-RT-Stem-loop Primer	GTCGTATCCAGTGCAGGGTCCGAGGTATTCGCACTGGATACGACCCTCAA	
619-RT-Stem-loop Primer	GTCGTATCCAGTGCAGGGTCCGAGGTATTCGCACTGGAACGACGGCTCA	
6842-RT-Stem-loop Primer	GTCGTATCCAGTGCAGGGTCCGAGGTATTCGCACTGGATACGACCTGCGG	
146a-RT-Stem-loop Primer	GTCGTATCCAGTGCAGGGTCCGAGGTATTCGCACTGGATACGACAACCCA	
146b-RT-Stem-loop Primer	GTCGTATCCAGTGCAGGGTCCGAGGTATTCGCACTGGATACGACCAGCCT	
548ah-Forward	TCGCTCAAAAACTGCAGTTAC	
151a-Forward	TCGCTCTAGACTGAAGCTCC	
619-Forward	TCGCTGCTGGGATTACAGGCA	

6842-Forward	TCGCTTTGGCTGGTCTCTGCT	
146a-Forward	TCGCTTGAGAACTGAATTCCA	
146b-Forward	TCGCTTGAGAACTGAATTCCAT	
Universal Reversal Primer 3'-5'		GTGCAGGGTCCGAGGT
U6	CTCGCTTCGGCAGCACA	AACGCTTCACGAATTTGCGT
PLG_External	AATGGACTATCATATGCTTACCGTAACTTGAAAGTATTTCG	CTTTAGTTTGTATGTCTGTTGCTATTATGTCTACTATTCTTTCC
Forward_staggered_1	AATGATACGGCGACCACCGAGATCTACACTCTTTCCCTACACGACGCTCTTCCGATCTAtcttgtggaaaggacgaaacaccg	
Forward_staggered_2	AATGATACGGCGACCACCGAGATCTACACTCTTTCCCTACACGACGCTCTTCCGATCTCTtcttgtggaaaggacgaaacaccg	
Forward_staggered_3	AATGATACGGCGACCACCGAGATCTACACTCTTTCCCTACACGACGCTCTTCCGATCTGACtcttgtggaaaggacgaaacaccg	

Forward_staggered_4	AATGATACGGCGACCACCGAGATCTACACTCTTTCCCTACACGACGCTCTTCCGATCTTCGAtcttgtggaaaggacgaaacaccg
Forward_staggered_5	AATGATACGGCGACCACCGAGATCTACACTCTTTCCCTACACGACGCTCTTCCGATCTATCGCtcttgtggaaaggacgaaacaccg
Forward_staggered_6	AATGATACGGCGACCACCGAGATCTACACTCTTTCCCTACACGACGCTCTTCCGATCTGTCAGAtcttgtggaaaggacgaaacaccg
Forward_staggered_7	AATGATACGGCGACCACCGAGATCTACACTCTTTCCCTACACGACGCTCTTCCGATCTTGCATCGtcttgtggaaaggacgaaacaccg
Forward_staggered_8	AATGATACGGCGACCACCGAGATCTACACTCTTTCCCTACACGACGCTCTTCCGATCTCTACGTGAtcttgtggaaaggacgaaacaccg
Forward_staggered_9	AATGATACGGCGACCACCGAGATCTACACTCTTTCCCTACACGACGCTCTTCCGATCTACTCGTGATtcttgtggaaaggacgaaacaccg
reverse_index3	CAAGCAGAAGACGGCATACGAGATGCCTAAGTGACTGGAGTTCAGACGTGTGCTCTTCCGATCTtctactattctttcccctgcactgt
reverse_index4	CAAGCAGAAGACGGCATACGAGATTGGTCAGTGACTGGAGTTCAGACGTGTGCTCTTCCGATCTtctactattctttcccctgcactgt
reverse_index6	CAAGCAGAAGACGGCATACGAGATATTGGCGTGACTGGAGTTCAGACGTGTGCTCTTCCGATCTtctactattctttcccctgcactgt

reverse_index10	CAAGCAGAAGACGGCATACGAGATAAGCTAGTGACTGGAGTTCAGACGTGTGCTCTTCCGATCTtctactattctttcccctgcactgt
reverse_index11	CAAGCAGAAGACGGCATACGAGATGTAGCCGTGACTGGAGTTCAGACGTGTGCTCTTCCGATCTtctactattctttcccctgcactgt
reverse_index12	CAAGCAGAAGACGGCATACGAGATTACAAGGTGACTGGAGTTCAGACGTGTGCTCTTCCGATCTtctactattctttcccctgcactgt
reverse_index13	CAAGCAGAAGACGGCATACGAGATTTGACTGTGACTGGAGTTCAGACGTGTGCTCTTCCGATCTtctactattctttcccctgcactgt
reverse_index16	CAAGCAGAAGACGGCATACGAGATGGACGGGTGACTGGAGTTCAGACGTGTGCTCTTCCGATCTtctactattctttcccctgcactgt
reverse_index17	CAAGCAGAAGACGGCATACGAGATCTCTACGTGACTGGAGTTCAGACGTGTGCTCTTCCGATCTtctactattctttcccctgcactgt

2.2.3 Functional Assays

2.2.3.1 Cell Viability Assay (NCI-SRB)

Growth inhibition was quantified by the sulforhodamine B (SRB) assay, which measures total cellular protein content after TCA fixation.

Cells were seeded in 96-well flat-bottom plates at 3,000 cells/well in 100 µL complete medium (monolayer) or as single-cell suspensions derived from dissociated spheroids. After 48 h attachment/equilibration, compounds were added in serial dilutions (typically 8–10 concentrations, 1:3 dilution series) in 100 µL to a final volume of 200 µL per well; vehicle controls received the corresponding solvent. Treatments were maintained for 72 h (standard) or 120 h (5 days) for Olaparib.

At endpoint, plates were cooled on ice and fixed by gently adding 50 µL of 50% (w/v) TCA to reach 10% final (v/v) and incubated at 4 °C for 60 min. Plates were washed 5× with deionized water, air-dried, and stained with 0.4% SRB in 1% acetic acid (100 µL/well, 30

min, dark). Excess dye was removed with 1% acetic acid washes (4–5×), plates were air-dried, and bound dye was solubilized with 10 mM Tris base (pH ~10.5) (100 µL/well, 10–15 min, gentle shaking). Absorbance was recorded at 515 nm (BioTek microplate reader); 650–690 nm background may be subtracted if available. Each plate contained blank wells (no cells) for background correction and vehicle wells for normalization. Percent viability was computed as:

$$\%viability = 100 \times ((Atreat - Ablank))/((Aveh - Ablank))$$

Where time-zero reference plates were included, GI% was calculated as:

$$GI\% = 100 \times (Atreat - At0)/((Aveh - At0))$$

values were obtained by nonlinear regression (four-parameter logistic). All conditions were run in technical triplicate and n = 3 biological replicates.

Notes/QC: Avoid edge effects by reserving outer wells for PBS/medium. Verify linearity of SRB signal with cell number in a pilot 96-well titration.

2.2.3.2 Colony Formation Assay

Monolayer cells or dissociated spheroid cells were seeded at 500 cells/well in 12-well plates (final volume 1.0–1.5 mL/well) in complete medium. Plates were incubated under standard conditions for 10–14 days without disturbance, with gentle medium refresh on day 5–7 if necessary. Colonies were fixed with 100% methanol (10 min, RT), stained with 0.5% crystal violet in 25% methanol (10–20 min, RT), rinsed with tap water, and air-dried. Wells were imaged on a flatbed scanner or bright-field microscope. Colonies containing ≥50 cells were counted using ImageJ (thresholding + particle analysis with a size cutoff). Data are reported as mean ± SD from n = 3 biological replicates.

Notes/QC. Ensure single-cell suspensions at seeding; gently pre-wet wells to improve uniform distribution.

2.2.3.3 Migration and Invasion Assays

Assays used polycarbonate transwell inserts for 12-well plates (pore size 8 µm, Sigma-Aldrich). For migration, uncoated inserts were used. For invasion, inserts were pre-coated with Cultrex (or equivalent basement membrane extract).

Monolayer or spheroid cultures were dissociated to single cells, filtered through 40 µm, and resuspended in spheroid medium (or serum-reduced medium, as indicated). For invasion assays, 10–50 µL Cultrex per insert was spread to form a uniform gel layer (manufacturer's instructions), polymerized at 37 °C for 30–60 min, and equilibrated with warm medium.

For each insert, 1,000 cells in 500 µL were added to the upper chamber. The lower chamber received 1.0 mL medium. (Where a chemoattractant gradient was applied, upper chamber contained 0–0.5% FBS and lower chamber 10% FBS; otherwise, the same spheroid medium was used in both chambers.) Migration was assessed after 7 days; invasion after 14 days. (In some pilot runs, earlier time points were monitored to avoid overgrowth.) At endpoint, non-migrated/non-invaded cells were removed from the upper surface with a cotton swab.

Inserts were fixed by immersion in cold methanol (10 min, RT) and washed 3× with cold sterile PBS. Nuclei on the lower membrane surface were stained with Hoechst 33342 (1 µg/mL in PBS) for 30–60 min at RT in the dark, washed with PBS, and imaged by epifluorescence microscopy. After fluorescence imaging, membranes were optionally stained with crystal violet (0.5%, 10–20 min) for bright-field imaging.

For each insert, ≥5 random fields were captured at 10×–20×. Migrated/invaded cells were counted manually or by automated segmentation in ImageJ; counts per field were averaged per insert, then per biological replicate. Results are presented as cells/field (mean ± s.e.m.) or normalized to control as % migration/invasion.

Notes/QC. Confirm pore size and coating thickness are consistent across inserts. Use gentle pipetting to preserve the matrix layer in invasion assays. If background attachment on the upper surface is high, extend the PBS rinse and increase the number of cotton-swab passes before fixation.

2.2.3.4 miRNA Mimic Transfection

Cells Cells at 60–70% confluence were transfected with miRNA mimics (hsa-miR-548ah-3p or a sequence-matched negative control; [vendor/cat#]) using Lipofectamine 2000 (Invitrogen) in 6-well plates. Unless otherwise stated, transfections were performed in DMEM/F12 spheroid medium (Section 1.2.1.2). For each well, 7.5 µL Lipofectamine 2000 and 100 pmol mimic were each diluted in 125 µL Opti-MEM (Thermo) in separate tubes and incubated for 10 min at room temperature. The diluted Lipofectamine and diluted mimic were then combined (total 250 µL), gently mixed, and incubated for a further 10 min to allow complex formation. Complexes were added dropwise to cells in 2.0 mL fresh medium per well (final volume ≈ 2.25 mL; estimated final mimic concentration ≈ 45 nM). Plates were rocked gently to distribute complexes evenly and returned to 37 °C, 5% CO_2. Medium was refreshed at 24 h to minimize reagent-related toxicity. Transfection efficiency, assessed by qPCR of the mature miRNA or by a fluorescent control duplex in pilot runs, peaked at ~48 h, and downstream assays were scheduled accordingly unless indicated.

For long-term exposure, transfections were repeated every 7–10 days to sustain miRNA activity throughout extended spheroid culture. Re-transfections were timed 24 h after passaging or medium renewal to ensure cells were metabolically active, using the same per-well doses (7.5 µL Lipofectamine 2000 + 100 pmol mimic in 250 µL Opti-MEM, added to 2.0 mL medium). Negative-control mimics were included at identical concentrations in every series. Cell health was monitored by morphology and SRB/viability readouts; if transient cytotoxicity was observed, the complex volume was kept constant while reducing the mimic amount to 75 pmol (final ≈ 34 nM) for that cycle, with the next cycle restored to the standard dose.

Notes/controls. Antibiotic-free medium during the first 4–6 h of transfection is recommended by the manufacturer; in our hands, maintaining standard spheroid medium did not alter efficiency, but all conditions within an experiment were handled identically. For spheroid experiments initiated from single cells, transfection was performed after cells re-adhered (≈6–12 h post-seeding) to standardize uptake. All transfections included no-template (vehicle) and negative-mimic controls.

2.2.4 CRISPR-Cas9 Functional Genomics

2.2.4.1 Plasmid Preparation

Plasmids encoding SpCas9 (blasticidin resistance), GFP reporters, and the custom epigenetic sgRNA library (EPI-KOL) were propagated in E. coli (library: a recombination-stable strain such as Stbl3/Endura). Transformants were selected on LB–agar with the appropriate antibiotic and grown in LB broth at 30–37 °C with shaking (library cultures at 30 °C to minimize recombination). Plasmid DNA was isolated using NucleoBond Xtra Midi (Macherey-Nagel) with endotoxin-reduction according to the manufacturer's protocol. DNA concentration and purity were assessed by NanoDrop (A260/280 ~1.8–2.0); library integrity was spot-checked by restriction digest and colony PCR before downstream use.

2.2.4.2 Lentiviral Production

Lentiviral particles were produced in HEK293T cells maintained in DMEM + 10% FBS. Cells were seeded to reach 60–80% confluence at transfection. For each 10-cm dish, plasmid DNA (transfer plasmid: Cas9-Blast or EPI-KOL; plus packaging plasmids psPAX2 and pMD2.G) was mixed at standard ratios (e.g., 10 µg transfer, 7.5 µg psPAX2, 2.5 µg pMD2.G) and complexed with PEI (1 mg/mL; DNA:PEI ~1:3 w/w) in Opti-MEM. Complexes were incubated 15 min at room temperature and added dropwise. Medium was refreshed after 6–16 h. Viral supernatants were collected at 48 h and 72 h, clarified (300 × g, 5 min), filtered (0.45 µm), and concentrated by PEG 6000 precipitation (final 8% PEG, 0.3 M NaCl, 4 °C overnight), then pelleted (e.g., 1,500–3,000 × g, 30–45 min) and resuspended in serum-free medium or PBS + 1% BSA. Aliquots were stored at –80 °C. All procedures were performed under BSL-2 conditions in accordance with institutional biosafety approvals.

2.2.4.3 OVCAR-3 Transduction and MOI Determination

OVCAR-3 cells were plated to 40–60% confluence and transduced with serial dilutions of lentiviral supernatant in the presence of polybrene (8 µg/mL). For Cas9, blasticidin selection was initiated 24–48 h post-infection; for the library, puromycin selection followed (concentrations determined by prior kill curves; typical ranges blasticidin 5–10 µg/mL, puromycin 1–2 µg/mL for OVCAR-3). Surviving cells were counted after 3–5 days of selection to estimate transduction efficiency. MOI was calculated from the fraction of survivors using a Poisson model $MOI = -ln(1 - funinfected)$. Conditions yielding ~30% transduction (MOI ≈ 0.3) were used for screening to favor single integrants. Where

applicable, flow cytometry of a fluorescent marker (or antibiotic-resistance outgrowth) provided an orthogonal MOI check.

2.2.4.4 Validation of Cas9 Activity

Cas9 activity was validated by co-transducing GFP reporter constructs. GFP expression was monitored by fluorescence microscopy and flow cytometry, confirming efficient editing activity.

2.2.4.5 CRISPR Screen Design

Stable Cas9-expressing OVCAR-3 cells were transduced with the EPI-KOL sgRNA library at MOI ~0.3 with ≥250–500× library coverage maintained at all times (cell numbers scaled to library size). Cells were cultured in parallel under monolayer and spheroid (ULA) conditions. After antibiotic selection, baseline samples (t_0) were collected; endpoint samples (t_{14}) were harvested after 14 days in the assigned condition. Genomic DNA was extracted from each replicate using a column-based large-prep kit (e.g., Qiagen Blood & Cell Culture kits), targeting ≥20 µg gDNA per 10^7 cells.

2.2.4.6 Nested (Multi-step) PCRs

All work was performed in a DNA-clean environment to minimize contamination. Prior to the experiment, work surfaces, pipettes, and racks were decontaminated sequentially with 10% bleach and 70% ethanol. All reagents (primers, dNTPs, nuclease-free water) were pre-aliquoted in single-use volumes and stored at –20 °C; reagents were thawed on ice immediately before use.

(8000 gRNAs×250×coverage×6.6 pg DNA/cell nucleus)≈13.2 µg gDNA/sample. To reach this target, gDNA was divided into four parallel PCR reactions with ~3.3 µg template each, provided that gDNA concentration exceeded 400 ng/µL.

External PCR (First Round)

- Each 100 µL reaction contained:
- 2 µL dNTP mix (10 mM each)

- 1 µL Phusion High-Fidelity DNA Polymerase (Thermo)
- 20 µL 6× GC buffer
- 5 µL forward primer (10 µM)
- 5 µL reverse primer (10 µM)
- 3.3 µg genomic DNA template
- Nuclease-free water to 100 µL

A no-template negative control (water instead of DNA) was included in each run. PCR tubes were kept on ice until cycling, and lids were opened one at a time to prevent cross-contamination.

Internal PCR (Second Round)

Products from the external PCR were directly used (5 µL per reaction, no cleanup) as templates for the nested amplification step. Each 100 µL internal reaction contained:

- 2 µL dNTP mix (10 mM each)
- 1 µL Phusion Polymerase
- 20 µL 6× GC buffer
- 5 µL staggered forward primer mix (10 µM, prepared by pooling 2 µL of each of nine staggered primers into 162 µL water)
- 5 µL reverse index primer (10 µM; barcoded for sample multiplexing)
- 5 µL external PCR product
- 62 µL nuclease-free water

Thermal Cycling Conditions

Both external and internal PCRs were carried out on a thermocycler with hot-start activation to reduce nonspecific amplification:

- 95 °C for 3 min
- 17 cycles (external) or 23 cycles (internal):
- 95 °C for 25 s
- 65 °C for 20 s

- 72 °C for 15 s
- Final extension: 72 °C for 3 min
- Hold: 4 °C

Visualization and Gel Purification

Internal PCR products were visualized on 2% agarose gels (12 µL per sample) alongside controls. Expected amplicon sizes were:

~357 bp for pLentiGuide libraries (352–361 bp range)

No-template controls were consistently negative. Multiple internal PCR reactions (2–3 tubes per sample) were pooled to achieve sufficient yield. Bands corresponding to the expected size were excised under minimal UV exposure using sterile razor blades, avoiding contaminating upper (~500 bp) or lower (~250 bp) bands. DNA was purified using a commercial gel extraction kit (Qiagen or Macherey-Nagel), and products were eluted in 30 µL of pre-warmed elution buffer.

Concentration was measured using NanoDrop spectrophotometry. Samples with <30 ng/µL were re-quantified on a Qubit fluorometer for accuracy. Preparations yielding <20 ng/µL after gel extraction were repeated starting from fresh gDNA to ensure adequate coverage.

2.2.4.7 Sequencing and Analysis

Next- Library QC and Illumina sequencing

PCR-amplified sgRNA cassettes was subject to Amplicon-seq by RefGen, GenEra. FASTQ files were gzip-compressed and subjected to FastQC to confirm Phred quality and absence of adapter contamination.

Read processing and sgRNA counting (MAGeCK "count")

Counts were generated with MAGeCK using the library reference (tab-delimited: sgRNA ID, 20-nt protospacer, target gene, control flag). Where staggered primers were used, the constant region was trimmed accordingly. Non-targeting sgRNAs served as internal controls.

Example command

```
mageck count \
--fastq t0_rep1.fastq.gz,sph_t14_rep1.fastq.gz,mono_t14_rep1.fastq.gz \
--sample-label t0_r1,sph14_r1,mono14_r1 \
--list EPI-KOL_library.txt \
--norm-method control \
--control-sgrna non_targeting_list.txt \
--trim-5 [N_if_stagger] \
--output-prefix counts_r1
```

Outputs for all replicates were merged into a single count matrix for downstream modeling.

QC metrics reported. Total reads per sample, mapping rate to library, number of detected sgRNAs, fraction of missing guides, and Gini index of sgRNA representation. Runs were accepted when mapping ≥80%, missing guides ≤5%, and Gini ≤0.2–0.25; replicate count vectors showed Pearson/Spearman ≥0.9.

Differential analysis (MAGeCK RRA and MLE)

Two complementary strategies were used.

Pairwise robust rank aggregation (RRA).

Primary contrasts were spheroid$_{t14}$ vs sphere medium monolayer$_{t14}$ and spheroid$_{t14}$ and sphere medium monolayer$_{t14}$ vs t_0, each with n = [3] biological replicates. RRA was run with non-targeting guides for normalization. Genes with FDR ≤ [0.1] and consistent direction across ≥[2] sgRNAs were retained.

Example:

```
mageck test rra \
  --count-table all_counts.txt \
  --norm-method control \
  --control-sgrna non_targeting_list.txt \
  --neg-control-sgrna non_targeting_list.txt \
  --treatment-label sph14_r1,sph14_r2,sph14_r3 \
  --control-label mono14_r1,mono14_r2,mono14_r3 \
  --output-prefix rra_sph_vs_mono
```

Multifactor modeling (MAGeCK-MLE).

To jointly account for condition (spheroid vs monolayer), time (t_0 vs t_{14}), and batch, we fit an MLE model with a design matrix. β-scores (per-gene effects) and Wald statistics were used to call hits (FDR ≤ [0.1]). Copy-number bias was assessed and, where applicable, corrected in downstream Flute steps.

Example:

```
mageck mle \
  --count-table all_counts.txt \
  --design-matrix design.txt \
  --norm-method control \
  --control-sgrna non_targeting_list.txt \
  --output-prefix mle_joint
```

Directionality. In the sign convention used, negative selection (depletion) in spheroids indicates genes required for spheroid maintenance; positive selection (enrichment) indicates relative growth advantage under spheroid conditions.

Downstream QC and bias correction (MAGeCK-Flute)

Counts and RRA/MLE outputs were processed in MAGeCK-Flute (R) to generate:

Quality reports: library coverage, count distributions, replicate correlations, and Gini indices.

Copy-number (CN) assessment/correction: optional CNV normalization using public OVCAR-3 CNA profiles or internal estimates (Flute functions CNV.Estimate, Flute.CNVCorrect)

Hit integration: combining RRA p-values and MLE β-scores to prioritize high-confidence genes with concordant signals across contrasts.

Filtering criteria. Unless noted, we required (i) FDR ≤ [0.1] in at least one spheroid comparison to spheroid medium monolayer (both normalized to t0 first), (ii) consistent sign across RRA and MLE, and (iii) median sgRNA $\log_2$ fold-change beyond [±0.5].

Functional annotation and enrichment analysis

Genes passing the above filters were functionally annotated using KEGG and Reactome pathway databases. Over-representation analysis was performed in R (e.g., clusterProfiler and ReactomePA) with the assayed gene set as background and BH correction for multiple testing. Pathways with FDR $q \leq 0.05$ were considered significantly enriched. Redundant terms were collapsed by semantic similarity or manual curation. Where appropriate, results were visualized as bar plots of normalized enrichment scores and network diagrams linking top pathways to leading-edge genes.

Example (R):

```
library(clusterProfiler)

library(ReactomePA)
```

```
library(org.Hs.eg.db)

hits <- unique(read.table("high_conf_hits.txt", stringsAsFactors=FALSE)[,1])

bg   <- unique(read.table("all_library_genes.txt", stringsAsFactors=FALSE)[,1])


# map to Entrez

map <- bitr(hits, fromType="SYMBOL", toType="ENTREZID", OrgDb=org.Hs.eg.db)

bgm <- bitr(bg, fromType="SYMBOL", toType="ENTREZID", OrgDb=org.Hs.eg.db)

ekegg <- enrichKEGG(gene=map$ENTREZID, universe=bgm$ENTREZID,

                    organism='hsa', pAdjustMethod="BH", qvalueCutoff=0.05)

ereact <- enrichPathway(gene=map$ENTREZID, universe=bgm$ENTREZID,

                        organism="human", pAdjustMethod="BH", qvalueCutoff=0.05)
```

Reporting and reproducibility

For every screen, we report: total and mapped reads per sample, mapping rate, detected sgRNAs (%), Gini index, replicate correlations, normalization method, statistical framework (RRA and/or MLE), FDR thresholds, and the non-targeting list used for control-based normalization. All code (command lines and R notebooks) and the library reference are available upon request and archived in [repository/DOI].

Note. Exact parameter values (e.g., --trim-5, read length, antibiotic doses, FDR cutoffs) are specified in figure legends or Supplementary Methods and match the versions reported here.

2.2.5 Statistical Analyses and Data Visualization

All experiments were performed with at least three independent biological replicates unless otherwise specified. Statistical analyses were conducted using GraphPad Prism 9, RStudio, and Python. Significance was tested using Student's t-test (two groups) or ANOVA (multiple groups) with post hoc correction. Significance thresholds were annotated in figures as follows: $p < 0.1$ (*), $p < 0.05$ (**), $p < 0.01$ (***), $p < 0.001$ (****).

Visualization of sequencing and CRISPR screen results was performed with R (ggplot2, pheatmap) and Python (matplotlib, seaborn). ImageJ was used for densitometric quantification of Western blot bands, and CytoFLEX software was used for flow cytometry data analysis.

2.2.5.1 RNA-seq Analysis and APA Determination Statistical Analysis

Read processing and alignment: Raw FASTQ files were assessed with FastQC and aggregated with MultiQC. Adapters and low-quality bases were trimmed (cutadapt/Trim Galore!; default stringency). Reads were aligned to the human GRCh38/hg38 reference using a splice-aware aligner against GENCODE v31 gene models. Only primary, uniquely mapped pairs with mapping quality MAPQ ≥10 were retained. BAMs were coordinate-sorted, indexed, and inspected with samtools (flagstat/idxstats). For visualization, CPM-normalized coverage bigWigs were generated with deepTools bamCoverage (--normalizeUsing CPM, --binSize 25, --ignoreDuplicates), and an identical y-axis was enforced across tracks within each IGV panel.

Gene-level differential expression (DE): Gene counts were obtained (featureCounts/htseq-count; strandedness matched library prep) and analyzed with DESeq2 (default size-factor normalization, dispersion estimation, Wald tests, Benjamini–Hochberg correction). The design formula was ~ condition for pairwise contrasts (MIM vs NC; MONO vs NC). Unless specified, significance was defined as FDR (padj) ≤ 0.05. Effect sizes are reported as $\log_2$ fold-change (LFC); where indicated for visualization filters, genes with $|LFC| \leq 0.4$ were considered "small-effect" DE.

Reference for APA*:* Alternative 3′UTR isoforms were restricted to known sites using the QAPA 3′UTRome derived from GENCODE v31 (hg38)

(qapa_3utrs.gencode_V31.hg38.bed). Poly(A) sites (PAS) were taken as the terminal coordinates of UTR intervals on the correct strand and exported as 1-bp features for browser display.

Quantification of 3'UTR isoform usage (Ψ): For each sample, strand-aware read coverage over each annotated 3′UTR isoform was quantified from BAMs (bedtools coverage/multiCov). For a gene with k UTR isoforms and counts $c_{i,s}$ in sample s, usage was computed as $\Psi_{i,s} = \frac{c_{i,s}}{\sum_{j=1}^{k}=c_{j,s}}$.

Genes were filtered if total UTR counts were insufficient (default: $\sum_j c_{j,s} < 30$ in ≥2 replicates per group) or if Ψ estimates were unstable (single-isoform dominance with near-zero alternatives across replicates).

Differential APA (ΔΨ) across conditions: For each isoform (or for a proximal vs distal summary when two major sites existed), replicate-level Ψ values were compared between groups. Two complementary tests were used:

- A two-sided Wilcoxon rank-sum on logit-transformed usage $logit(\Psi) = \frac{\Psi}{log1-\Psi}$ to stabilize variances at the boundaries.
- A beta-binomial model (sensitivity analysis) using isoform counts and gene-wise totals to account for overdispersion.

P-values were BH-adjusted per contrast (α = 0.05). We report ΔΨ as the difference in mean usage between groups (e.g., $\Delta\Psi = \Psi_{MIM} - \Psi_{NC}$). “Shortening” indicates increased proximal usage (or decreased distal usage), whereas “lengthening” indicates the converse. Because Ψ is a within-gene proportion, ΔΨ is independent of gene-level expression changes; DE results (DESeq2 LFC/padj) are reported alongside ΔΨ for context but are not used in Ψ normalization.

Multiple contrasts and replicate handling: APA analyses were performed for MIM vs NC (spheroids) and MONO vs NC, each with n = 3 biological replicates per group. Unless noted, genes were considered APA-significant in a contrast if BH-adjusted P ≤ 0.05 and |ΔΨ|

exceeded a minimal practical threshold (e.g., ≥0.10) with concordant direction across replicates.

Quality control for APA: As global checks, we computed (i) the fraction of annotated PAS with non-zero coverage (100-bp windows), and (ii) metaprofiles of CPM signal around PAS (±2 kb; deepTools computeMatrix/plotProfile). Replicate concordance was assessed by pairwise correlations of Ψ and by ΔΨ consistency plots. For figure panels, IGV snapshots used CPM bigWigs with a shared y-axis and PAS tracks underneath to illustrate local usage differences near annotated sites.

Integration with DE and candidate selection: To aid visualization and reduce DE-driven height differences in IGV, we prioritized examples with small DE (e.g., |LFC| 0.1–0.4) but significant ΔΨ. Genome-wide statistical conclusions were based strictly on replicate-level Ψ tests (above), not on browser signal amplitudes.

Software and reproducibility. Analyses used samtools, bedtools, deepTools, DESeq2 (R), and in-house R scripts for Ψ/ΔΨ and FDR control. All thresholds (coverage filters, ΔΨ minimum, FDR) are reported in figure legends where they differ from the defaults above.

CHAPTER 3

RESULTS

1.1 Comparison of 3D Culture Methodologies and HGSOC Cell Lines

1.1.1 Optimization OVCAR-3 Spheroid Generation with Ultra Low Attachment Plates

Optimal Seeding Density for OVCAR-3 Spheroid Generation

After OVCAR-3 cells are counted and carefully reduced to single cells, they are seeded to ULA plates. Cell density suggestions in the literature range between $1x10^3$-$5x10^4$ cells/well. Although this research concludes that seeding too low cell numbers delay or disrupt spheroid formation. This is probably due to the cell-to-cell signaling (intracellular communication) being too sparse inside a 6-well sized medium. Given that OVCAR-3 cells almost immediately switch to a slower proliferation behavior when seeded to ULAs from conventional 2D cultures, low initial seeding densities is not favorable for downstream analyses with spheroids. Therefore, even though $5x10^4$ cells/well is found to generate spheroids much better than smaller cell densities, this number of cells still required too long to obtain the optimal cell number for the downstream experiments and applications. Maximum cell/well number was determined as $3x10^5$, as going higher than this number produced high amounts of cell death and debris. To summarize, the optimal seeding density of OVCAR-3 cells to 6-well ULA plates was found to range between $5x10^4$-$3x10^5$ cells per well. According to the downstream application's cell number need, initial seed density was used at maximum (for instance with CRISPR-KO Screen) or lower.

Optimal Medium Volume and Medium Change Intervals

Cells were found to be nutrient depleted and subject to more cell death under 5 ml spheroid media and too early medium addition disturbed aggregates and spheroid generation. 5-7 ml was the optimal range for initial seeding volume and higher amounts delayed spheroid formation substantially. Given that the proliferation rate is significantly lowered, medium color change is observed as late as week 2-3 time period (Days 14-21 after seeding). If the

culture was to be sustained for 21 to 3, one or two medium addition (medium change) applications were required. At least 3 ml medium addition helped spheroids to thrive and Corning ULA plates could take up to 15 ml of media. Not to risk spilling, initial seeding volume was determined as 5 ml and medium additions were performed as 3-4 ml, until the medium color turned back to orange/red.

Optimal Time Points for OVCAR-3 Spheroids to Generate While Maintaining a Healthy Culture Environment

Between day 6-12 after cells seeded as single cells, cells start to cluster together in groups. Sometimes these groups can compile at the middle of the well but the groups still remain separate. This stage is known as the aggregate formation stage. These small aggregates later combine with other aggregates or proliferate to represent larger aggregates. At that stage aggregates start to resemble grapes and may situate as long lines. Day 12-21 time point is where we observe these structures. Later on, some cells in the culture behave differently than just forming clusters but they generate another structure we called “compartmentalized spheroids” they might sometimes be referred to as “compact spheroids” in the literature. These structures has loose cells in the middle and a tightly packed outer-layer, resembling organoids defined in the literature. Compartmentalized spheroids are signs of OVCAR-3 spheroid culture’s health and proper maintenance and when they appear, CSC characteristics enrichment follow. They can be a result of “differentiation favoring over proliferation” of the cells. As the culture continues to be maintained with medium additions and minimal disturbances, these compartmentalized spheroids gets higher in both number and size. Optimal cell passaging time point was determined as around the first month of the passage, between days 21-28. After P1, culture is enriched greatly in size and number of these defined structures and culture is ready for downstream analysis. (This stopping time point is not only determined with visual observations but also with the analysis of CSC traits enrichment experiments, which will be presented in the following sections.) After passage number 2, cell death rate increases and was not found optimal for analyses.

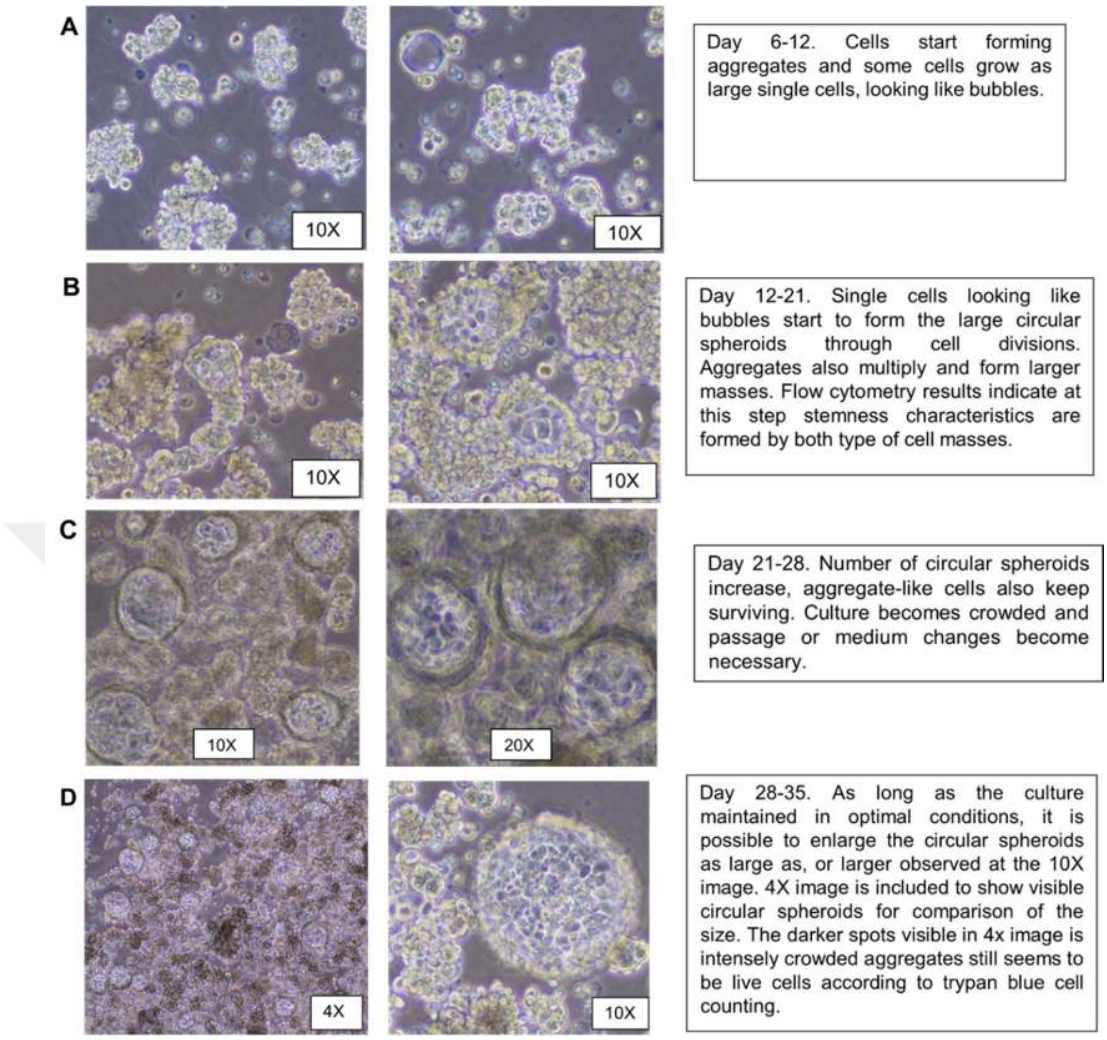

Figure 3.1: Spheroid Generation of OVCAR-3 Cell Line With Ultra Low Attachment Plates. (A) Between day 6-12 after cells seeded as seperate single cells starts to form small aggregates. **(B)** Between day 12-21 Aggregates gets larger and small compartmentalized spheroids start to appear in the culture. **(C)** Number of compartmentalized spheroids and their size increase until time point day 28. Medium color turns yellow as cell numbers increase and medium addition is performed. **(D)** As the culture is kept steady and medium refreshed, spheroids keep growing in size and number and they become visible even in 4X magnification of the brightfield microscopy. *Representative fields from n=3 biological replicates. Scale bars and magnifications are as indicated on the pictures.*

1.1.2 Optimization of OVSAHO Spheroid Generation with Ultra Low Attachment Plates

OVSAHO cell line behaved dramatically different from OVCAR-3 cell line. First notable difference was the continuation of proliferation capacity as they do in 2D conventional cultures. This requires seeding less cells initially. Even with the low cell number starting points, OVSAHO ULA 3D culturing required frequent medium changes and up to 4 passages because medium addition was not enough to keep the cell media non-acidic (red/orange in color). Second important difference is the absence of the compartmentalized structures in OVSAHO ULA culture. Even as late as 60 day time period (and onward as well) these structures did not form. This initially led the assumption that differentiation was not favored enough and CSC enrichment was probably not occurring. However, CSC trait enrichment experiment results proved otherwise, which will be presented in the following sections.

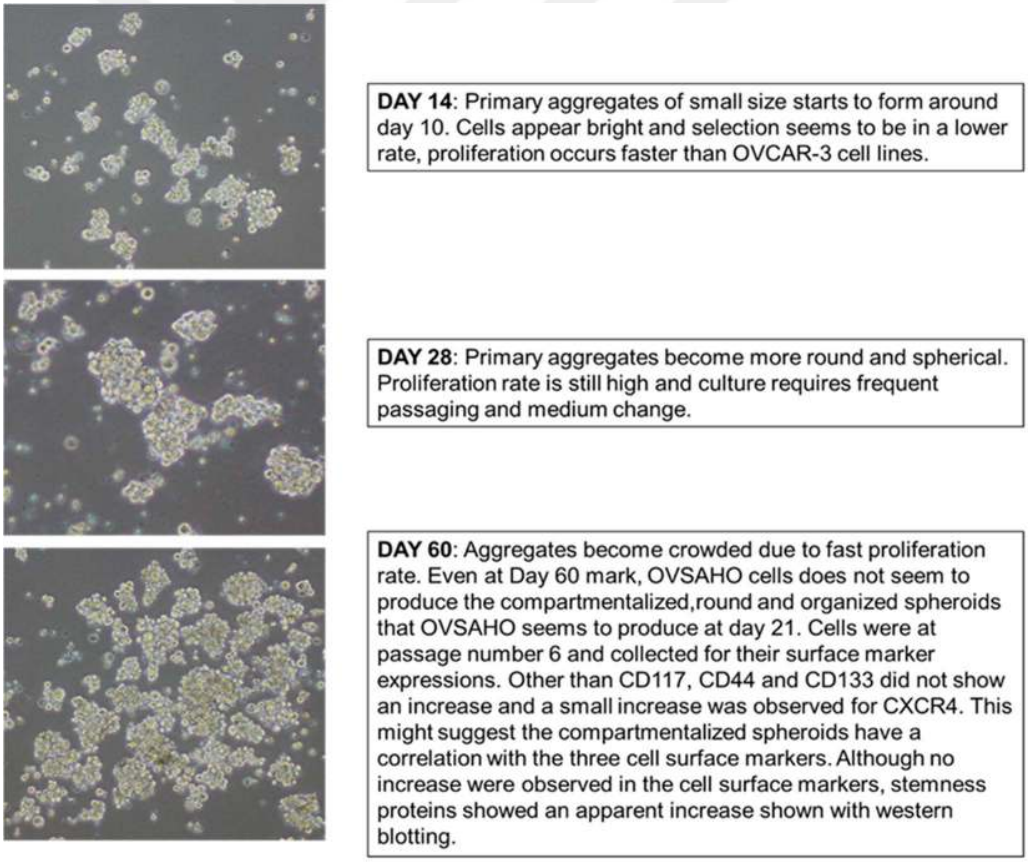

Figure 3.2: Spheroid Generation of OVSAHO Cell Line With Ultra Low Attachment Plates. (A) After 14 days following the cells seeded as seperate single cells, small groups of cell clusters are observed. **(B)** Until day 28 they start to resemble aggregate formations.

Proliferation is rapid compared to OVCAR-3 cell line. This leads to increased cell population in the culture and medium changes are required more frequently. **(C)** Even at day 60 mark (2 months of culturing) compartmentalized spheroid formations are not observed in the culture, leading to the assumption that OVSAHO cell line is not enriching in CSC traits. *Representative fields from n=3 biological replicates. Magnifications are 4X.*

1.1.3 Morphology and Size Measurements of OVCAR-3 ULA Generated Spheroids

Size Measurements

To represent the compartmentalized spheroids enlargement, brightfield microscopy images were taken with a scale axis lines included, after the first passage time point (Day 30-50). As the figure shows, at the time of cell collection, the culture consists of many compartmentalized spheroids of different sizes.

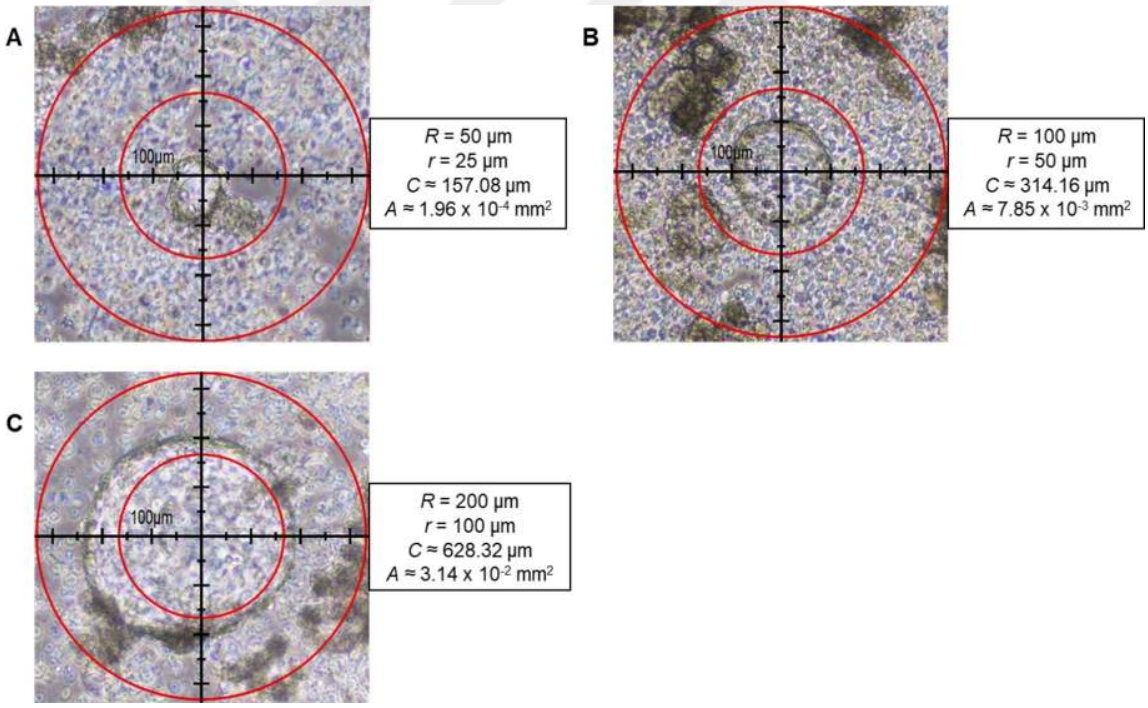

Figure 3.3: Measurements of Compartmentalized Spheroids. (A) A smaller spheroid in the culture. **(B)** A mid-sized spheroid and its measurements. **(C)** One of the largest spheroids obtained in this time period. n=3 biological replicates. Scale as indicated by the axis.

Cellular State Investigation

In addition to size evaluation, cellular states in the spheroids were also investigated. According to the literature, the outer layer of compact spheroids are the proliferative zone, cells right under that layer are considered quiescent and the middle layer is considered necrotic (Senrung et al., 2023). DAPI and α-tubulin staining of spheroids and imaging with confocal microscopy using the z-stack feature showed that even with smaller spheroids, the core of the spheroids remain unstained with DAPI. This showed that our compartmentalized spheroids match the literature's defined cellular states within them.

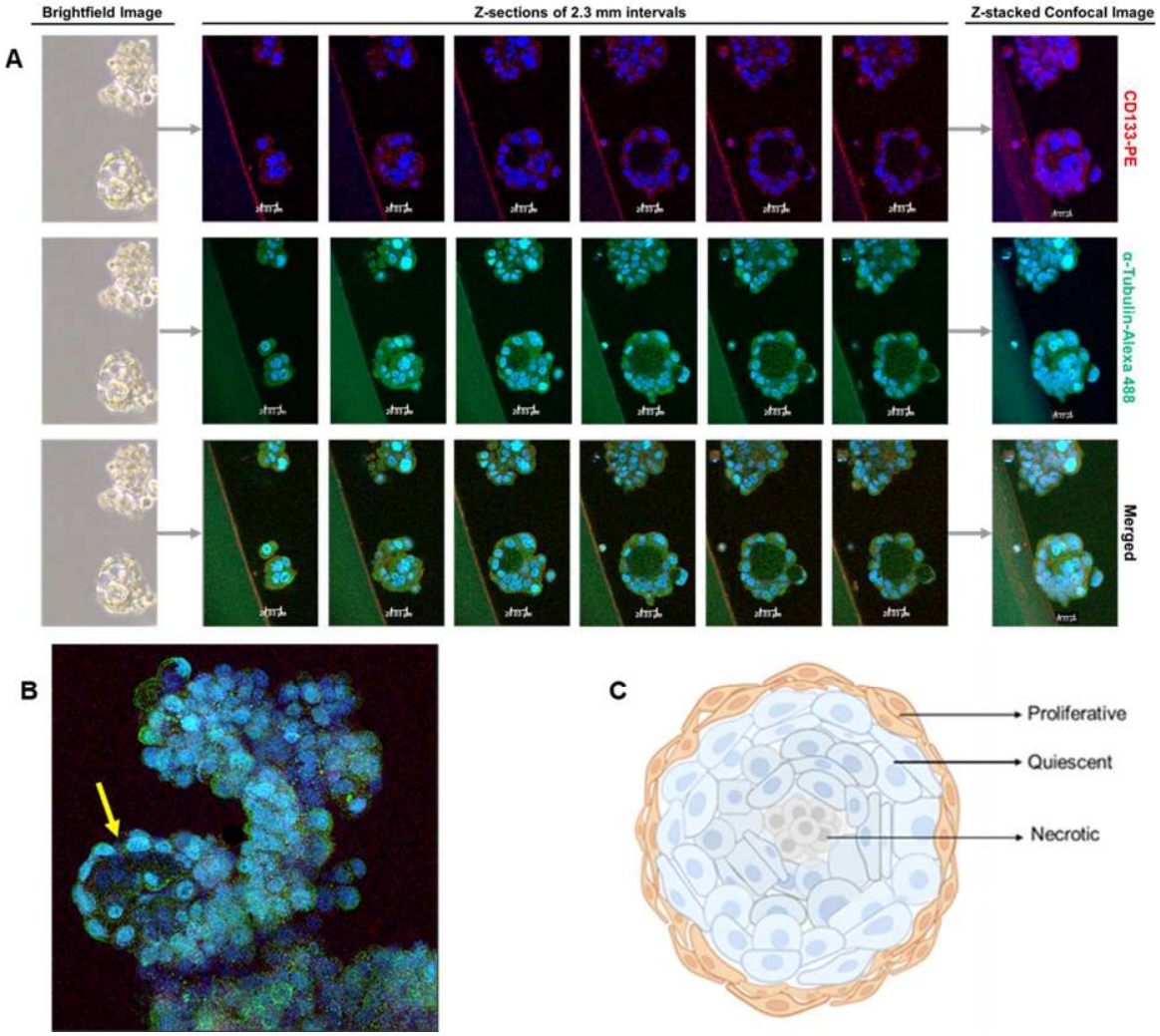

Figure 3.4: Confocal Images and Cellular States of Spheroids. (A) Spheres imaged in brightfield microscopy was dyed for alpha tubulin (green) and DAPI (blue). Multiple z-axis images are shown next to each other (following the first grey arrow) and the final image represents the merged image of the z-stack pieces (after the second grey arrow). Different channels are shown separately and scale bar is included. **(B)** Another compartmentalized

spheroid structure (larger one) is seen in the picture connected to a string of aggregates. Mid-section (pointed with a yellow arrow) is shown unstained and some blue are observed in the far dimension, representing 3D spherical structure. (Image is stacked z-sections captured every 2.1 mm, in 63X magnification.) **(C)** Spheroid morphology illustration, adapted from (Acland et al., 2018). *Representative of n=3 biological replicates. z-step ≈2.1 μm; scale bars as indicated.*

1.1.4 Optimization OVCAR-3 Spheroid Generation with GelMA Encapsulation

For evaluating GelMA Encapsulation and its spheroid generation facilitation abilities, we initially tried to UV-crosslink a 10-20 μl droplet on a glass confocal dish and culture it with spheroid media. The droplet was composed of PBS-GelMA-Irgacure mixed with OVCAR-3 cells of 4 million cells/ml density. Cells did not show any ability to proliferate or form spheroids in such a structure. Comparison of MTT results of Day 0 (seed day) and Day 14, showed no differences. This system probably led to GelMA extracellular matrix to be too thick to allow for medium additives to diffuse freely to the cells.

To make the GelMA encapsulate thinner and in a more organized structure, we used photomasks of different shapes. The square shaped photomask yielded significantly healthier culture appearance and rapid spheroid formations. The system and the spheroids produced with it is represented in **Figure 3.5**. This GelMA encapsulation will be referred to as GelMA-Pm abbreviation from this point onward.

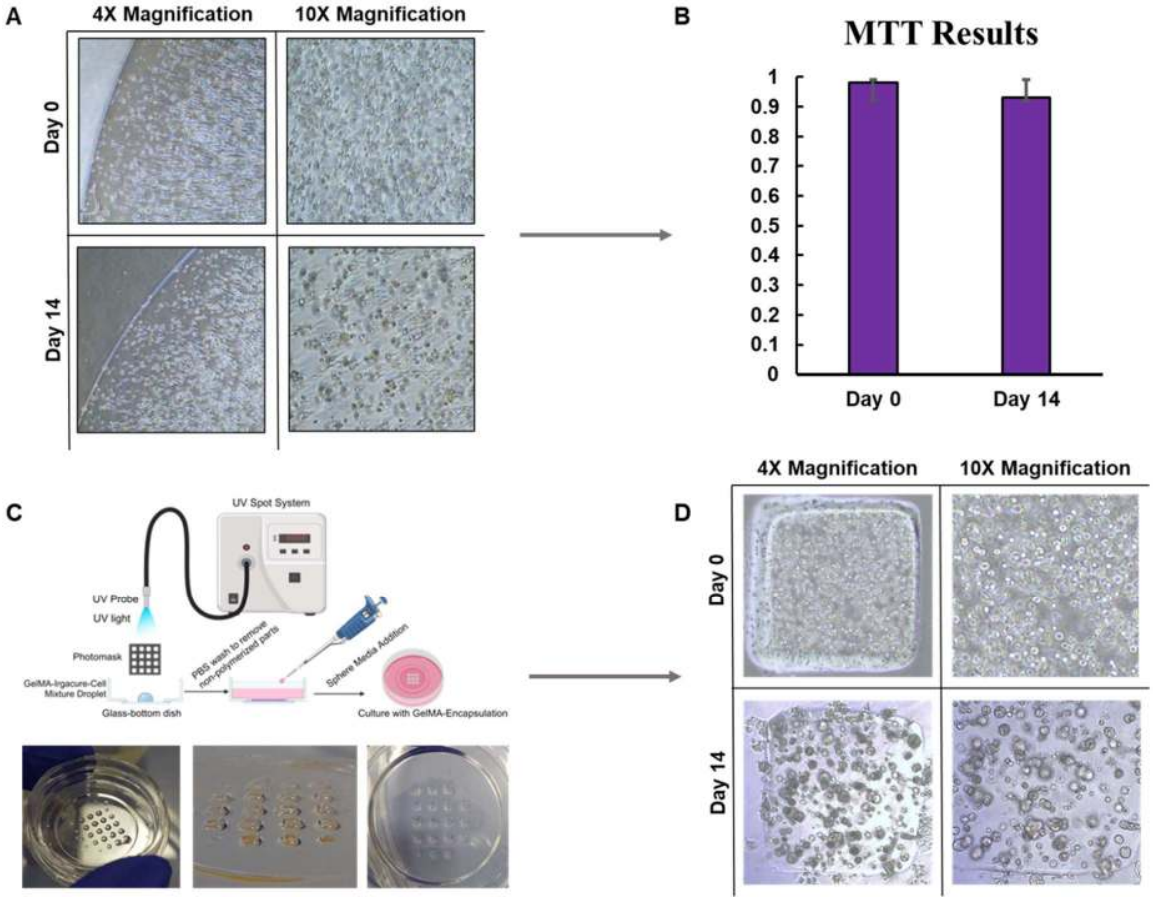

Figure 3.5: Optimization OVCAR-3 Spheroid Generation with GelMA Encapsulation. (A) Brigfield images of GelMA encapsulation method without using photomasks and using UV crosslinking directly on the droplet. (B) MTT results of GelMA encapsulation without using photomasks. The difference is non-significant and no cell growth could be observed in 14 days of culturing. (C) Representative illustration of GelMA encapsulation using photomask chambers and actual photographs of square-shape solidified matrix units. (D) One of the square-shaped GelMA masks (GelMA-Pm structure) at Day 0 and Day 14. Spheroid generation and overall culture health is drastically enhanced with photomasking. *Representative fields from n=3 biological replicates.*

1.1.5 Optimization OVCAR-3 Spheroid Generation with GelMA Encapsulation

Observing OVCAR-3 cell line spheroid generation thrive in photomasks, same technique was applied to OVSAHO cells. Interestingly, OVSAHO cell line that was not able to form compact spheroids in ULA technique, showed a high number of spheroids with GelMA-Pm technique.

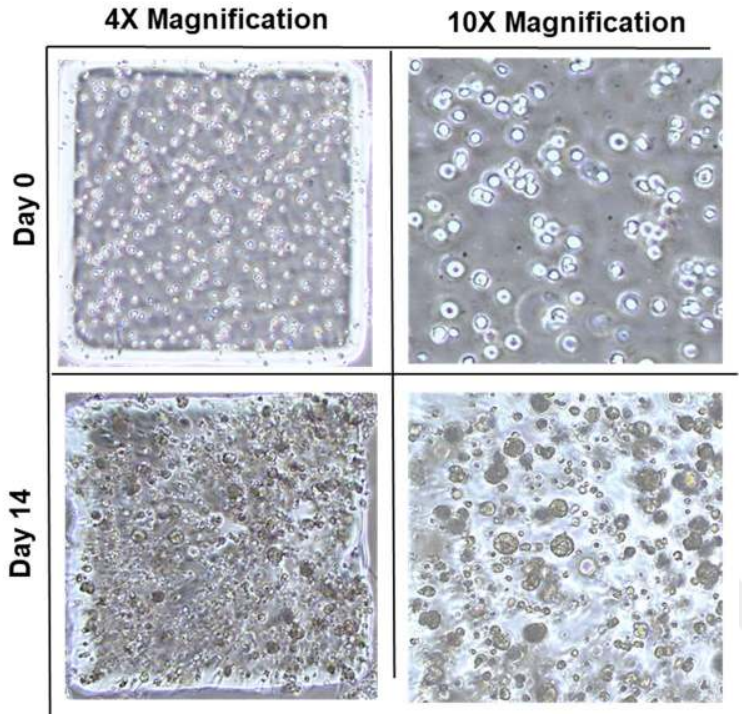

Figure 3.6: OVSAHO Spheroid Generation with GelMA-Pm Encapsulation. Brightfield microscopy images of GelMA-Pm encapsulation technique with OVSAHO cell lines, Day 0 and Day 14 comparison. Representative fields from n=3 biological replicates.

1.1.6 Evaluation of Ultra Low Attachment Plate Culturing CSC Trait Enrichment

Brightfield Microscopy Images and CSC Marker Proteins

Collective brightfield microscopy images of both cell lines were put side by side at the same time points for better comparison. Although OVSAHO cell line did not show the same morphology as OVCAR-3 cells, they still got enriched in terms of cancer stemness markers: ALDH1A1, NANOG, OCT-4 and SOX-2.

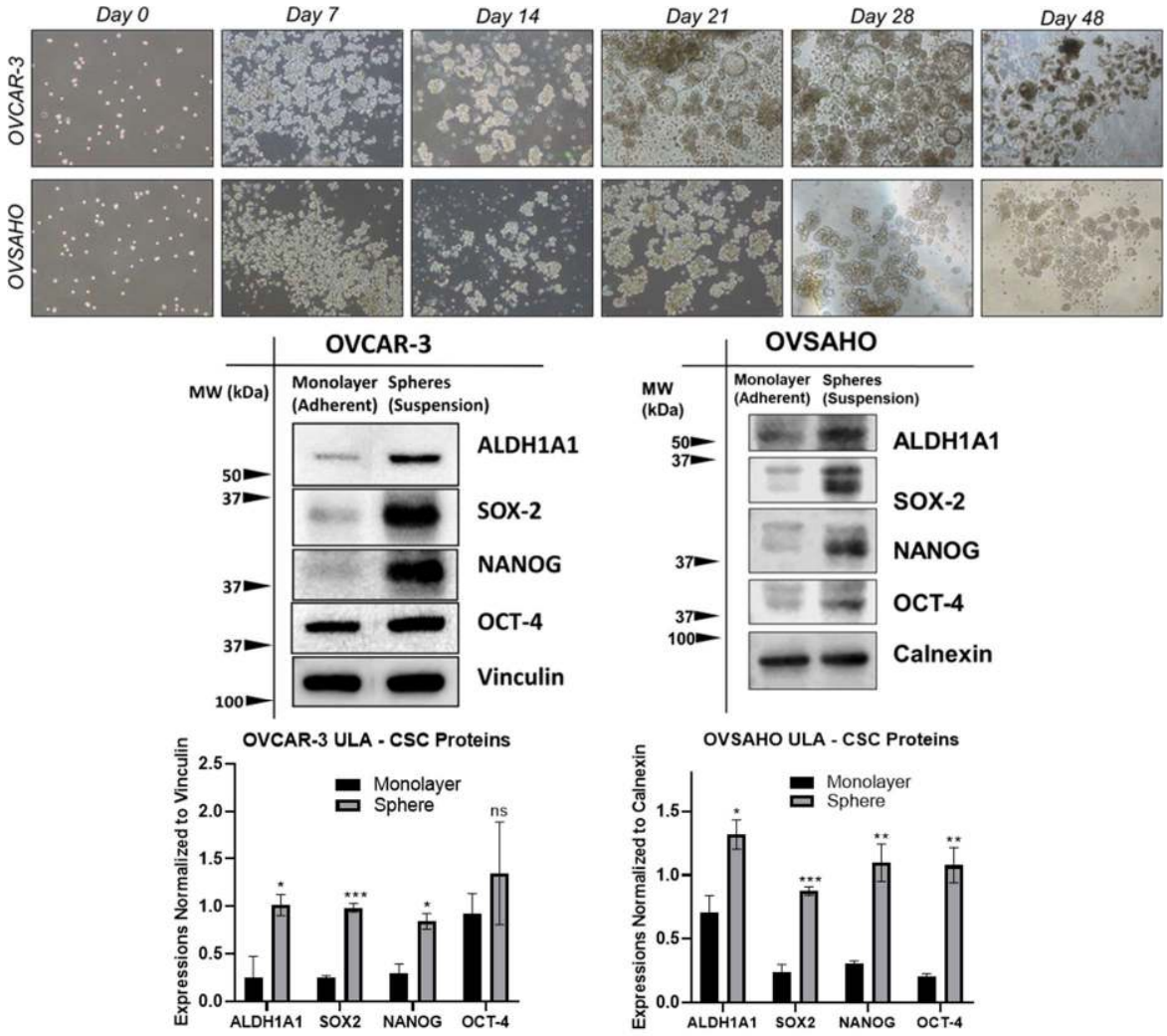

Figure 3.7: Brightfield Image Summaries and Cancer Stemness Marker Proteins Enrichment with Ultra Low Attachment Plates. Collective brightfield microscopy images of both cell lines followed with ALDH1A1, SOX-2, NANOG, OCT-4 proteins western blot images and their quantitative data summarized in bar graphs. Densitometry normalized to loading control. n=3 biological replicates; mean ± SD. Two-sided t-tests (ULA vs monolayer within line) $p < 0.1$ (*), $p < 0.05$ (**), $p < 0.01$ (***), $p < 0.001$ (****).

Confocal Microscopy Images and CSC Cell Surface Marker Flow Cytometry

Cell surface markers reported to be present in HGSOC, CD133, CD117, CD44 and CXCR4 levels were evaluated with flow cytometry analysis. OVCAR-3 showed significant increase in all four markers, most signifant ones being CD133 and CD117, whereas OVSAHO only showed moderate (but statistically significant) increase in CD117. For CD44 and CD133 no change was observed and for CXCR4 a significant decrease was observed. Therefore, the confocal microscopy images were performed with OVCAR-3 spheroids, where DAPI is represented with blue, α-Tubulin is represented with green and CD133 is represented with red.

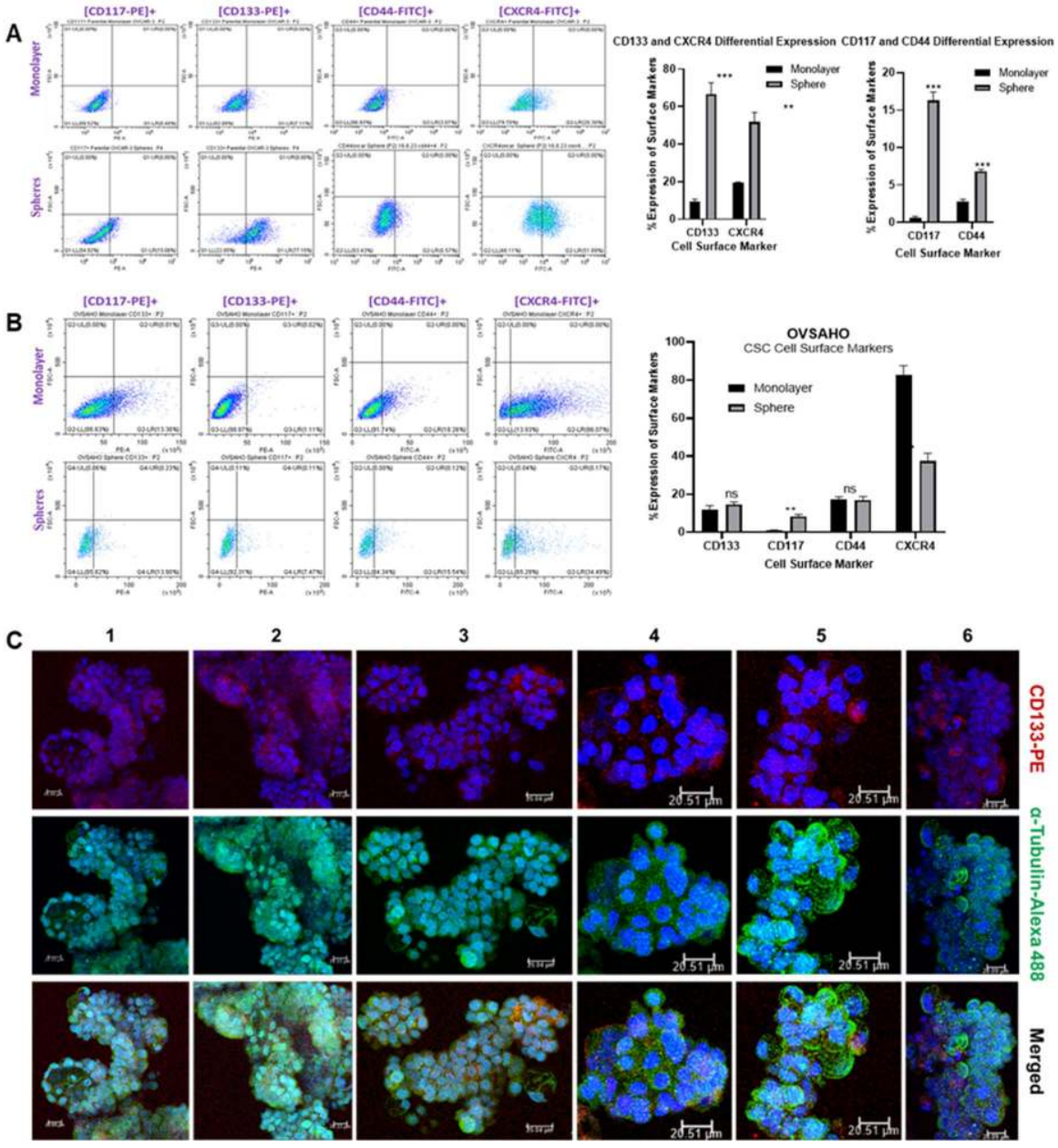

Figure 3.8: Cell Surface Marker Proteins Enrichment with Ultra Low Attachment Plates. (A) OVCAR-3 ULA 3D cultured cells CD133, CD117, CD44, CXCR4 cell surface markers flow cytometry dot plots and their quantitative representation with bar graphs. **(B)** OVSAHO ULA 3D cultured cells CD133, CD117, CD44, CXCR4 cell surface markers flow cytometry dot plots and their quantitative representation with bar graphs. **(C)** Confocal microscopy images of 3D ULA cultured OVCAR-3 cells. (Images are stacked z-sections of 2.1 mm intervals where blue is DAPI, green is α-Tubulin and red is CD133-PE.

OVCAR-3 spheroids obtained with ULA system yielding significant increases in all cell surface markers in the panel was a promising result, therefore to make sure it was indeed due to growing in a suspension in ULA plates and not due to the sphere media additives (such as FGF or depleted FBS) we performed another flow cytometry analysis adding sphere medium grown monolayer control group. It was safe to conclude that sphere media was not the major driving factor for cell surface marker enrichment because either no change from conventional monolayer culture was observed, or they were not found statistically significant as ULA experimental group. Only exception was CXCR4, which has also increased significantly with only spheroid enrichment media. (All the following evaluations after this point in the thesis also includes sphere medium grown monolayer controls.)

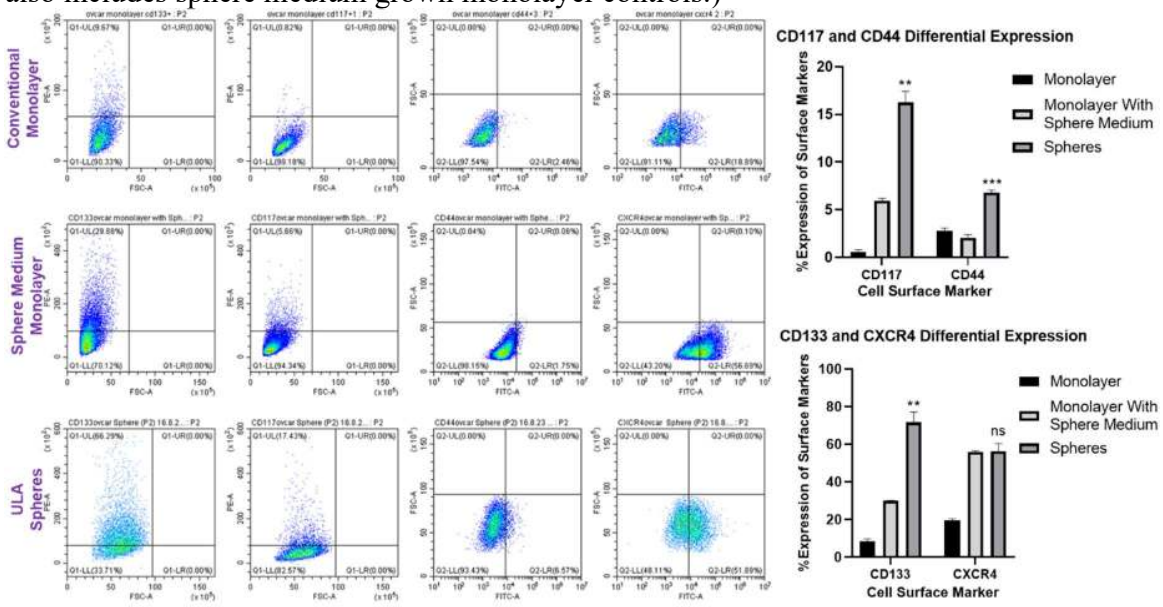

Figure 3.9: Addition of Sphere Medium Grown Monolayer OVCAR-3 Control Group to Validate CSC Surface Markers Increase with ULA System. Pseudo-dot plot graphs represent flow cytometry results and bar graphs summarize the quantitative measurements.

n=3; mean ± SD, paired t-test applied and ns= not significant, $p < 0.1$ (*), $p < 0.05$ (**), $p < 0.01$ (***), $p < 0.001$ (****).

1.1.7 Evaluation of GelMA-Pm Culturing CSC Trait Enrichment and Comparison of Culture Systems-Cell Line Pairs

Brightfield Microscopy Images and Confocal Microscopy Images of GelMA-Pm System

Similar CSC characteristics evaluations were done with GelMA-Pm cultures of OVCAR-3 and OVSAHO with a few limitations the system raises.

The following are some inconveniences for western blot analyses:

- GelMA-Pm structures are extremely small scale microenvironments therefore to obtain enough cells for downstream applications, one has to seed at least 10 systems for each cell line.
- The UV exposure requires to be in the same distance and imaging requires glass bottom confocal dishes.
- In addition to these, there is the step where GelMA is melted with collagenase and removed from the culture. This removal step may lower the final cell yield and leftover collagenase or GelMA particles could interfere with BCA experiment.

Owing to these limitations western blot analysis with GelMA system is fewer than ULA system.

There were also limitations detected for flow cytometry analysis. Flow cytometry experiments are sensitive experiments where large molecules can clog the probe, such as larger dyes, cell clusters or gelatin leftovers. However staining and imaging with confocal microscopy was applicable and yielded valuable results where OVCAR-3 cells yielded more CD133-PE staining than OVSAHO cells.

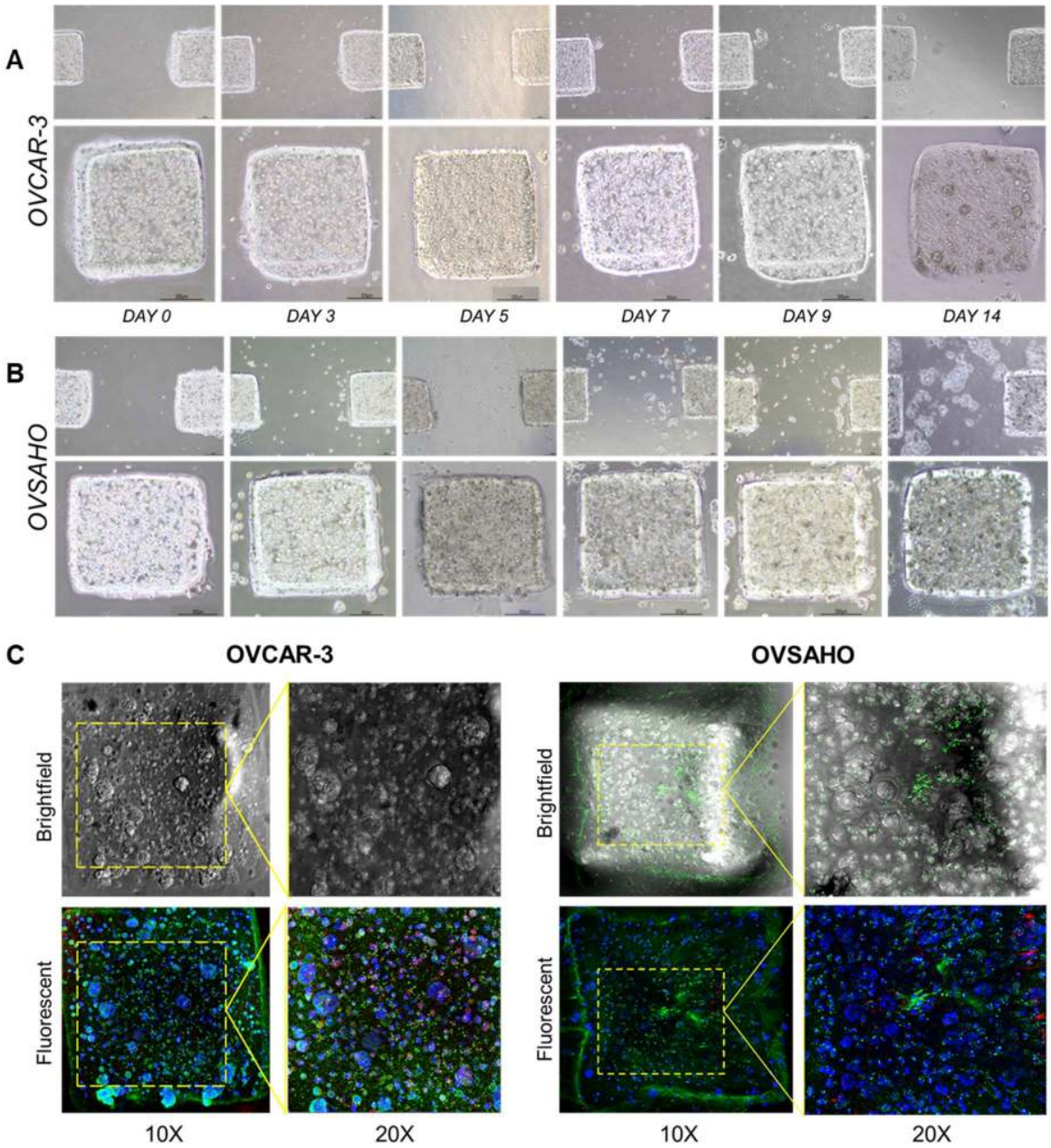

Figure 3.10: Brightfield Microscopy Images and Confocal Microscopy Images of GelMA-Pm System. (A) Brightfield images of different time points with OVCAR-3 GelMA-Pm and spheroid generation. **(B)** Brightfield images of different time points with OVSAHO GelMA-Pm and spheroid generation. **(C)** Confocal microscopy images of 3D GelMA-Pm cultured OVCAR-3 and OVSAHO cells. (Images are stacked z-sections of 2.1 mm intervals where blue is DAPI, green is α-Tubulin and red is CD133-PE.)

Comparison of 3D culture methods (ULA vs GelMA-Pm) CSC traits enrichment abilities

Due to the above mentioned limitations, for comparison of the two cultures mostly qPCRs were performed. This comparison also required an additional control group, to rule out the UV exposure effects. Surprisingly, UV exposure was not found ineffective on CSC traits. It was mostly an active contributor to OVSAHO traits rather than OVCAR-3. Although increasing CSC traits is the end-goal, not being able to rule out UV exposure effects and difference in cell line responses, left GelMA-Pm system questionable in this aspect. One explanatory theory for cell line behavior differences is their distinct BRCA1/2 mutation status, where OVCAR-3 is not mutated (wild-type) but OVSAHO is mutated for BRCA2 and loss of heterozygosity is observed in BRCA1.

Advantages of GelMA-Pm system was significantly faster spheroid generation time and increase in spheroid numbers and viability. Other than that, for mass production and high-thorughput downstream applications, ULA plating was found more advantageous.

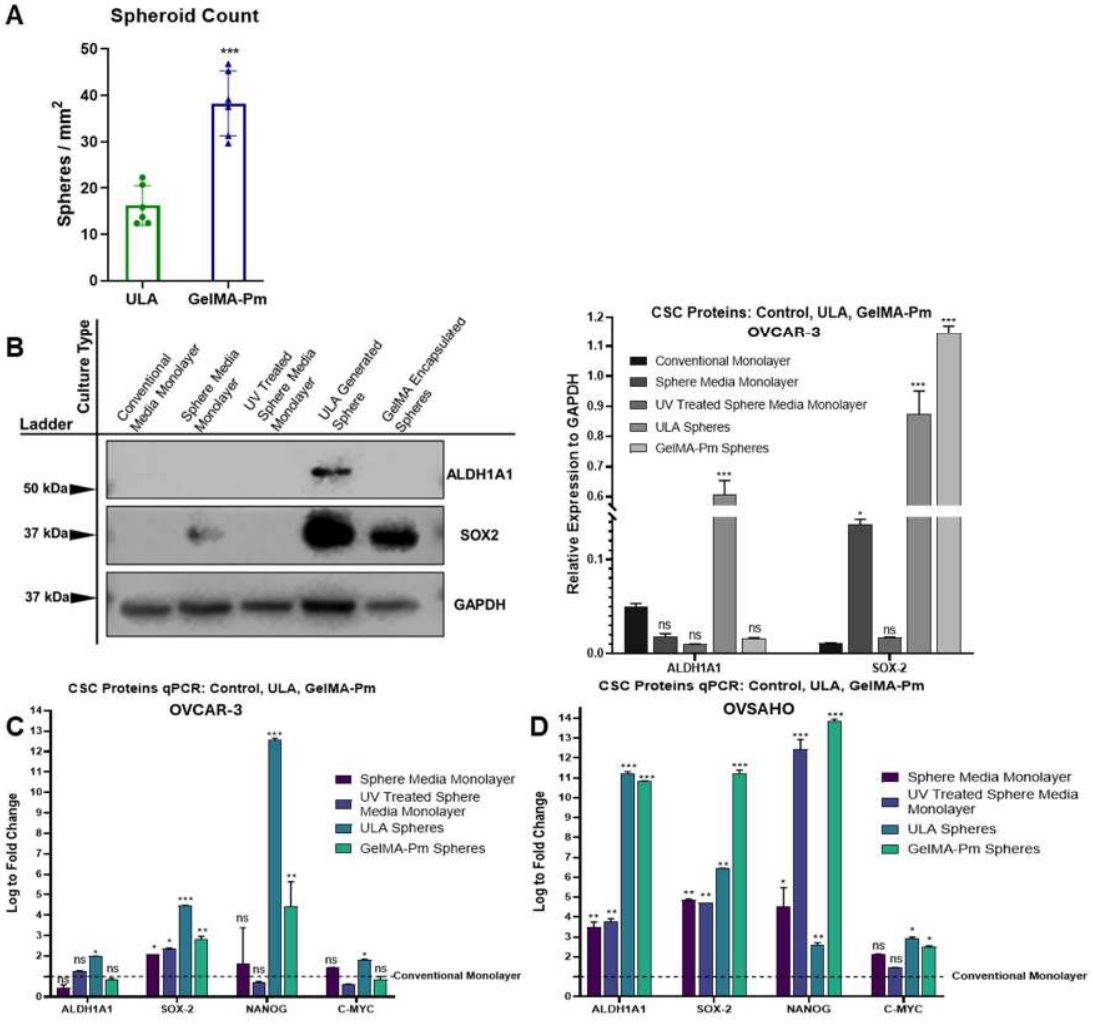

Figure 3.11: Cancer Stemness Marker Enrichment with GelMA-Pm vs. ULA 3D culturing. (A) A bar graph representing sphere number per mm2 of ULA or GelMA-Pm cultures **(B)** Western blot images of ALDH1A1 and SOX-2 proteins for groups Conventional Monolayer, Sphere Medium Monolayer, UV exposed Sphere Medium Monolayer, ULA spheroids and GelMA-Pm Spheroids. **(C)** OVCAR-3 cell line ALDH1A1, SOX-2, NANOG and c-MYC mRNA expression level comparisons obtained with qPCR results for groups: Sphere Medium Monolayer, UV exposed Sphere Medium Monolayer, ULA spheroids and GelMA-Pm Spheroids. Data was normalized to Conventional Monolayer control group, which is represented as 1. **(D)** OVSAHO cell line ALDH1A1, SOX-2, NANOG and c-MYC mRNA expression level comparisons obtained with qPCR results for groups: Sphere Medium Monolayer, UV exposed Sphere Medium Monolayer, ULA spheroids and GelMA-Pm Spheroids. Data was normalized to Conventional Monolayer control group, which is represented as 1. n=3; mean ± SD, paired t-test applied and ns= not significant, $p < 0.1$ (*), $p < 0.05$ (**), $p < 0.01$ (***), $p < 0.001$ (****).

1.1.8 Selection of OVCAR-3 ULA Cell Line-Method Pair Reasoning

In addition to CSC marker proteins and cell surface markers, cancer stem cells may be enriched in other functions. These functions include epithelial to mesenchymal transition (EMT) characteristics, drug resistance behavior and colony formation abilities. When both cell lines were tested against these traits, OVCAR-3 showed significant gain of function phenotypes. These traits weren't as significant and notable in OVSAHO cell line.

EMT Marker Proteins

Among the proteins checked in the panel namely, Slug, Snail, TWIST1, Vimentin, Fibronectin, N-cadherin all showed increasing patterns compared to monolayer controls. E-cadherin which was expected to decrease, showed no change but overall N-cadherin/E-cadherin ratio increased nonetheless. In addition to these, cell cycle regulation proteins Cyclin D1 and and CDK2 was also found differentially expressed in spheroids.

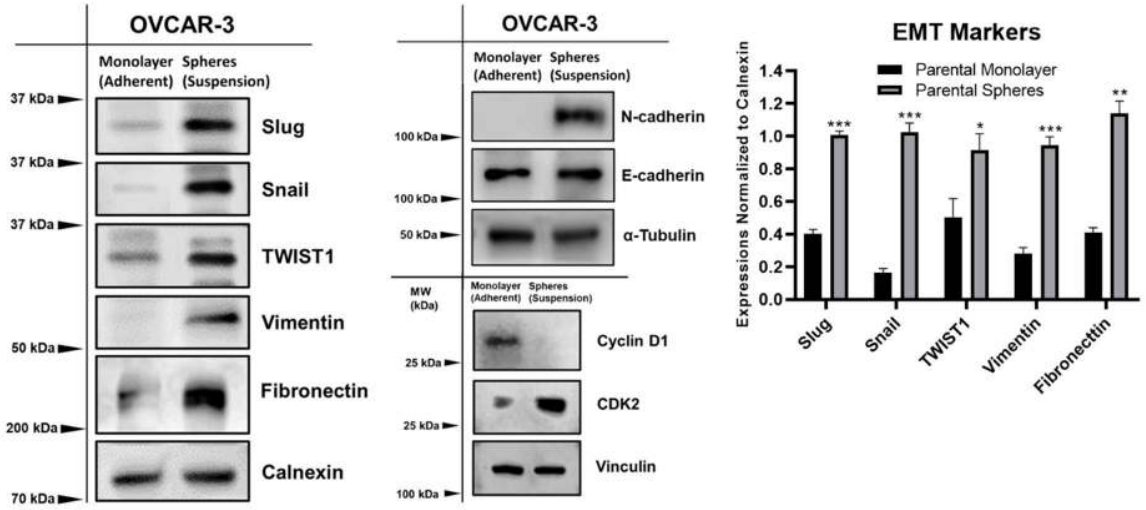

Figure 3.12: EMT marker and Cell Cycle Regulation Proteins Western Blots. Monolayer (adherent) vs. Spheroid enriched (ULA 3D cultured) OVCAR-3 cells western blot images and their quantitative analyses collected in bar graphs. Expressions were normalized to their respective house-keeping genes in the same membranes. n=3; mean ± SD, paired t-test applied and ns= not significant, $p < 0.1$ (*), $p < 0.05$ (**), $p < 0.01$ (***), $p < 0.001$ (****).

Multi-drug Resistance

A large panel of clinically used chemotherapeutic agents were applied to both monolayer and ULA spheroid enriched populations of OVCAR-3. The results were striking given that spheroid enriched group was found to have gained resistance to all but one drug in the panel. That drug was VEGF inhibitor Sunitinib and was found logical to have selectivity towards spheres enriched in many cell surface markers and EMT markers closely related to VEGF pathways. Rest of the drugs in the panel that have given significantly higher IC_{50} values were Carboplatin, Cisplatin, Niraparib, Olaparib, Paclitaxel and Doxorubicin. This NCI-SRB panel also included Olaparib and Carboplatin resistant subtypes of OVCAR-3 obtained by prolonged increasing dose treatment of the drugs. They were part of Irem Durmaz Sahin's laboratory cell line archive and was used as controls to compare spheroid resistance extent. In addition to NCI-SRB panel, for Carboplatin and Niraparib which showed approximately two-fold IC_{50} values, colony formation assays were performed and the results served as

visualization of the resistance phenotype and increased colony formation abilities of the OVCAR-3 ULA spheroids.

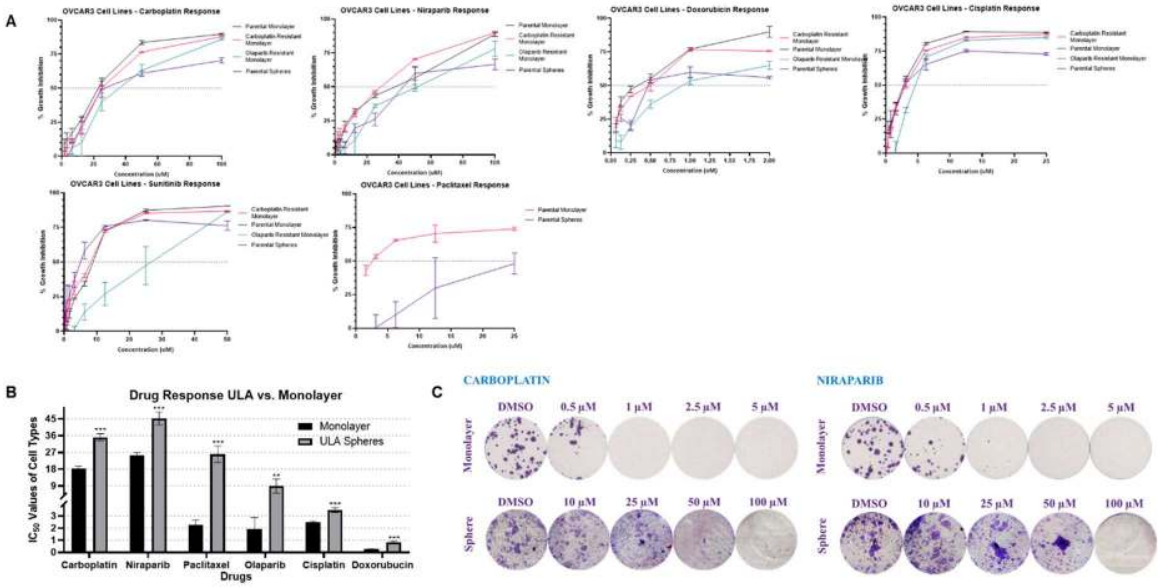

Figure 3.13: Drug Resistance Phenotypes of OVCAR-3 ULA Spheroids. (A) Growth inhibition graph summaries of NCI-SRB assays with Parental Monolayer, Olaparib Resistant, Carboplatin Resistant and ULA Spheroid OVCAR-3 strains. **(B)** Bar graph summary of IC_{50} values of Monolayer vs ULA Spheroid OVCAR-3 cells. **(C)** Colony formation assays for Monolayer vs ULA Spheroid OVCAR-3 cells. n=3; mean ± SD, paired t-test applied and ns= not significant, $p < 0.1$ (*), $p < 0.05$ (**), $p < 0.01$ (***), $p < 0.001$ (****).

While OVCAR-3 cell line showed these abilities with ULA method, it was found inapplicable or inconsistent with GelMA-Pm method. For drug resistance assays, drugs needed additional applications such as being labelled or trackable to verify it is indeed resistance behavior and not GelMA ECM blocking or slowing down diffusion. In addition, western blotting posed the limitations mentioned above therefore to detect EMT markers and other proteins, confocal microscopy imaging was required which would in turn call for mass production of GelMA-Pm structures (at least 3 samples for each protein in question). To sum up, for many analyses ULA method was concluded to be more productive and handy.

Regarding the cell line choice for following experiments, this thesis hypotheses required two groups to compare to each other where one shows significant increases in CSC traits, drug resistance characteristics, EMT increase was a bonus that could not be overlooked. Expanding

all these reasons, OVCAR-3 cell line was found more appropriate to the hypotheses, stable and reproducible model when grown with ULA+spheroid enrichment media as described in detail in the prior sections. From this point on, the thesis will refer to this selected cell line-method pair as spheroid group for short. Sphere media monolayer can be referred to as SMM and adherent conventional 2D grown OVCAR-3 cells can be referred to Mono or Monolayer for short.

1.2 Evaluating the Established 3D Culture Techniques with Patient Derived Primary (*ex-vivo*) Cells

To extend our findings beyond established cell lines, four primary samples were obtained from HGSOC patients during cytoreductive surgery (two from tumor tissues and two from ascites). Cells were successfully cultured under both ULA and GelMA-Pm conditions, forming spheroids with comparable efficiency. Representative brightfield images of patient-derived spheroids in both culture systems are shown in the following figure. (Figure 3.14-A).

Drug sensitivity was assessed using SRB assays with four clinically relevant agents (Carboplatin, Paclitaxel, Olaparib, Niraparib) (Figure 3.14-B). Parallelly, baseline SOX-2 expression levels were determined from patient tissue RNAs, serving as a reference unaffected by in vitro culture. A general trend of higher SOX-2 expression correlating with greater drug resistance was observed. For instance, Patient 1, with the lowest SOX-2, displayed the greatest sensitivity to three of the drugs, while Patient 2, with the highest SOX-2, showed resistance across most treatments. Patient 3 was notably resistant to Carboplatin, whereas Patient 4 deviated from this correlation pattern (Figure 3.14-C).

qPCR analysis of CSC markers SOX-2 and NANOG under monolayer, ULA, and GelMA-Pm conditions demonstrated that GelMA-Pm more strongly promoted CSC marker expression across most samples (much like OVSAHO cell line), though variability existed (Figure 3.14-D). Correlation heatmap analyses revealed that ULA enrichment was more consistent with patients' baseline SOX-2 status, whereas GelMA-Pm occasionally induced CSC traits in samples with initially low CSC representation (Figure 3.14-E). Interestingly, spheroid number did not align positively with CSC traits or resistance, suggesting that higher spheroid counts do not necessarily equate to a more stem-like or drug-resistant phenotype.

In summary, both ULA and GelMA-Pm supported CSC enrichment in patient-derived samples. ULA tended to reflect patients' intrinsic CSC status more faithfully, while GelMA-Pm provided a stronger induction of stemness features, even in samples with low initial CSC marker expression. This distinction highlights the complementary value of the two systems for ex vivo modeling of CSC biology.

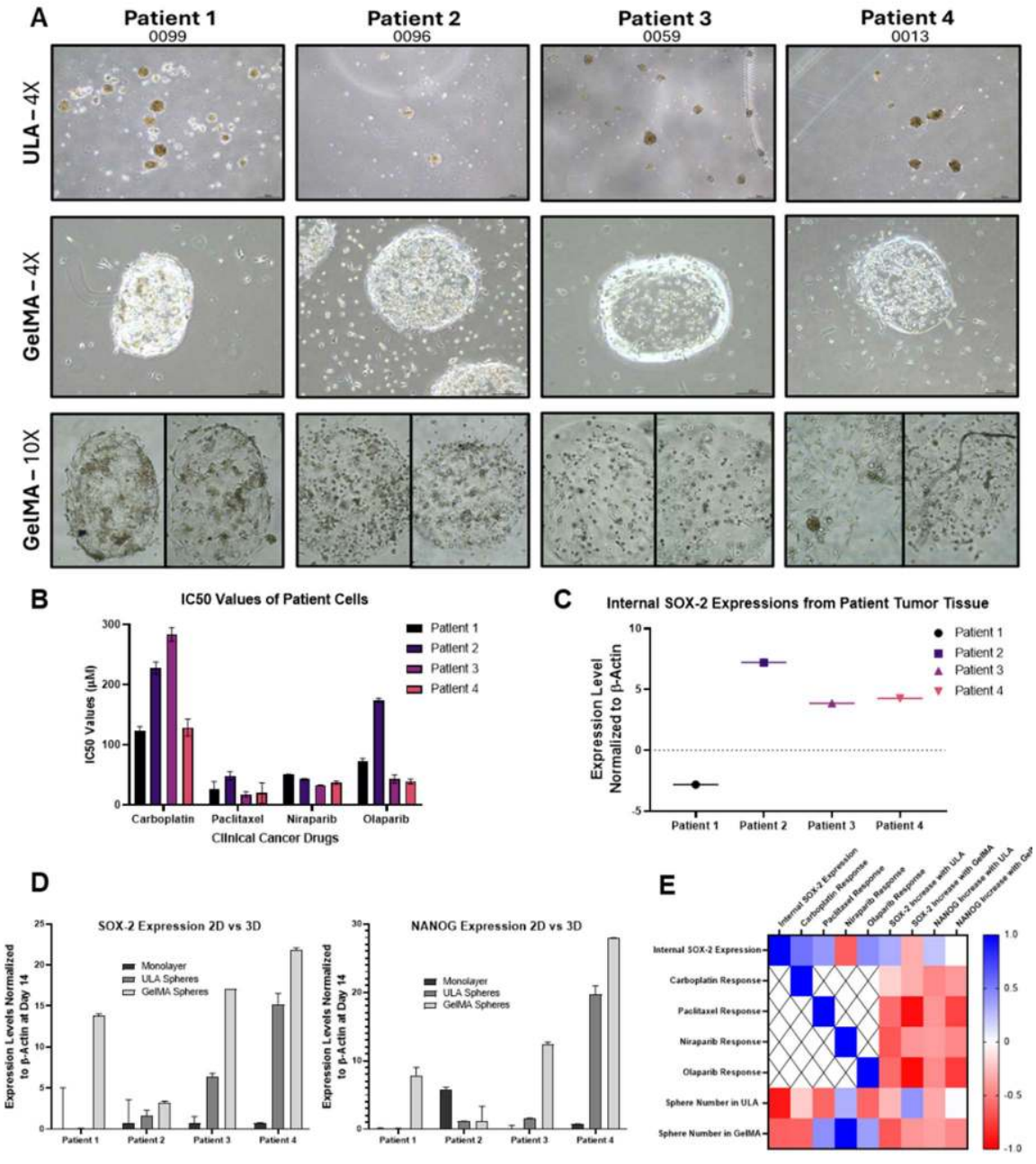

Figure 3.14: ULA and GelMA-Pm as CSC representation models with HGSOC patient-derived primary cells. (A) Brightfield images of primary cells cultured in ULA and GelMA-Pm conditions (top: 4X; bottom: 10X magnification of GelMA-Pm structures). **(B)** IC_{50} values of patient-derived cells against Carboplatin, Niraparib, Paclitaxel, and Olaparib in 2D monolayer cultures, determined by NCI-SRB assay. **(C)** Baseline SOX-2 expression levels measured from patient tumor tissues, normalized to β-actin. **(D)** RT-qPCR analysis of CSC-associated transcripts (SOX-2, NANOG, ALDH1A1, c-MYC) in 2D, ULA-3D, and GelMA-Pm-3D cultures, normalized to β-actin. **(E)** Correlation heatmap of drug responses, spheroid formation, and CSC marker expression (blue = high correlation; red = low correlation). n=3; mean ± SD, paired t-test applied and ns= not significant, $p < 0.1$ (*), $p < 0.05$ (**), $p < 0.01$ (***), $p < 0.001$ (****).

1.3 Small RNA-Seq and Differential miRNA Expression Analysis Between CSC-Traits-Enriched Spheres and Monolayer

1.3.1 Analysis and General Results

Small RNA-Seq procedure was applied between OVCAR-3 monolayer and sphere cultures. Analysis of raw data was performed with a pipeline optimized according to several publications in the literature. Analyses were performed on a Linux based computer using classical bash codes and DESeq2 analysis and graph production was performed with R Studio. Summary of the analysis pipeline and the miRNA counts volcano plot is found in the following figure (**Figure 3.15**).

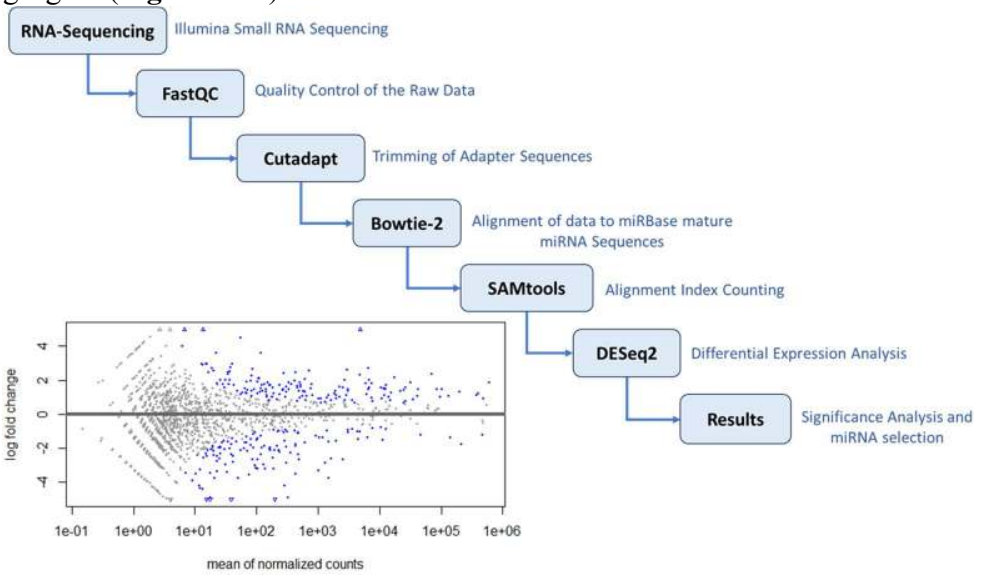

Figure 3.15: Small RNA-Seq Pipeline and miRNA Count Volcano Plot. Bioinformatic tools used for analysis is listed in the scheme and miRNA counts are represented. DESeq2 volcano plot for OVCAR-3 spheres vs monolayer (n=2 per group). Differential expression by DESeq2 Wald test with BH correction; colored points denote significantly deregulated miRNAs (padj threshold as indicated on the plot). Top candidates used for downstream qPCR are labeled.

1.3.2 miRNA Selection After qPCR Validations and Patient Sample Investigations

According to the overexpression and downregulation tables obtained from small RNA-Seq results, most "log to fold change" showing 20 downregulated and 20 upregulated miRNAs were isolated and literature was scanned to detect most novel candidates in ovarian cancer and stemness contexts. 3 upregulated and 7 downregulated miRNAs were selected to further validate with qPCRs.

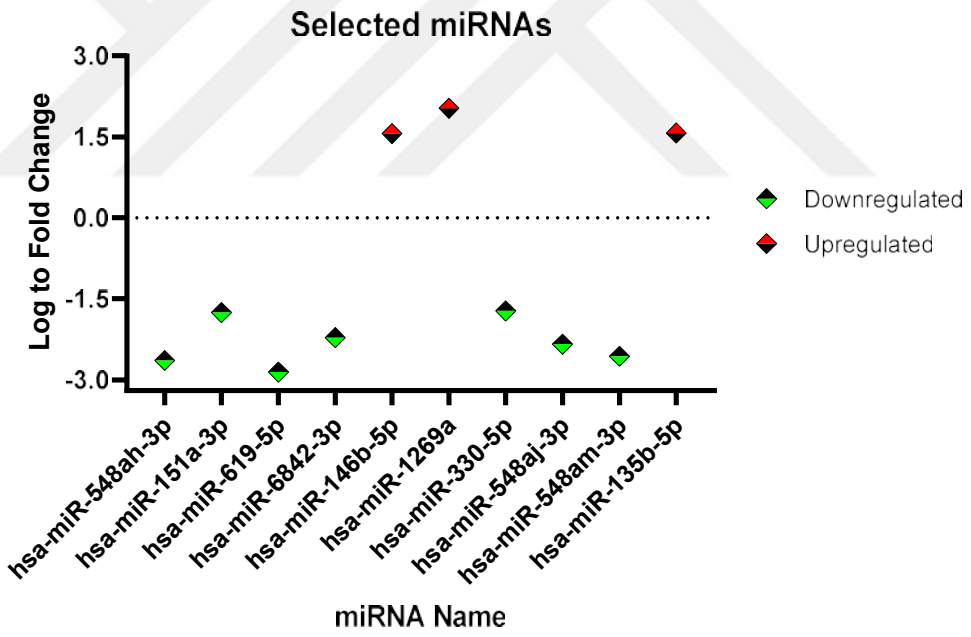

Figure 3.16: Selected 10 miRNAs from small RNA-Seq Results. Chosen from the top 20 downregulated and top 20 upregulated lists after literature curation for novelty in ovarian/CSC contexts. These candidates were taken forward for RT-qPCR screening. (n=3)

Above graphed 10 miRNAs and 2 additional miRNAs in our lab were used in a series of qPCRs. Among these 12 miRNAs, 4 miRNA RT-qPCR results were found most consistent

with the small RNA-seq results. These were hsa-miR-548ah-3p, hsa-miR-let7b-5p, hsa-miR-146a-5p, hsa-miR-146b-5p, two of them downregulated and two of them upregulated respectively. Later on the most novel and underexplored one hsa-miR-548ah-3p was also

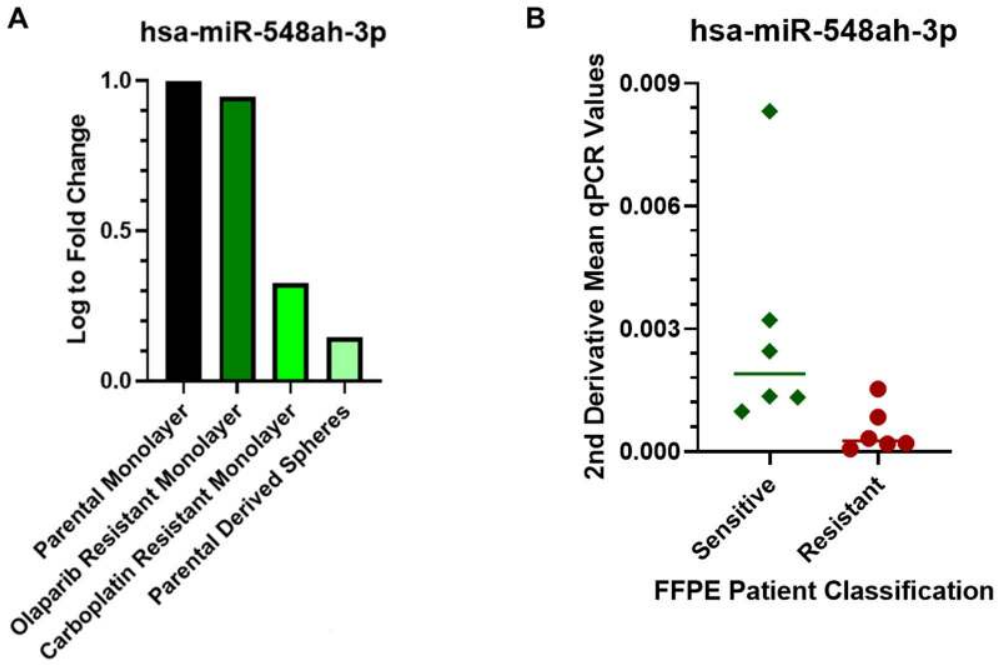

found downregulated in Olaparib resistant and Carboplatin resistant strains of OVCAR-3. Not only that, but an FFPE patient tissue cohort of 14 patients were also evaluated. According to their clinical characteristics, these samples were classified as resistant or sensitive by the gynegological oncologists of Koç University Hospital. The classified patient samples showed downregulated hsa-miR-548ah-3p levels in resistant classified ones compared to the sensitive group.

Figure 3.17: OVCAR-3 Resistant Subtypes and FFPE Patient Samples hsa-miR-548ah-3p Levels. (A) OVCAR-3 subtypes: miR-548ah-3p expression is lower in Olaparib-resistant, Carboplatin-resistant, and spheroid subtypes versus parental monolayer (each n=3). Statistics: one-way ANOVA with BH-adjusted post-hoc comparisons vs parental; *, **, *** shown above bars. **(B)** Patient FFPE cohort: miR-548ah-3p is decreased in clinically resistant vs sensitive samples (n=14 total; group sizes indicated on plot). Statistics: two-sided Mann–Whitney U (non-parametric across patients); exact p reported on the plot; $p < 0.1$ (*), $p < 0.05$ (**), $p < 0.01$ (***), $p < 0.001$ (****).per legend.

1.4 Downregulated hsa-miR-548ah-3p Expression Restoration with Mimic Experiments and CSC Traits Reversal

1.4.1 Cell Surface Marker Expressions Under miR-548-ah-3p Mimic Treatment

Flow Cytometry Results of CSC Surface Marker Expressions

After hsa-miR-548ah-3p was found as a promising tumor suppressor miRNA, mimic treatment experiments were conducted. Within the experimental set-up as a negative control, a non-targeting miRNA molecule was delivered in the same conditions miR-548ah-3p mimic was delivered. In addition to rule out transfection reagent toxicity, "lipofectamine only" sphere control group was added. Among every CSC surface markers detected upregulated in spheres earlier, was found to decrease in expression upon mimic treatment and was found unchanged or insignificantly changed with negative control treatment.

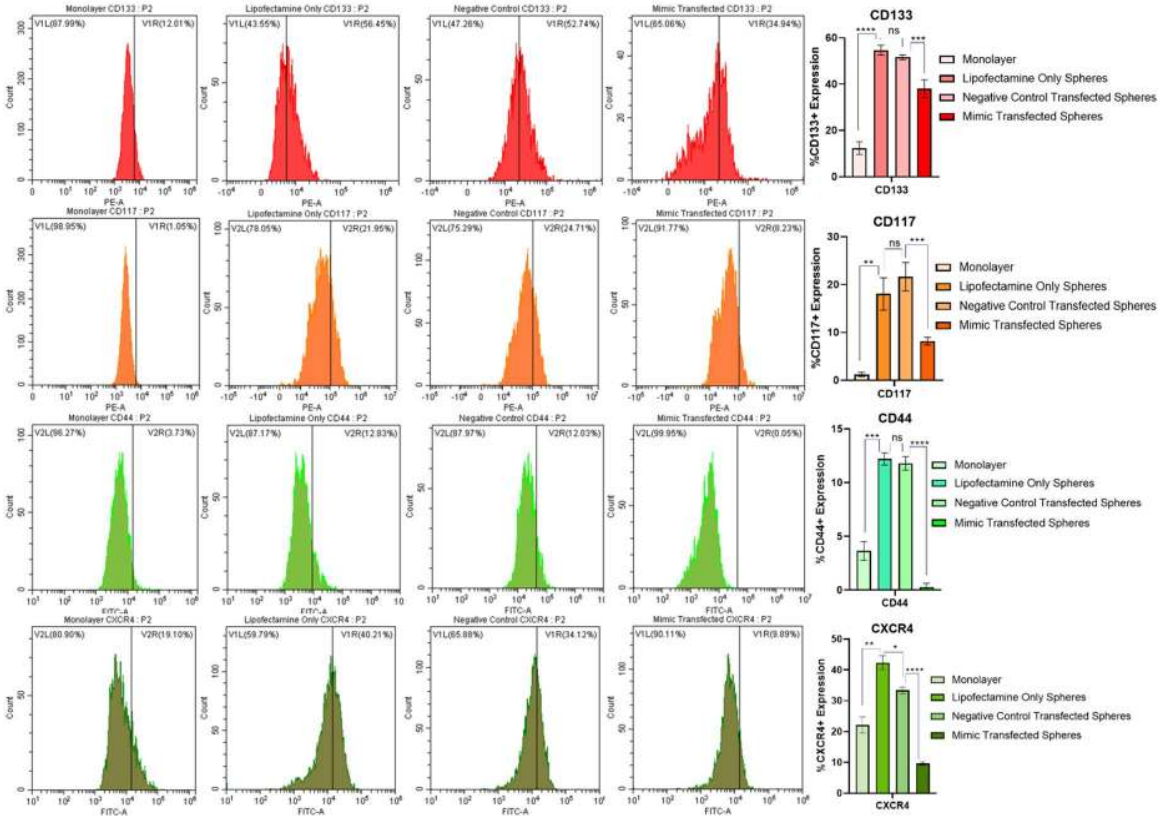

Figure 3.18: Flow Cytometry Results of CSC Surface Marker Expressions Restoration with Mimic Treatment. Percent-positive cells for CD133-PE, CD117-PE, CD44-FITC, CXCR4-FITC under mimic, negative control (NC), and lipofectamine-only sphere conditions

(n=3 each). One-way ANOVA across the three groups for each marker with BH adjustment across markers; mimic < NC for all markers (CXCR4 decreases as well) with $p < 0.1$ (*), $p < 0.05$ (**), $p < 0.01$ (***), $p < 0.001$ (****).indicated above comparisons. Bars = mean ± sd.

Confocal Microscopy Images of Some CSC Surface Marker Expressions

For cell surface markers CD44 and CD133, apparent decrease was observed in confocal microscopy images as well. Reason for the choice of these cell surface markers were primarily to be able to double stain so different conjugates were needed to be selected. Among PE conjugates CD133 expression is high and plausible to image. Among CD44 and CXCR4 the prior was chosen because within biological replicas it gives more consistent results and according to flow cytometry results it shows the most significant decrease upon mimic treatment.

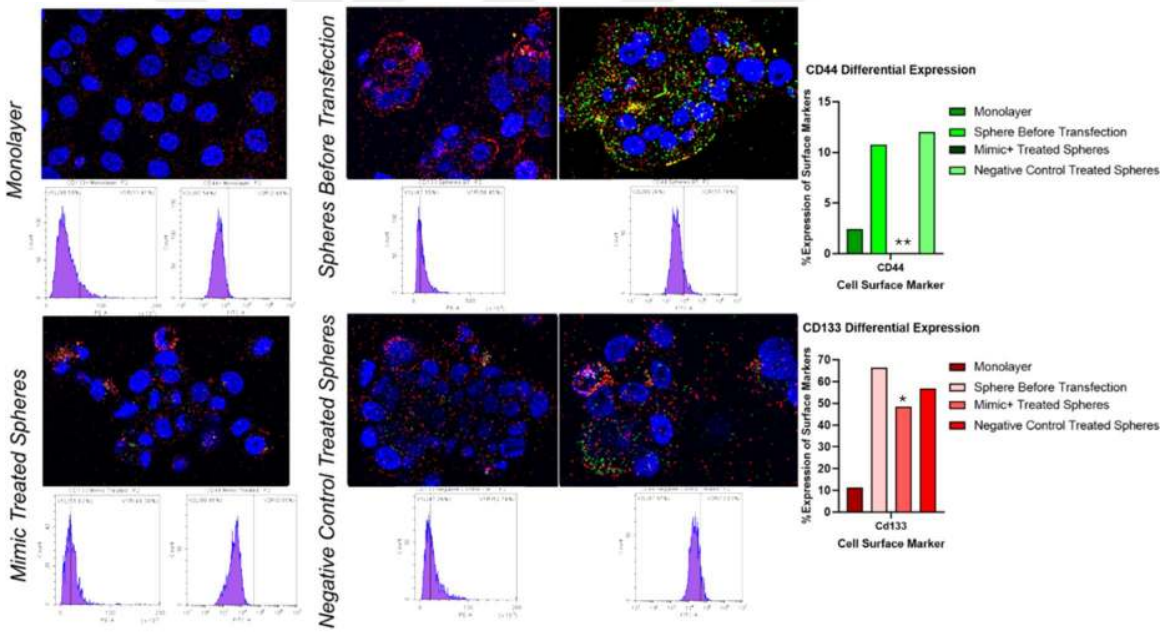

Figure 3.19: Flow Cytometry Results and Confocal Images of CSC Surface Marker Expression with Mimic Treatment. Left: flow-cytometry quantification for CD133 and CD44 shows significant decreases with miR-548ah-3p mimic vs NTC (n=3; two-sided t-tests with BH for two markers; $p < 0.1$ (*), $p < 0.05$ (**), $p < 0.01$ (***), $p < 0.001$ (****).). Right: representative confocal z-stacks (DAPI/α-tubulin/CD133-PE or CD44-FITC) illustrate visibly diminished surface staining in the mimic group relative to NTC. Scale bars as indicated.

1.4.2 Cancer Stem Cell Marker Proteins Expressions Under miR-548-ah-3p Mimic Treatment

CSC marker proteins' expression levels were evaluated with western blot experiments. All CSC markers checked except NANOG showed a meaningful and significant decrease in western blot experiments. Western blots were performed 48h after miRNA mimic treatment application. (OCT-4 was excluded from the panel due to showing no increase in sphere group in the first place.)

In addition, one of these markers, SOX-2 has a high target match score in miRDB target search platform with miR-548ah-3p miRNA. Therefore investigating mRNA levels of SOX-2, at the same time evaluating the mimic expression levels after the treatment was a practical experimental approach. The results showed that mimic expression remains drastically high, even at the 7 day mark after the initial treatment. SOX-2 mRNA levels started to fall after day 5 and reached to a significant drop at day 7.

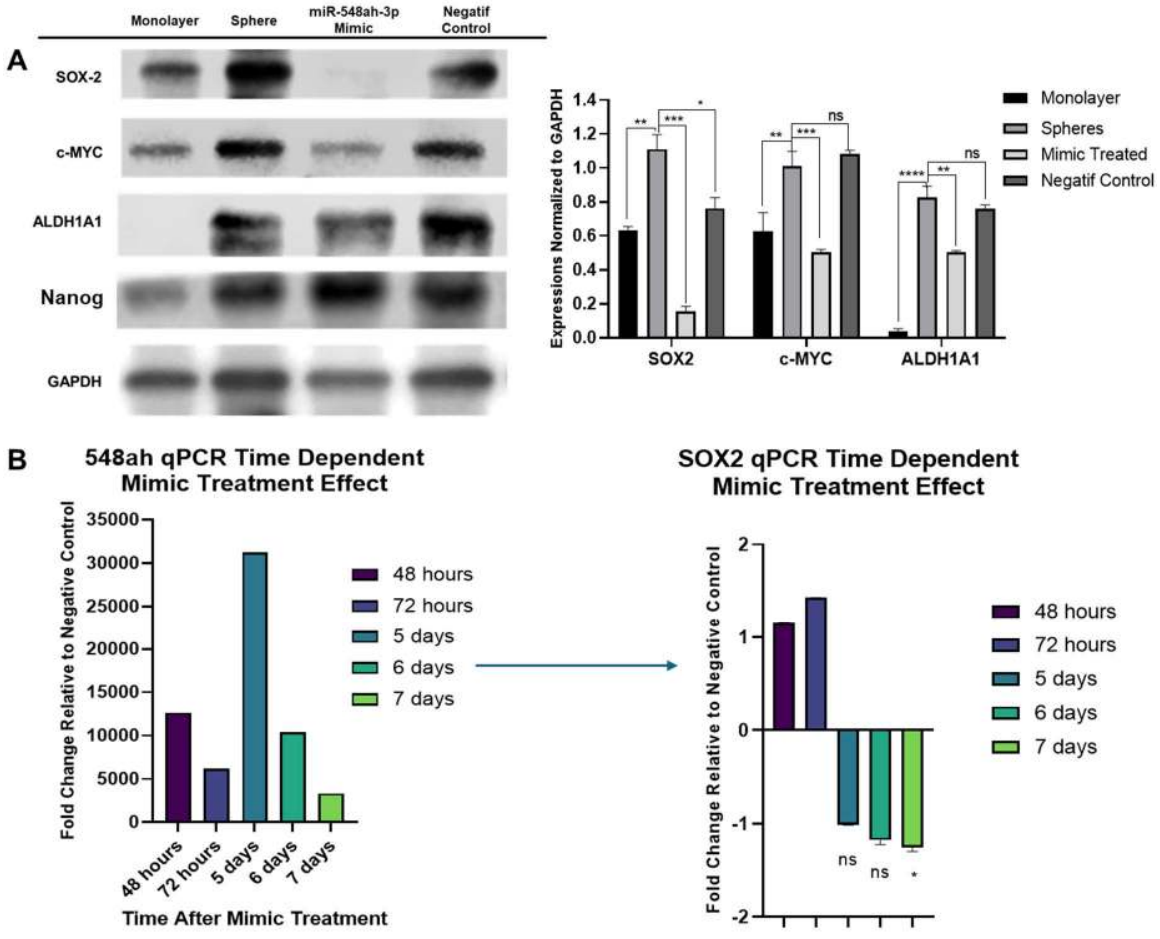

Figure 3.20: Cancer Stem Cell Marker Proteins and mRNA Expressions Under miR-548-ah-3p Mimic Treatment. (A) Western blots for SOX2, ALDH1A1, CD133, CD117, CD44 (NANOG unchanged) 48 h after miR-548ah-3p mimic vs NTC in spheres (n=3). Densitometry normalized to loading control and NTC (=1). Statistics: two-sided t-tests per marker with BH correction; markers show significant decreases with mimic $p < 0.1$ (*), $p < 0.05$ (**), $p < 0.01$ (***), $p < 0.001$ (****).; NANOG ns. **(B)** RT-qPCR time course shows sustained high mimic levels (miR-548ah-3p) and a progressive decrease in SOX2 mRNA (noted at day 5, significant by day 7) relative to day 0 (n=3). Statistics: one-way ANOVA with Dunnett's multiple comparisons vs day 0; $p < 0.1$ (*), $p < 0.05$ (**), $p < 0.01$ (***), $p < 0.001$ (****) on the plot.

1.4.3 Drug Resistance Phenotypes Under miR-548-ah-3p Mimic Treatment

After seeing the reversal (or can be called rescue) of CSC traits with internal CSC protein and cell surface markers expression levels the drug resistance phenotype was revisited and investigated under mimic treatment, lipofectamine treatment, negative control miRNA treatment compared with monolayer drug responses and each other's. Indeed miR-548ah-3p mimic treatment, spheres showed an apparent sensitization to all four drugs in the panel. From the initial panel Carboplatin, Olaparib, Paclitaxel and Niraparib were selected due to them being standard of care in HGSOC clinical practices. The negative control usually remained unaffected and as resistant as lipofectamine control spheres whereas mimic treated spheres

showed increased growth inhibition with lower doses of drugs approaching the response of monolayer control group.

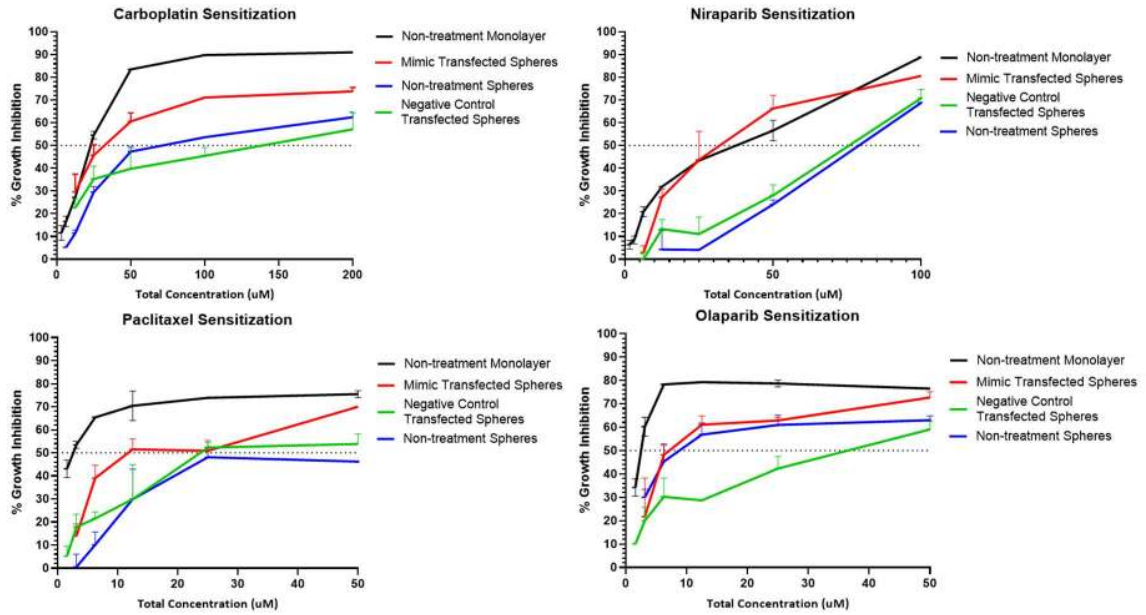

Figure 3.21: Drug Sensitization Effect of miR-548ah-3p Treatment. miR-548ah-3p mimic treatment resulted in sensitization to chemotherapeutic agents Carboplatin, Olaparib, Paclitaxel, Niraparib in drug resistance acquired spheroids. n=3 all mimic treatments were found significant with two-way ANOVA.

1.4.4 Migration and Invasion Abilities Under miR-548-ah-3p Mimic Treatment

Given the reversal of CSC characteristics, next question was if spheroids gain the migration and invasion abilities and if mimic treatment could reverse their capacity. As expected, miR-548ah-3p mimic treatment had a significant inhibiting effect on both migration and invasion. To evaluate this, spheroids were reduced to single cells and seeded onto Cultrex covered or normal trans-well migration assay inserts. Cell numbers were kept equal as the monolayer group and same control groups were applied. Treatments were done before trans-well insert seeding, knowing that mimic effect remains for at least 7 days.

Although the migration and invasion traits are low in all groups, ImageJ colony counting yielded that spheres have significantly higher mobility than monolayer group and mimic treated group were observed decreased at both abilities, lower than monolayer control group.

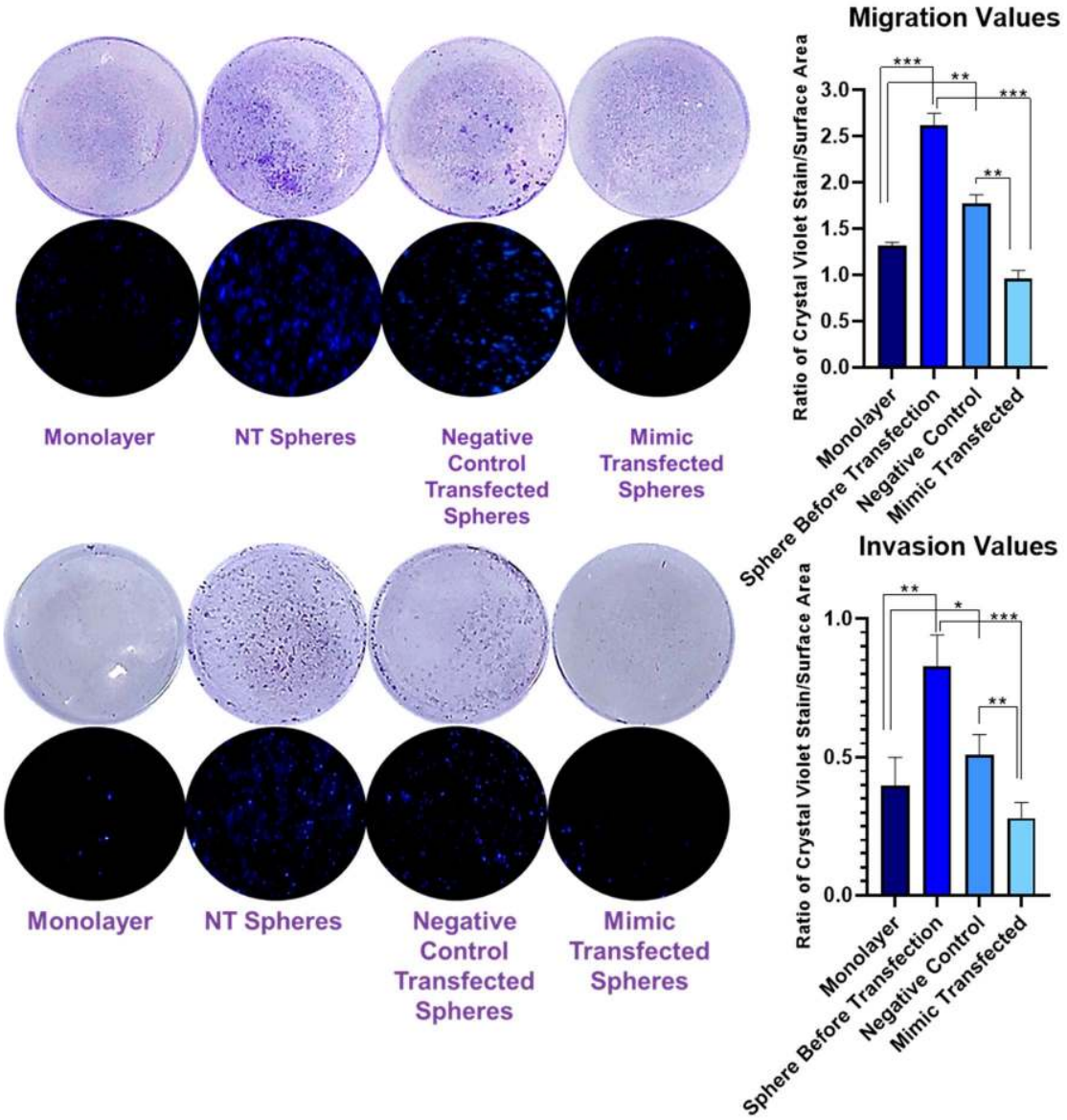

Figure 3.22: Migration and Invasion Assays with miR-548ah-3p Treatment. Transwell migration (no matrix) and invasion (Cultrex-coated) quantified by ImageJ colony/field counts (n=3). One-way ANOVA across Monolayer, NTC spheres, Mimic spheres (per assay) with BH-adjusted post-hoc tests: NC > Monolayer (higher motility in spheres), while Mimic < NC and Mimic ≤ Monolayer $p < 0.1$ (*), $p < 0.05$ (**), $p < 0.01$ (***), $p < 0.001$ (****) as shown. Representative images included.

1.5 Investigation of mRNA Expressions and Alternative Polyadenylation Patterns in CSC Traits Enriched Spheres and Spheres Under Prolonged miR-548ah-3p Mimic Treatment

Although miRNA functional studies bear valuable in vitro results, the clinical applications are still behind the vast information accumulated about miRNAs. While unveiling miR-548ah-3p as an important regulator of cancer stemness, for it to be a candidate to enter clinical trials, many aspects could be researched. Along with *in vivo* studies that is the major pre-requisite of clinical trials, we could also investigate some of the side effects or disadvantages of miR-548-ah-3p using molecular techniques and bioinformatic analyses.

For this aim, an RNA-Seq analysis was performed for three groups: Sphere Medium Monolayer (SMM or Mono), Negative Control miRNA treated Spheres (NC-) and miR-548-ah-3p Mimic treated Spheres (Mim+). To capture long term effects of mimic treatment on the cells, mimic were not treated once and sent to sequencing, rather both NC and Mim+ groups were given the respective molecules for over a month (6 weeks). miR-548ah-3p Mimic and non-targeting miRNA molecules were treated to spheroid maintained cultures in 7-10 days to keep their levels constantly high in the spheroids for a prolonged time period. One notable thing during this prolonged treatment was neither NC- nor Mim+ groups were disturbed in a way that blocked compact spheroid formations. During this period, spheroids were counted in NC- and Mim+ controls as well as lipofectamine receiving group. No meaningful change in spheroid numbers were observed, although all three groups produced smaller spheroids due to frequent disturbance of the culture environments.

Another absent effect of miR-548ah-3p mimic was cell death. Although one could assume maybe the lethal dose of mimic were not being delivered to spheres, qPCR results of mimic treated spheres tells otherwise. Thousand-fold raises of the subject miRNA was observed in the early days after the treatment and the levels were remained steadily high for long periods of times, especially with prolonged treatment. miR-548-ah-3p mimic was also not observed lethal towards monolayer grown OVCAR-3 cells which was a promising result for it to be a clinical trial candidate in the future. Other promising results, along with some disadvantages were acquired with our RNA-Seq results which are presented in the following section.

3.5.1 Conventional RNA-Seq Analysis for Transcriptome Profiling and Detecting Differentially Expressed mRNAs in Spheres and Mimic Treated Spheres

Our RNA-Seq results delivered results that are both intriguing and somewhat coherent with some clinical trials of miRNA delivery to cancer patients as treatment.

Overexpressed and Downregulated Genes Between Monolayer and Spheres

RNA-seq results yielded important significantly upregulated and downregulated genes of different pathways. Gene Onthology (GO) Analysis matched downregulated genes to mostly cell cycle related genes. Some of the matched terms are: cell cycle, cell cycle process, regulation of cell cycle, mitotic cell cycle, mitotic cell cycle process, cell division, cell cycle phase transitions, cell cycle checkpoint signaling and other similar pathway names. Among the top downregulated cellular processes there are also DNA metabolic process, DNA repair, DNA replication, DNA templated DNA replication, chromosome organization, chromosome segregation, sister chromatid segregation, which will gain important meaning and correlation in the CRISPR screen results section.

Among the overexpressed genes pathway matches include: Regulation of cell differentiation, epithelial cell differentiation, secretion, export from cell, defense mechanism and system process. These pathways can be linked to CSC-EMT characteristics and drug resistance phenotypes.

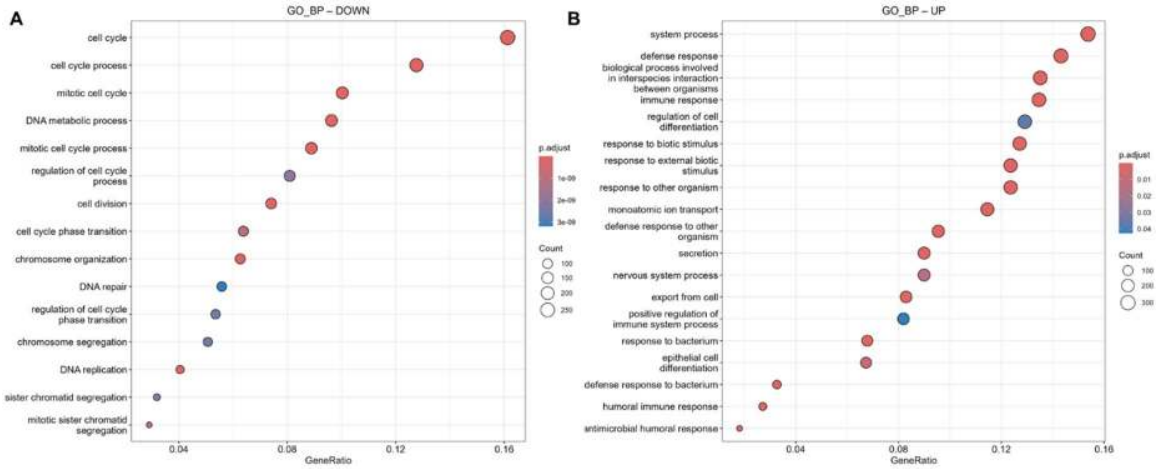

Figure 3.23: GO Pathway Analysis of Downregulated and Upregulated Transcripts Between Monolayer and Sphere Samples. (A) Downregulated in Spheres: enrichment for

cell cycle, mitotic processes, DNA replication/repair, checkpoint signaling. **(B)** Upregulated in Spheres: enrichment for differentiation, secretion/export, defense/system processes. DE by DESeq2 (padj ≤ 0.05); GO by BH-adjusted over-representation; dot size = gene count, color = $-\log_{10}$(padj). (n=3 per group.)

Differential Expression Patterns of Monolayer, Sphere and Mimic Treated Spheres

A heatmap of differentially expressed significant transcripts were drawn. Many genes are differentially expressed between monolayer vs. spheres group and some genes are returning to the expression more similar to monolayer than the spheres group after prolonged mimic treatment. These sections are marked with yellow squares in the heatmap.

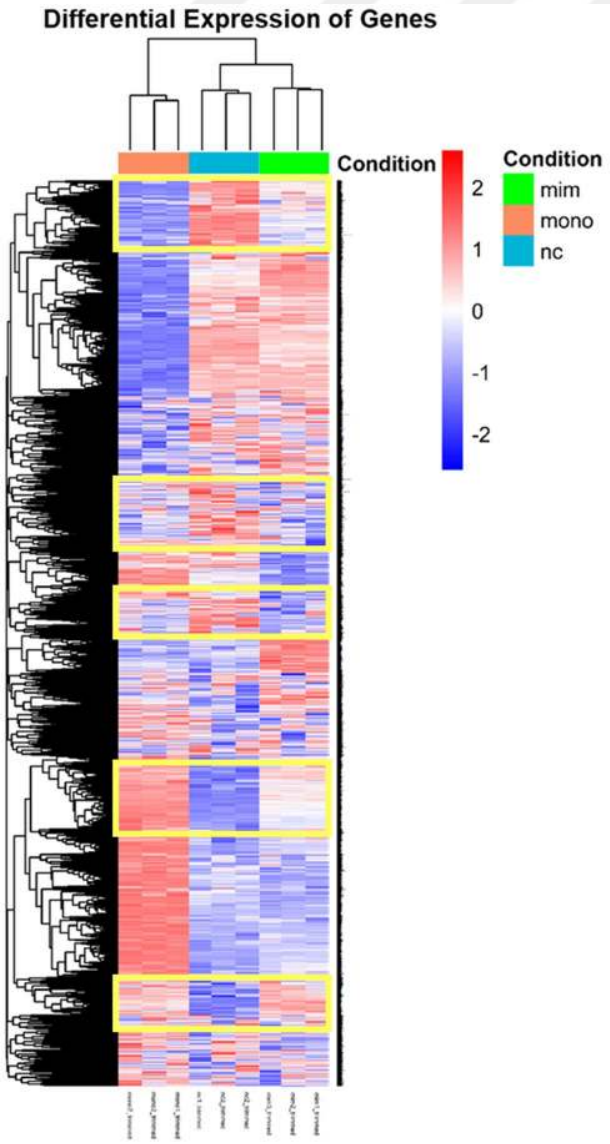

Figure 3.24: Differential Expression Heatmap and Mimic Drived Expression Restoration Regions. Variance-stabilized, row-z-scored counts for significant DE transcripts across Monolayer, NC- Spheres, Mimic+ Spheres (n=3 each). Yellow boxes highlight loci whose expression shifts toward Monolayer after prolonged Mimic (padj ≤ 0.05 vs NC-).

Differentially Expressed Transcripts Filtered for "CSC-EMT" from GO Annotations

After a general analysis and observing some "reversed" expressions with mimic treatment, the differentially expressed transcripts were then filtered for keywords on GO reported as part of CSC and EMT pathways. Later on from these genes, the ones overexpressed comparing monolayer to spheres but downregulated with mimic treatment (NC vs Mimic) genes were filtered again. This expression pattern will be called "rescue genes" from now on. Both heatmaps are represented in the following figure.

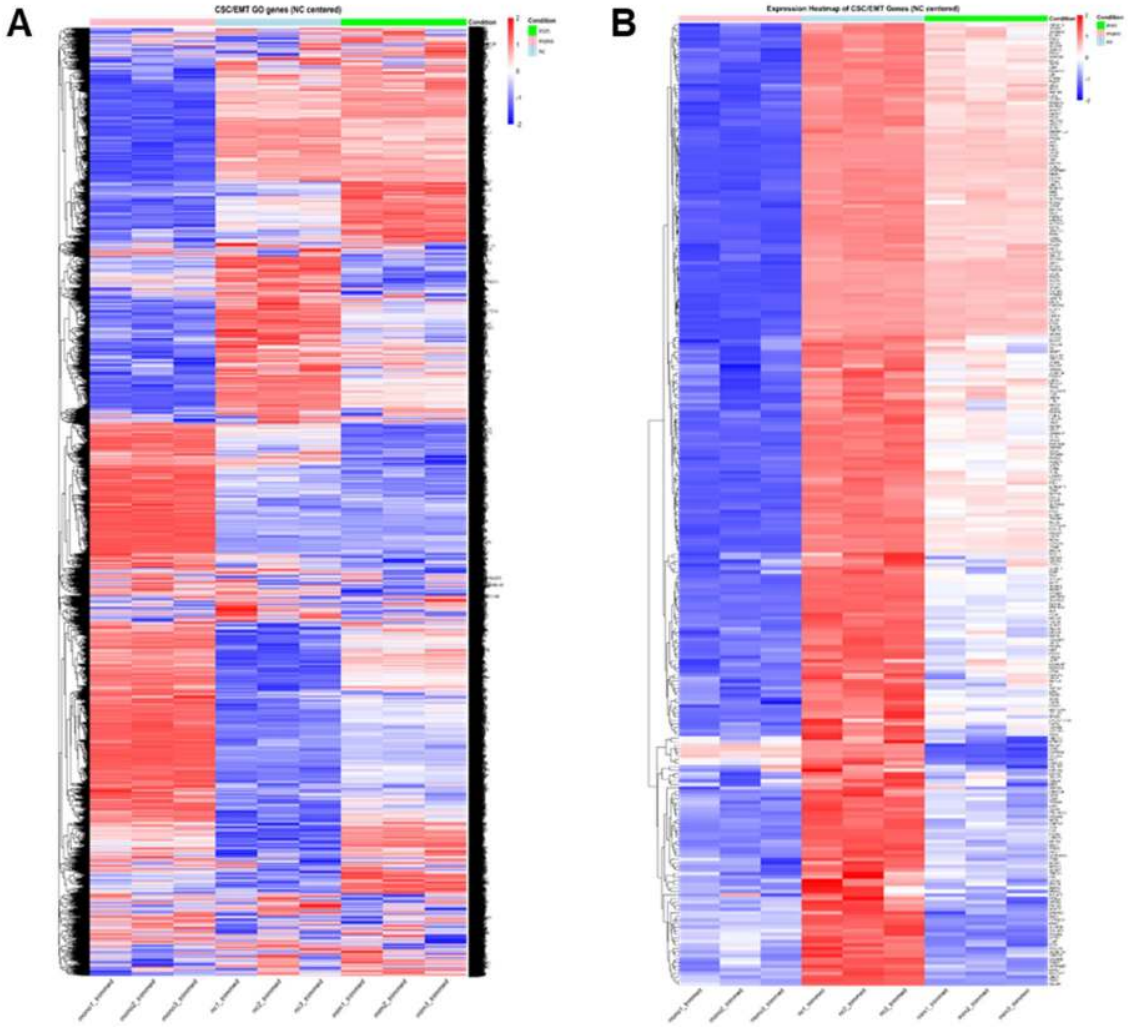

Figure 3.25: Heatmap of CSC-EMT Genes and Filtering "Rescue" Phenotypes. (A) DE genes annotated to CSC/EMT terms (GO keyword filter) across groups. **(B)** Rescue pattern subset: up in Monolayer vs NC- and down in Mimic+ vs NC- (padj ≤ 0.05 in both contrasts). Heatmaps show row z-scores; n=3 per group.

Among the Differentially Expressed Transcripts, Rescue Pattern Showing Ones Matched to miRNA Target Databases for Potential hsa-miR-548ah-3p Target mRNAs

Since miR-548ah-3p expression is downregulated when monolayers are grown as spheroids, its targets should be upregulated in spheres compared to monolayers. Same logic applies for when comparing Negative Control Spheres to miR-548ah-3p Mimic Treated group, miR-548ah-3p targets would be downregulated. From the significant differentially expressed gene lists, overexpressed ones in "Mono" vs "NC-" and downregulated ones in "NC-" vs "Mim+" were filtered and these genes were called "Rescue Pattern Transcripts". However, for target search this filter by itself was not enough to call these candidates miR-548ah-3p targets. To achieve a better filtering, miR-target prediction databases online were explored and all their target scores were combined to obtain a more reliable score table. (miRNA target databases studied, namely TargetScan, miRDB, DIANA-microT-CDS, miRmap, miRWalk, mirDIP, RNA22, RNAhybrid.) In the end, highest "log to fold change" overexpression numbers, lowest "log to fold change" downregulation negative values, and highest miRNA target match scores were combined to obtain a score we called "Rescue Score". Below the lollipop plot summarizes the top 50 transcripts with descending rescue scores, high potential of being miR-548ah-3p's mRNA targets.

Rescue-based analysis integrating RNA-seq differential expression with multi-database target prediction produced a ranked list of 100 high-confidence candidate targets of miR-548ah-3p (Figure 3.26). Several top candidates map directly onto CSC/EMT and drug-response programs, including VIM (vimentin), CXCR4, and KIT (CD117)—the latter two matching our flow-cytometry and imaging data, where surface CXCR4 and KIT levels significantly decreased after mimic treatment (see Figures 3.18–3.19). Additional high-ranked genes (PDGFA, KLF10, FRZB, SOX9, AKT3) align with stemness, ECM remodeling, and survival pathways. Collectively, these findings support a model in which miR-548ah-3p exerts

distributed repression across a network of CSC/EMT and resistance genes, rather than acting through a single dominant effector.

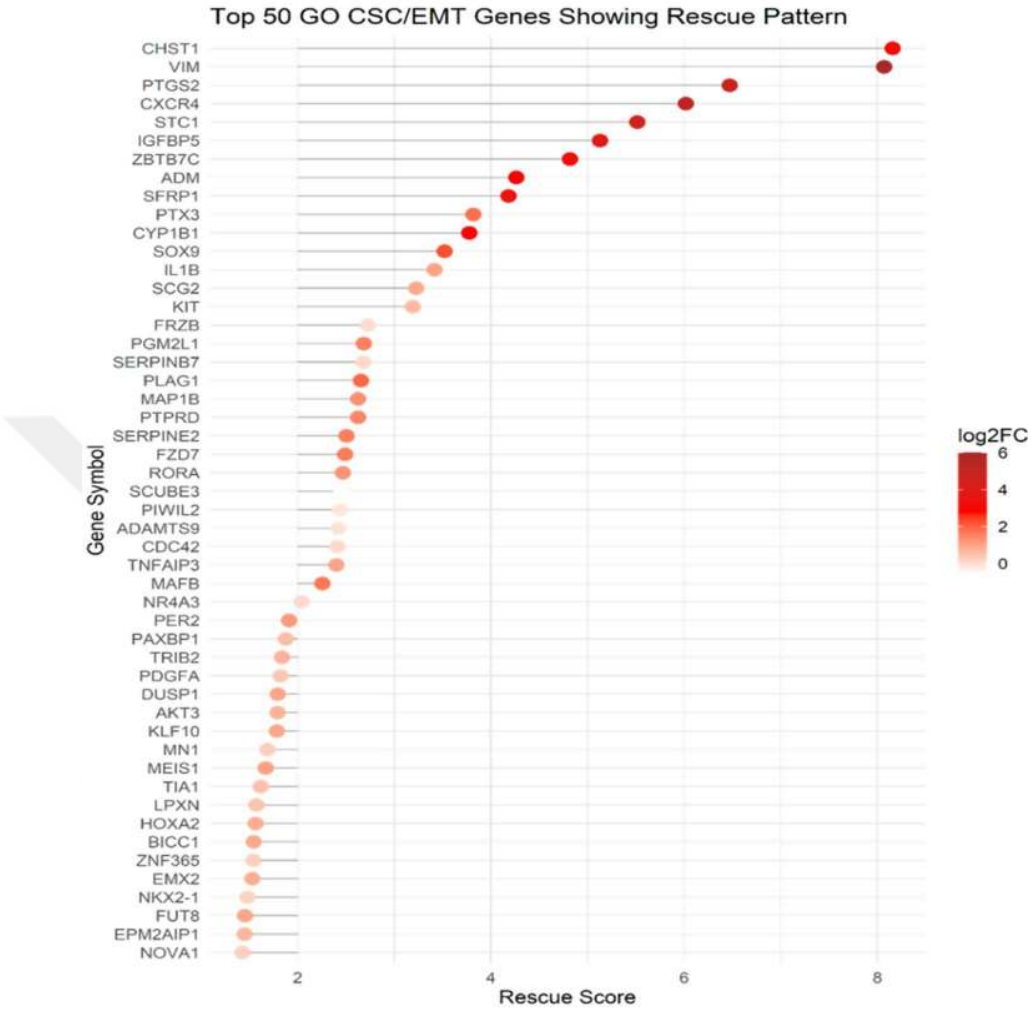

Figure 3.26: Top 50 high rescue score transcripts predicted as miR-548ah-3p targets. Lollipop plot ranking transcripts by an integrated Rescue Score combining (i) up in Monolayer vs NC-, (ii) down in Mimic+ vs NC-, and (iii) multi-database target predictions (TargetScan, miRDB, DIANA, miRmap, miRWalk, mirDIP, RNA22, RNAhybrid). Notables include VIM, CXCR4, KIT (CD117), KLF10, SOX9, AKT3, PDGFA. Concordant protein decreases for CXCR4/KIT with Mimic are shown in Figs. 3.18–3.19. (n=3 per group for RNA-seq contrasts.)

3.5.2 APA Profiling and 3'UTR Length Analysis

Alternative Polyadenylation mechanism is found responsible in come cancer driving mechanisms mostly by shortening the oncogenic mRNA 3'UTRs and escaping miRNA regulation. To address this mechanism in the context of cancer stemness and to evaluate if differential APA profiling might be a player, bulk RNA-Seq data were analyzed for 3'UTRs shortening and lengthening events. This analysis was done with QAPA tool.

Interestingly, more aggressive (migration and invasion capable, CSC-EMT enriched) and multidrug resistant spheres did not show major shortening of mRNAs, rather more lengthening events. This behavior is consistent with some iPSC and embryonic stem cell findings, which seems to favor longer mRNA 3'UTRs. These results can be interpreted as slowing metabolism and downregulation of most proliferative and cell cycle regulation genes. Quiescence and staying dormant while chemotherapy applications of CSCs is one of the major reasons they survive the primary treatment, later leading to recurrence when conditions are favorable for CSCs to switch to proliferative state.

While this trait may make CSCs more resilient towards chemotherapeutic agents, it may also make them more susceptible to miRNA therapies. Below heatmaps of common genes between differentially expressed mRNAs and differential 3'UTR length presenting transcripts were filtered and heatmaps of them are shown side by side. Heatmaps were not clustered (--FALSE) to show the dominant colors in each event, where blue represents downregulation of mRNAs and lengthening of 3'UTRs, and red represents upregulation of mRNAs and shortening of 3'UTRs. Spheroid Negative Control column is more blue than monolayer in both heatmaps, downregulation events are correlated with lengthening of 3'UTRs, as the general knowledge about APA mechanisms expects. On the other hand, mimic treated spheroids remain lengthened but mRNA expressions are upregulated back. The red distribution does not reach

the level of monolayer in the mimic treated group but it is still significantly higher than negative control spheroids.

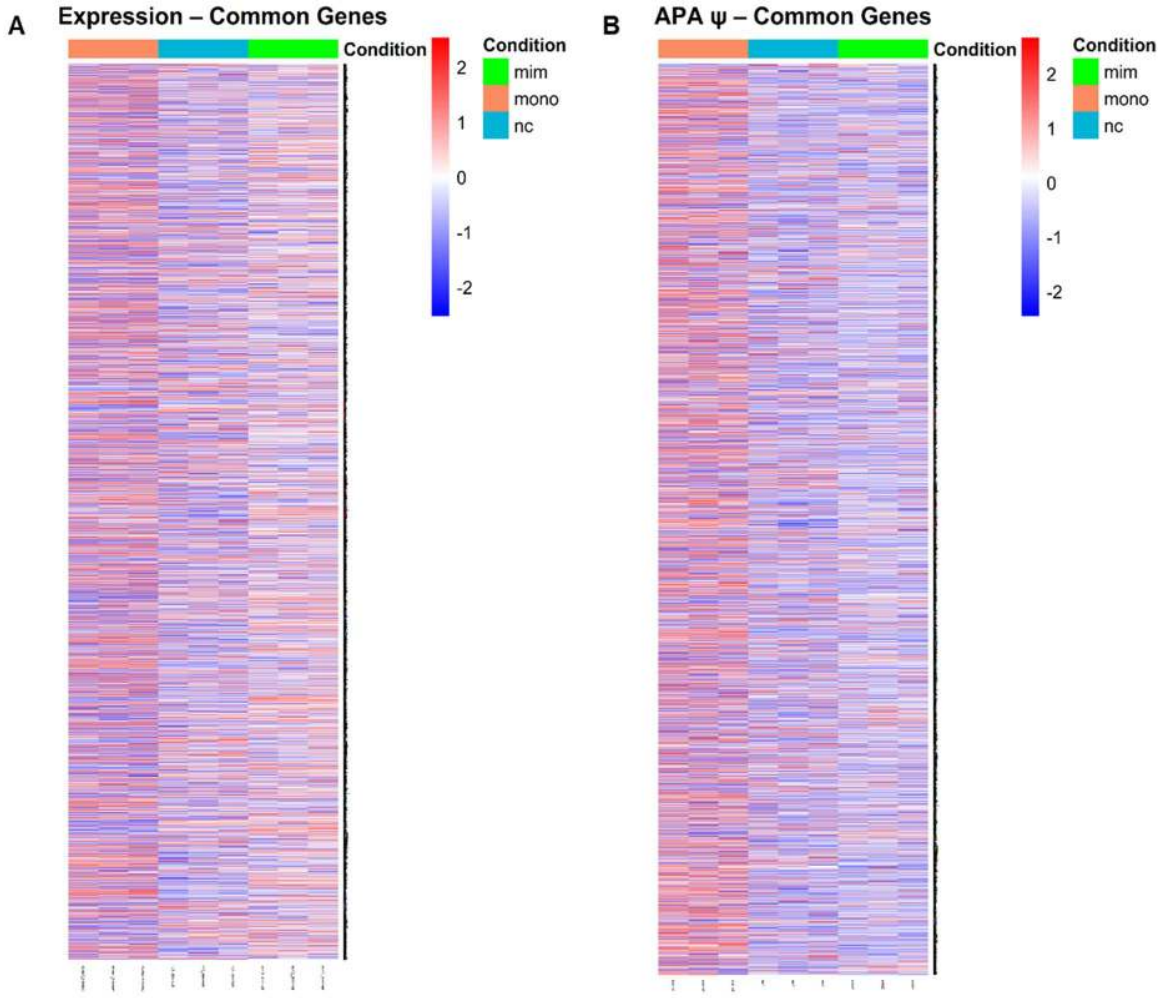

Figure 3.27: Heatmaps of Common Genes Between Differentially Expressed mRNAs and Differential 3'UTR Length Presenting Transcripts. Side-by-side heatmaps for genes shared between DE lists and APA-changing transcripts (QAPA ΔΨ). Blue = downregulated / lengthened; red = upregulated / shortened (legend on plot). NC- Spheres show a blue-shift relative to Monolayer (down + lengthened). Mimic+ shows partial expression restoration while remaining lengthened at many loci. DE by DESeq2 (padj ≤ 0.05); APA by ΔΨ with FDR filtering (threshold indicated); n=3 per group.

Correlation analysis was performed between Monolayer and NC- Spheres differentially expressed transcripts and their APA profiles, as well as NC- spheres and Mimic+ groups.

There is a positive correlation between the prior compared groups whereas the latter group has a negative correlation curve. Figure 3.28 also contains a correlation dot plot with the transcripts names, APA and mRNA expression patterns. Red dots represent NC- vs Mim+ and blue dots represent Mono vs NC-. Blue dots are situated around the x-axis while red dots are more scattered. Some housekeeping genes are observed in these common genes.

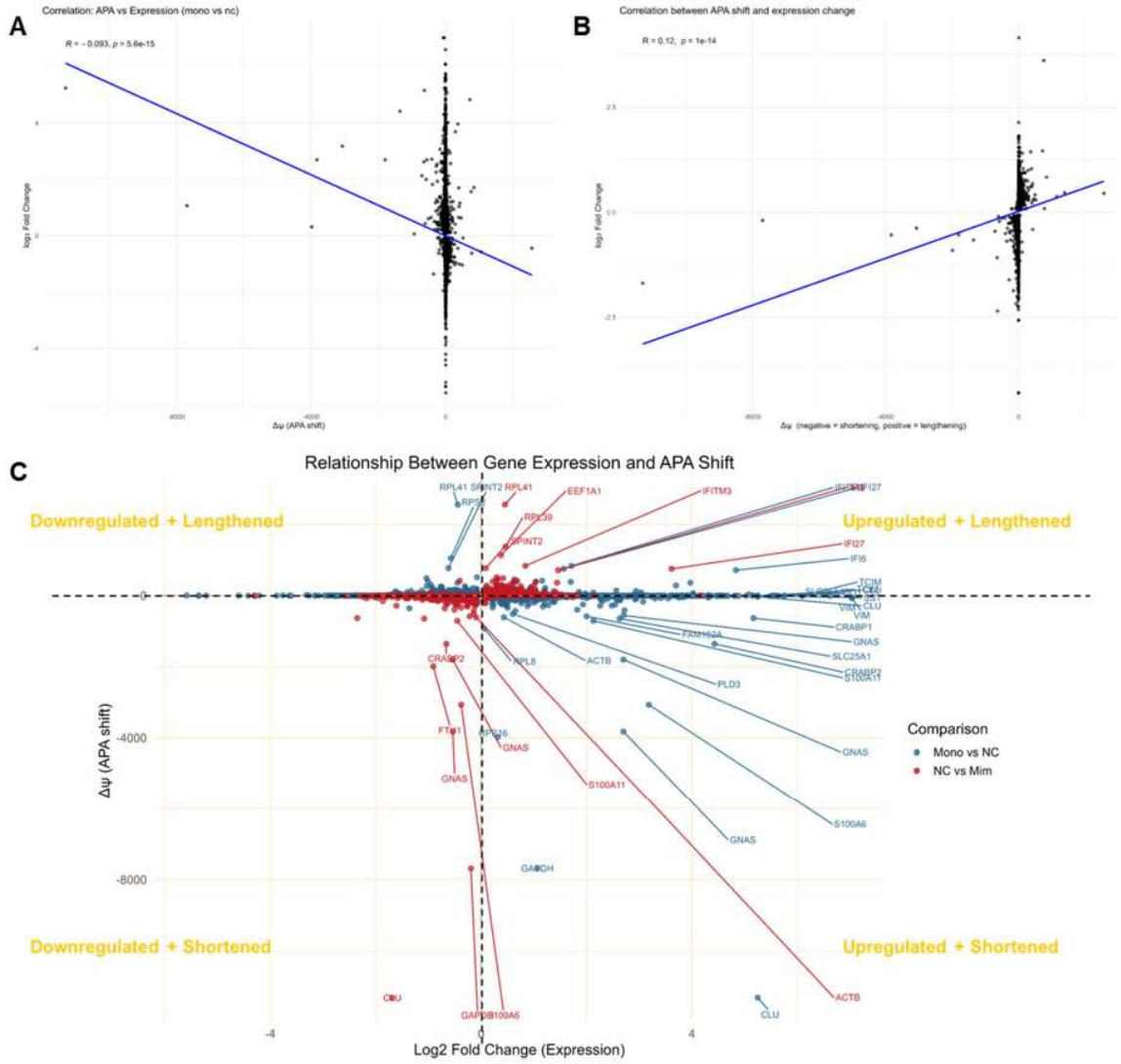

Figure 3.28: Correlation Analysis of Differentially Expressed Transcripts and Their APA Profiles Between Groups. (A) Monolayer vs NC-: positive correlation between log_2FC and ΔΨ (lengthening associates with downregulation). **(B)** NC- vs Mimic+: negative correlation (expression recovery despite sustained lengthening at many loci). (C) Labelled scatter of transcripts with quadrant annotation (Q1 up/lengthened; Q2 down/lengthened; Q3

down/shortened; Q4 up/shortened). Spearman ρ and exact p values shown on each panel; n=3 per group.

A possible scenario is hsa-miR-548ah-3p is also targeting some key APA regulatory units and cell's APAlytion is also restrained. One such gene is CPEB4 of APA.

1.6 Epigenetic Regulators CRISPR Knockout Screen (EPI-KOL) Between CSC Enriched Spheres and Conventional Monolayer Cells

Along with post-transcriptional investigations as the 3D culturing system yielded valuable results about CSC trait enrichment, performing a CRISPR-KO system and detecting essential genetic regulators of CSC enrichment was applicable and plausible. In cancer stemness contexts, CRISPR screening is still rare in the literature, due to culture restrictions and obtaining CSC specific control vs experimental groups. Although CSC process in the organisms are highly diverse and cancer-type and patient specific, applying a screen in the established system could yield noteworthy results and ideas about what CSC maintenance depends on. For this aim, as we focused on post-transcriptional regulations so far, we wanted to perform an "epigenetics" focused CRISPR dropout screen.

1.6.1 Preparation for CRISPR-KO Screen Utilizing EPI-KOL sgRNA Library

EPI-KOL library was prepared and functionally tested by (Yedier-Bayram et al., 2022) and the plasmids were kindly provided by Tugba Bagci Onder's laboratory. After obtaining the plasmids viral production and MOI calculations for transfection on OVCAR-3 cells were conducted as detailed in the methods section. During this time, OVCAR-3 cells were also transducted with Cas9 expression viruses. This step was also crucial because low cas9 expression could drop the screen efficiency whereas high cas9 expression could negatively affect cell line viability. To test the Cas9 activity efficiency, a GFP gRNA containing viral transduction was applied to Cas9 expressing OVCAR-3 cells (MOI = 2.0). Cas9 expressing OVCAR-3 cells were transfected with GFP plasmids and after green fluorescence was validated with fluorescent microscopy, GFP targeting and Non-targeting viral particles were

given to them. Flow cytometry results showed a significant decrease in GFP signal, validating OVCAR-3 cells function with the amount of Cas9 they express.

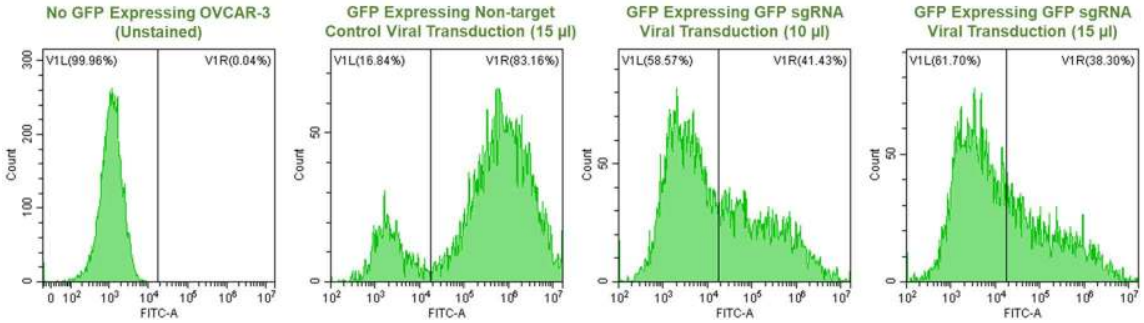

Figure 3.29: Cas9 Activity Efficiency Test with GFP transduction. Flow cytometry histograms for GFP-expressing OVCAR-3 ± GFP-targeting vs non-targeting virus (two input doses). %GFP$^+$ cells significantly decrease with targeting virus in Cas9-expressing cells (n=3; two-sided t-tests vs non-targeting at each dose). Representative fluorescence micrographs provided.

1.6.2 Results Obtained from Epigenetic CRISPR-KO Screen and Potential Essential Elements of CSC enrichment in HGSOC

Following validation of Cas9 activity, the pooled epigenetic sgRNA library (EPI-KOL) was introduced into OVCAR-3 cells cultured under monolayer condition then to identify essential regulators of CSC maintenance, transduced cells were divided randomly, some were seeded as monolayer culture some were seeded as ULA suspension cells and spheroid formation was waited. Genomic DNA was extracted at baseline (t_0) and after 14 doubling times (t_{14}). These doubling times were measured prior to screen initiation since spheres have slowed proliferation times, time doubling time between spheroids and sphere medium grown monolayers had a 2-fold doubling time difference, that was taken into account.

sgRNA cassettes were amplified by nested PCR, and libraries were sequenced on an Illumina platform. Quality control of raw reads confirmed uniform representation of sgRNAs at t_0, ensuring adequate coverage of the library. Processed reads were mapped to the reference guide set, and count matrices were generated. Downstream analysis was carried out with MAGeCK, which uses a maximum-likelihood framework to estimate gene-level selection scores by comparing sgRNA abundance between conditions. Negative selection highlighted

genes whose loss impaired spheroid formation, what can be called as “essential genes for CSC enrichment and non-adherent growth”.

Validation of Screen Performance

The following figure (Figure 3.31) includes confirmation analyses of the reliability of the CRISPR-Cas9 knockout screen. Several quality control steps were carried out. Analysis of sgRNA read count correlations across biological replicates showed strong agreement, reflecting stable library distribution and reproducible screening performance. When β scores were ranked, the expected enrichment of both non-targeting controls and essential gene controls was observed, supporting the screen’s ability to separate genuine dependencies from background noise. In addition, volcano plot visualization highlighted significant depletion of known housekeeping and core essential genes—including ribosomal proteins and DNA replication factors—consistent with their well-established necessity for cell survival. Taken together, these evaluations indicate that the screen maintained sufficient coverage, sensitivity, and specificity, and thus provides a sound foundation for identifying essential regulators in the context of HGSOC spheroids.

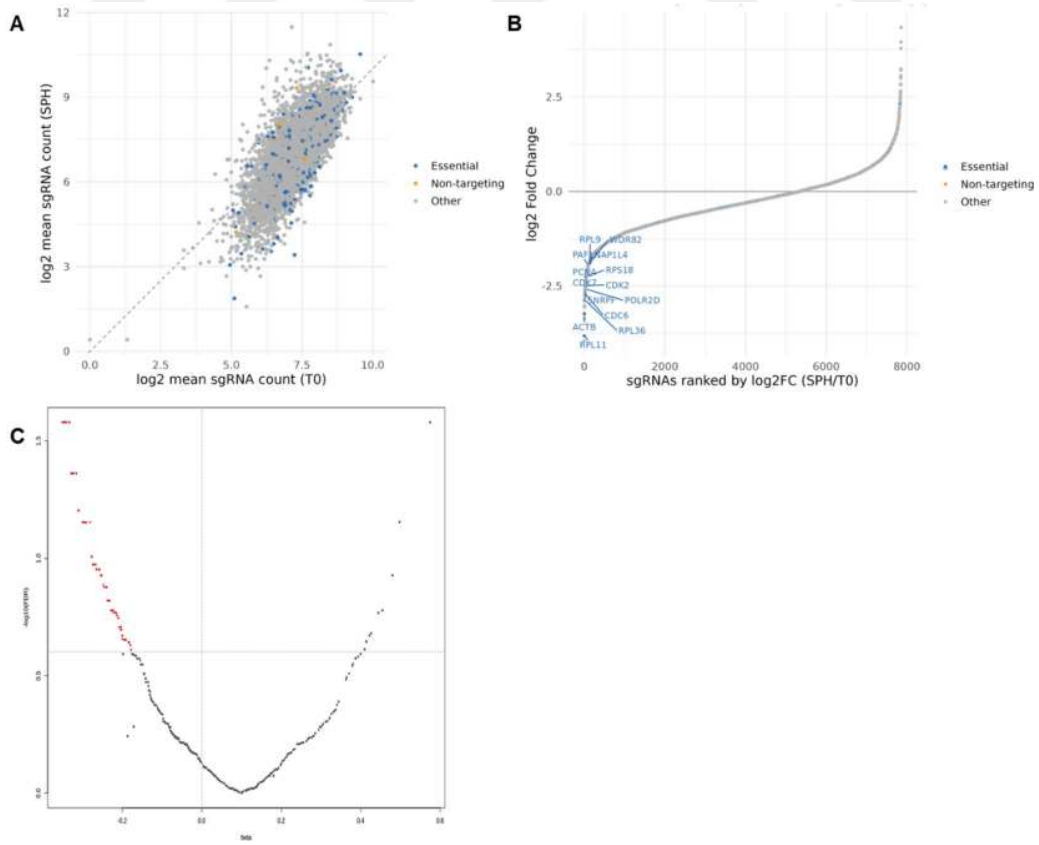

Figure 3.30: Confirmation of CRISPR-KO Screen Reliability and Validation of Performance. (A) Replicate concordance: scatter of normalized sgRNA counts with high Pearson r across replicates (values on plot). **(B)** Rank plot of gene β-scores with core essential genes depleted and non-targeting controls neutral. **(C)** Volcano of β vs $-\log_{10}$(FDR) showing significant depletions (red). Library coverage, Gini indices, and sample-wise count distributions summarized on the figure; FDR by MAGeCK (BH).

Epigenetic CRISPR-Screen "Hits" and Their Pathway Analyses

Pathway enrichment of the most stringent hit list (FDR < 0.1) revealed strong convergence on DNA damage response and chromatin-related processes. Among the top categories were regulation of DNA repair, histone modification, homologous recombination, recombinational repair, and epigenetic regulation of gene expression. Additional terms included DNA replication, regulation of mRNA processing, and cell cycle G1/S transition. These results indicate that the highest-confidence dependencies for spheroid survival involve safeguarding genome integrity, maintaining proper chromatin architecture, and tightly regulating transcriptional and replication programs—all processes critical for sustaining CSC traits in high-grade serous ovarian cancer.

Expanding the threshold to FDR < 0.25 uncovered a broader network of biological processes, extending the stringent hits with categories linked to stem cell biology and checkpoint control. In addition to DNA repair, chromatin modification, and replication, enriched terms included stem cell population maintenance, negative regulation of stem cell differentiation, cell number homeostasis, and mitotic G2/M transition checkpoints. These findings suggest that, beyond core DNA repair and chromatin regulators, ovarian CSCs also depend on broader stemness-maintaining and cell cycle checkpoint pathways, further underscoring their reliance on transcriptional plasticity and cell fate control mechanisms.

All genes were mapped to GO database with GO enrichment tool in R.

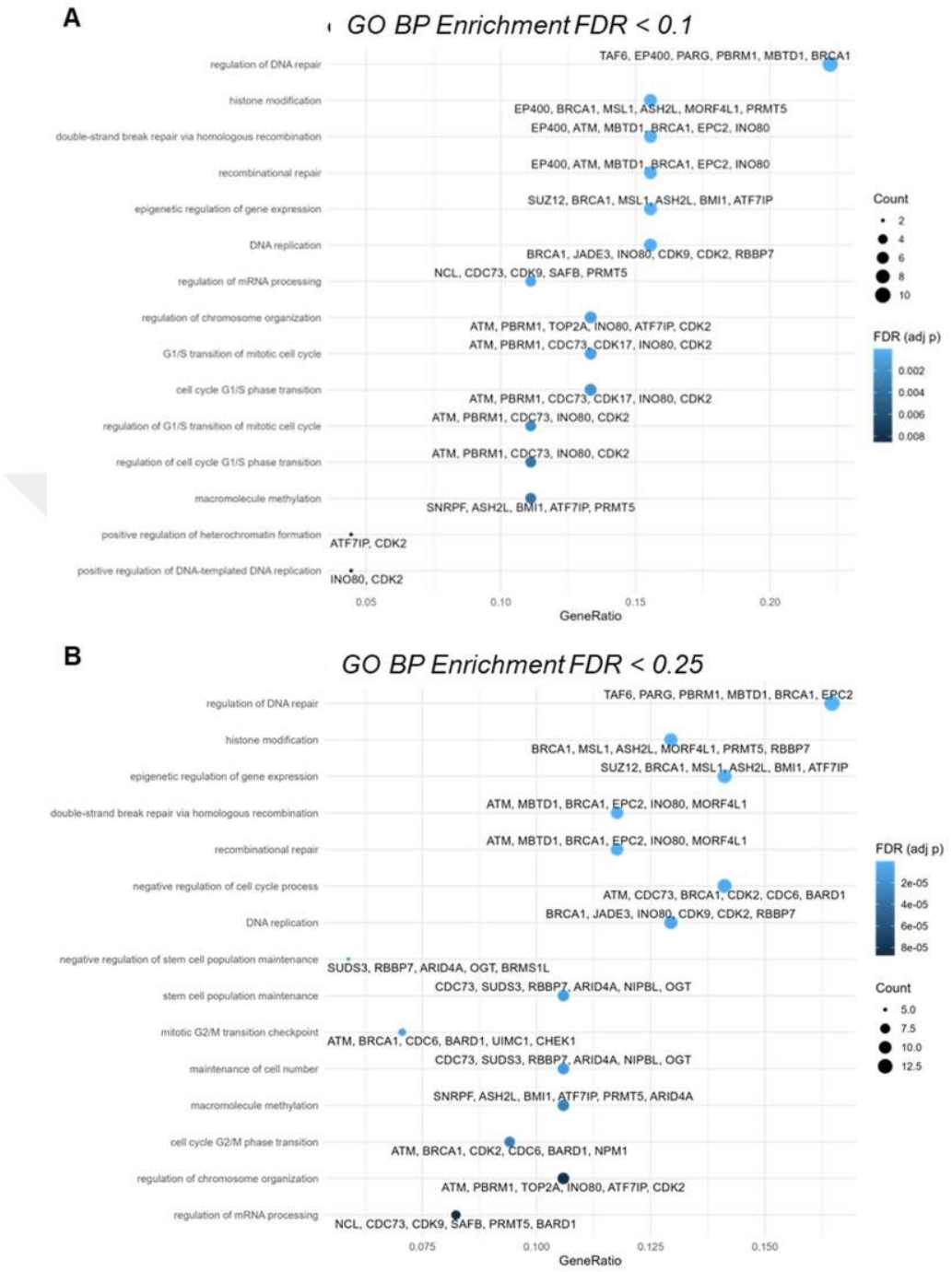

Figure 3.31: Epigenetic CRISPR-Screen Hits and Their Pathway Analyses. (A) Stringent set (FDR < 0.10): GO terms concentrate on DNA repair, histone modification/PRC2, homologous recombination, chromatin regulation, replication, cell-cycle control. **(B)** Broader set (FDR < 0.25) recapitulates core terms and adds stem-cell population maintenance, negative regulation of differentiation, checkpoint control. Dot size = gene count; color = –

$\log_{10}$(padj).*Epigenetic CRISPR-Screen "Hits" That Confer CSC Enrichment/Non-adherent Growth*

Analysis of the ranked gene-level results (ordered by FDR (< 0.1) and then by β) revealed a coherent set of regulators that are selectively essential for spheroid maintenance. Among the top hits were canonical DNA damage response genes such as ATM and BRCA1, notable examples because ovarian cancer prognoses highly dependent on DNA damage repair pathway deficiencies and BRCA1/2 mutations. The identification of multiple polycomb complex components—including SUZ12, EPC2, EP400, PBRM1, and MBTD1—further underscores the importance of chromatin remodeling and epigenetic silencing in sustaining stem-like properties. Additional depleted genes included splicing and RNA processing factors (SNRPF, SYNCRIP), transcriptional regulators (TAF6, MUM1), and PAR metabolism (PARG), reflecting the broad dependency of CSCs on transcriptional and RNA metabolic plasticity. Collectively, these results suggest that ovarian CSC spheroids may be depending on an integrated network of DDR effectors and polycomb-associated chromatin regulators, thereby linking DNA repair, epigenetic control, and RNA processing as convergent vulnerabilities in this context.

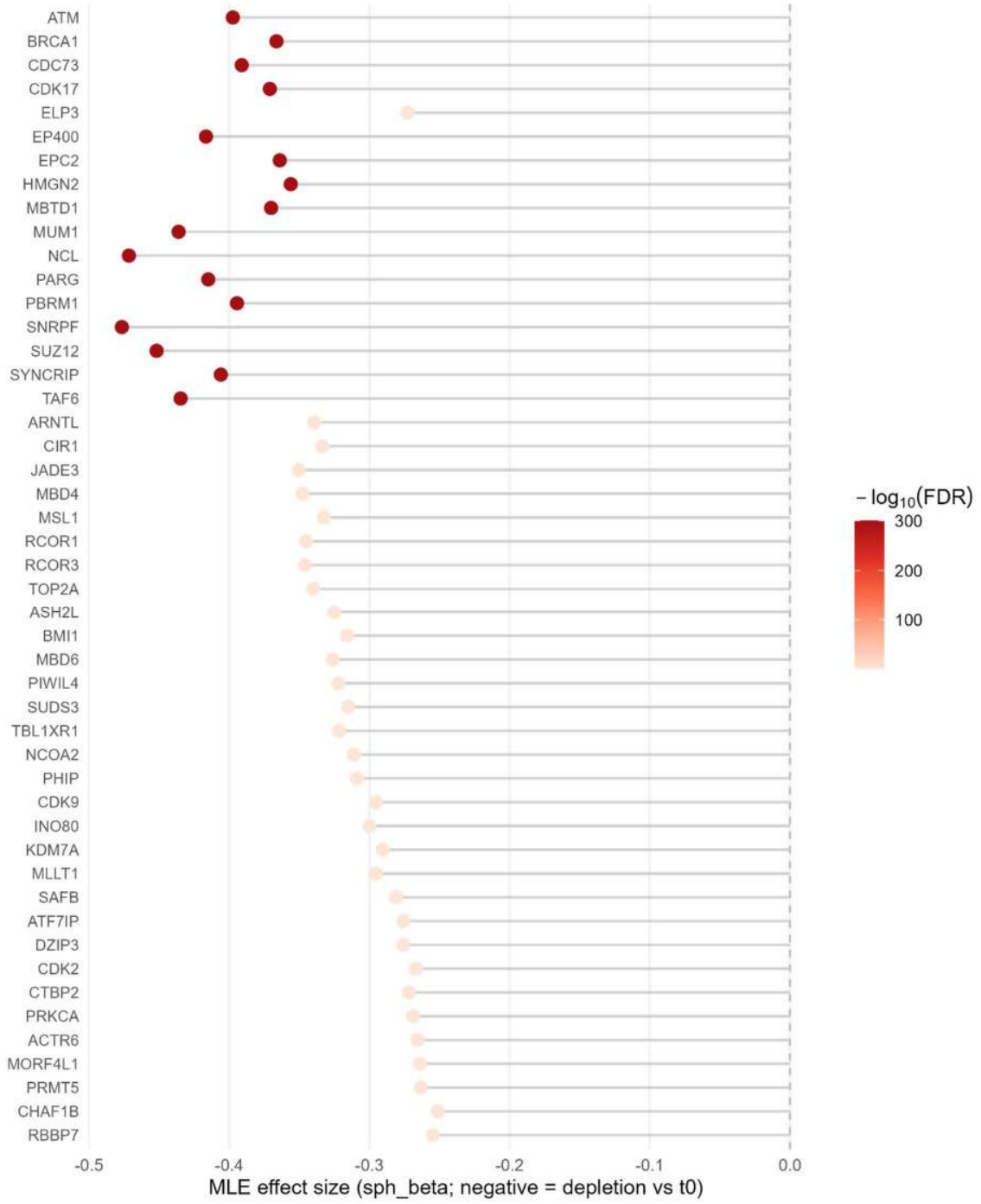

Figure 3.32: Ranked depleted genes in spheroids (FDR < 0.1). Lollipop plot of ranked depleted genes (MAGeCK-MLE β scores) called only in spheroids. *Comparisons:* Gene β/FDR were computed separately for each arm relative to t_0: (i) SMM/Monolayer t_{14} vs t_0 and (ii) Spheres (ULA) t_{14} vs t_0.

Sphere-selective call: Genes were kept if they showed significant depletion in Spheres ($\beta_{Sphere} < 0$ with FDR < 0.10) but not in SMM/Monolayer (FDR ≥ 0.10 and/or $|\beta_{SMM}| \approx 0$), with a more negative effect in spheroids ($\Delta\beta = \beta_{Sphere} - \beta_{SMM} < 0$). Genes significant in both arms (pan-essential) were excluded.

Display: Points are ordered by FDR (then by β). Negative β = stronger depletion. Highlighted examples include ATM, BRCA1 (DDR), SUZ12, EPC2, EP400, PBRM1, MBTD1 (polycomb/chromatin), SNRPF, SYNCRIP (RNA processing), and PARG (PAR metabolism). Exact β and FDR are shown on labels for the top hits.

CHAPTER 4

DISCUSSION AND CONCLUSIONS

An integrated view of CSC maintenance and therapeutic evasion in HGSOC

High-grade serous ovarian cancer (HGSOC) remains difficult to cure because tumor cells, particularly cancer stem cell (CSC)–like subpopulations, flexibly rewire gene regulation to survive therapy and seed relapse. In this thesis we combined two complementary 3D culture systems (ULA spheroids and GelMA-photomasked hydrogels), miRNA gain-of-function experiments, bulk RNA-seq with alternative polyadenylation (APA) profiling, and a focused CRISPR knockout screen of epigenetic regulators. Across these strands, a coherent picture emerges: CSC persistence appears to rely on the interplay of DNA damage response (DDR), chromatin-mediated transcriptional control, and post-transcriptional programs (miRNAs, 3′UTR isoforms), enabling slow-cycling survival, immune evasion, and plasticity under drug pressure. While our data are preclinical and inference-heavy in places, the convergence across orthogonal assays increases plausibility, and many observations align with recent literature on APA regulation, polycomb/DDR dependencies, and miRNA network effects in stem-like states (Mitra et al., 2015).

Model systems: Reasoning behind ULA and GelMA, and OVCAR-3/OVSAHO

We optimized two 3D systems because spheroid context enriches CSC traits and better models peritoneal spread/ascites biology than 2D culture. Prior work shows ovarian spheroids acquire self-renewal, EMT, metabolic rewiring, and drug tolerance—phenotypes we also observed (e.g., CD117/CD133/CD44/CXCR4, SOX2/NANOG/ALDH1A1/c-MYC). ULA allows intrinsic spheroid organization while GelMA-photomasking supplies defined microenvironments, and both have been used to enrich ovarian CSCs and recapitulate resistance behaviors (Liao et al., 2014).

Regarding cell lines, OVCAR-3 is sometimes criticized, yet comparative genomics/transcriptomics that re-benchmarked ovarian models against TCGA-like HGSOC

tumors recently ranked OVCAR-3 among the most faithful in-vitro models, and confirmed OVSAHO as highly representative as well. Using both lines therefore spans BRCA-wildtype/HR-proficient (OVCAR-3) and HR-defective contexts (OVSAHO), which is relevant for DDR-targeted therapies. Earlier analyses emphasizing model fidelity likewise highlighted OVSAHO/Kuramochi as top HGSOC surrogates, while retaining OVCAR-3 as a widely used, genomically characterized line (Xia et al., 2014). Taken together, our platform choices are defensible: ULA/GelMA capture distinct aspects of spheroid biology, and OVCAR-3/OVSAHO bracket clinically important DDR states.

miR-548ah-3p: a distributed regulator rather than a single-target switch

Small RNA-seq pointed to broad miRNA remodeling in spheroids, with miR-548ah-3p consistently reduced in CSC-enriched and drug-tolerant settings. Mimic restoration decreased CSC/EMT markers and sensitized cells to agents used clinically. We interpret these changes as network-level dampening—miR-548ah-3p likely suppresses several nodes at once (e.g., CXCR4, KIT, VIM, SOX-family members) rather than solely one dominant target. This is consistent with the general "many targets, modest per-target effects" logic of miRNA control and with dose-/time-dependent consequences of miRNA perturbations reported by others (Jafari et al., 2021).

To address whether 100 pmol/well dose (6-well, ~2 mL) was appropriate dose, which is a commonly raised question in miRNA mimic studies, this thesis cites literature. This equals ~50 nM, a mainstream working concentration for miRNA mimics in cancer lines, including OVCAR-3. For example, independent OVCAR-3 studies commonly use 50 nM mimics for 24–72 h readouts, and bench guidelines recommend optimizing in the ~10–50 nM range (scaling by volume/format). Our dose thus falls squarely within typical practice (Fang et al., 2017).

At the same time, prolonged or repeated transfections can produce adaptation, altering both direct and indirect readouts; reviews caution that miRNA phenotypes are concentration- and kinetics-dependent, particularly at the protein level. We therefore interpret long-term effects cautiously and propose explicit time-course designs below (Jafari et al., 2021).

Unmodified ssRNA mimics can activate TLR7/8 and other sensors, complicating interpretation of interferon/innate pathways. This is well documented and mitigated by 2′-O-methyl or other chemical modifications. We observed immune-response signatures in short-term mimic conditions and consider them likely platform effects, not biology specific to miR-548ah-3p; future work should use appropriately modified mimics (Bradbury et al., 2020).

Future validation: priority targets and assays

Our in-silico prioritization flagged SOX2 among high-scoring candidates (miRDB), and proteins such as Vimentin and CPEB4 emerged in "rescue-style" analyses; we propose dual-luciferase (pmirGLO) 3′UTR reporters for SOX2, VIM, and CPEB4 to test direct targeting. CPEB4 is mechanistically appealing, because Genome Biology work shows CPEB4 can assemble a repressor complex with CCR4–NOT to drive mRNA deadenylation, beyond its classically described polyadenylation-activating role—providing a plausible bridge between miRNA perturbation and global RNA stability/APA crosstalk (Poetz et al., 2022).

APA Analysis under miRNA treatment and CSC enrichment

APA is dynamically regulated by stress, growth signals, and RBP dosage (e.g., CFIm25/NUDT21, PCF11, CSTF), shifting 3′UTR isoforms to tune miRNA/RBP site landscapes and translational efficiency (Mitschka & Mayr, 2022). Notably, stress-responsive APA is an established phenomenon that helps preserve mRNAs in adverse conditions (Zheng et al., 2018). We therefore examined whether sustained miR-548ah-3p exposure nudges global/polygenic APA programs—independent of individual DE—toward isoform repertoires that blunt or redistribute regulatory pressure as well as investigating APA shifts in our more CSC traits expressing spheroids to see if it may in fact play a role in CSC-like phenotype shift and if that behavior changes with our potentially CSC pathway regulator miRNA hsa-miR-548ah-3p.

Interpreting our APA patterns

Across comparisons we observed a tendency toward 3′UTR lengthening in spheroids, consistent with quiescence/senescence-like adaptations reported in other systems. While proliferative states often show 3′UTR shortening (exposing fewer regulatory sites), quiescent

or stress-adapted states can lengthen 3′UTRs to alter translational restraint and circuitry. Our data fit the latter narrative in CSC-enriched spheroids, and prolonged mimic treatment partially normalizes expression of CSC/EMT genes without collapsing the global lengthening trend—suggesting APA and transcriptional programs are partially decoupled (Sommerkamp et al., 2021).

A point to acknowledge is, conventional bulk RNA-seq can bias APA calls when read coverage tapers at distal 3′ ends. We addressed this with three safeguards:

- *Annotation-anchored quantification.* We used the QAPA framework's logic—quantifying isoform usage relative to known, curated 3′UTR ends (GENCODE-based), which mitigates false novel sites and coverage artifacts. QAPA was designed for exactly this use case and is widely adopted (Ha et al., 2018).
- *Cross-method convergence.* Orthogonal RNA-seq methods like DaPars infer de-novo distal/proximal switches from coverage; newer tools (e.g., PAQR2, (Ghosh et al., 2022)) benchmark favorably across diverse datasets. The broader field accepts careful RNA-seq–based APA quantification considering other tools are newer, therefore rarer, especially when grounded in known PAS and validated by locus-level inspection (Xia et al., 2014).
- *Visual QC in IGV*. For representative loci we verified that bigWig density peaks coincide with annotated 3′UTRs/PAS across conditions, avoiding misinterpretation from off-by-annotation artifacts—an extra belt-and-suspenders step.

Altogether, while 3′-end–enriched protocols (3P-seq, 3′READS, long-read or nanopore-seq) are gold-standard, well-constrained RNA-seq remains informative for relative isoform usage; that is precisely the measurement (ΔPSI) we emphasize (Fahmi et al., 2022).

CRISPR screen: polycomb/DDR and RNA-processing dependencies

Our epigenetic CRISPR screen nominated PRC2 components (EZH2/SUZ12), DDR genes (ATM, BRCA1), and several RNA processing factors among the strongest spheroid-selective dependencies. The polycomb signal is biologically coherent: EZH2 helps maintain undifferentiated (Wen et al., 2017), chemoresistant phenotypes in ovarian models;

mechanistic work ties EZH2 to CHK1 signaling and repression of tumor-suppressive programs (e.g., DAB2IP) in OCSC contexts (Wen et al., 2021).

Recent studies also place PRC2 as a resistance hub in platinum-refractory disease, and multi-omic analyses of patient-derived models have highlighted polycomb pathways as drivers of undifferentiated states (Bharti et al., 2024).

The DDR hits likewise make sense in spheroids: maintaining genome integrity during slow cycling and hypoxia-like stress is essential for long-term survival. Literature in breast/ovarian systems links ATM activity to maintenance of stem-like traits and mammosphere/spheroid formation under stress, while BRCA1 status modulates stemness and therapeutic responses. Our results are consistent with that broader theme, although we do not claim direct causality in our lines without single-gene validation (D. Yang et al., 2020).

Finally, the appearance of PARG among notable genes is interesting given its counter-position to PARP; PAR metabolism increasingly surfaces as a vulnerability in HR-proficient ovarian cancers and, in some contexts, in CSC maintenance. This might rationalize future PARP±PARG or PARP±EZH2 combination tests in spheroids (Matanes et al., 2021).

Clinical context: BRCA/HRD trade-offs and what our models say

Clinically, BRCA-mutated/HR-deficient HGSOC derives substantial benefit from PARP inhibition (e.g., SOLO1), with prolonged PFS versus placebo. Meta-analyses also suggest better prognosis in BRCA-mutant disease relative to HR-proficient tumors when contemporary therapy is used. Our data provide a mechanistic angle: BRCA-WT, HR-proficient contexts (OVCAR-3) may lean more heavily on CSC/EMT programs and chromatin/DDR crosstalk to survive, making them adaptively resilient but harder to debulk biologically; BRCA-defective contexts (OVSAHO) show greater intrinsic drug sensitivity despite aggressive presentation (Moore et al., 2018). This interpretation fits with the differing reliance on microenvironmental support we saw (OVSAHO benefits from GelMA-Pm), and helps justify why targeting polycomb + DDR or miRNA network + DDR might be fruitful particularly in HR-proficient disease. These findings highlight the strength of PARP inhibitors

as maintenance therapy, potentially targeting residual CSCs during the process but this hypothesis requires more research to be claimed.

Limitations

We explicitly acknowledge: (i) bulk RNA-seq lacks cell-type resolution; future scRNA-seq + scAPA would deconvolve CSC subclusters; (ii) miRNA mimic immunostimulation likely contributed to innate-immune signatures unless chemically mitigated; (iii) the CRISPR screen pinpoints associations, not causal hierarchies—single and combinatorial knockouts are needed; (iv) APA calls from RNA-seq are conservative when constrained to known PAS/3′UTRs but still benefit from targeted 3′-end assays; (v) some groups/replicates had lower RNA yields historically; we therefore present representative IGV views, ΔPSI-style isoform usage (less sensitive to total abundance), and avoid over-interpreting single-gene APA switches.

Future directions

Time-resolved miRNA programs. Run longitudinal series at 1, 3, 10, and 15 weeks with modified mimics at multiple doses (e.g., 10, 25, 50 nM) to map dose–time–phenotype surfaces. Readouts: CSC markers, invasion/migration, drug sensitivity, and APA trajectories. Dosing and kinetic considerations are well known to alter miRNA phenotypes; capturing this landscape explicitly will distinguish durable network shifts from transient effects .

Direct target validation. Test SOX2, VIM, and CPEB4 3′UTRs in pmirGLO dual-luciferase assays (wild-type/mutated seed sites); then enforceability with CRISPRi/CRISPRa of each target followed by rescue with seed-mutant 3′UTRs to confirm specificity. The CPEB4 literature supports a context-dependent repressor function via CCR4–NOT, making it a high-value mechanistic node.

APA resolution. 3′-focused RNA-seq (e.g., QuantSeq/3′READS+) and/or long-read isoform profiling (Iso-Seq/Nanopore) in selected conditions; perturbation of APA factors (e.g., CFIm/NOVA/CPEB) to test causality.

Single-gene tests. For top CRISPR hits (e.g., ATM, PARG, SUZ12, EP400), perform individual KO/CRISPRi or siRNA across multiple lines, followed by spheroid formation assays, drug-response profiling (GI50/AUC), migration/invasion assays, and EMT/CSC marker panels. Include rescue experiments with sgRNA-resistant cDNAs.

Epigenetic–DDR combinations. Based on screen hits, evaluate EZH2 inhibition (tool compounds or clinical-grade) ± PARP inhibitors in OVCAR-3 spheroids; prior work suggests EZH2 connects to CHK1 and can sensitize HR-proficient EOC to DNA-damage therapies. Extend to PARG genetic/chemical probes in combination with PARP or chemotherapy .

Genetic background stratification. Comparing CSC enrichment, APA profiles, and miRNA responses across BRCA1/2-mutant vs. wild-type lines (e.g., OVSAHO/Kuramochi vs. OVCAR-3/OVCAR-8/CA-OV3) to address the question "are these effects OVCAR-3-specific?". Given the updated benchmarking placing OVCAR-3 among top HGSOC models, we expect shared phenomena with line-specific nuances. For this purpose, breast cancer genes can also be checked.

Limiting-dilution assays. Determining tumor-initiating cell frequency across conditions; performing serial transplantation to assess self-renewal.

In vivo. To validate aggressiveness of OVCAR-3 spheroids, monolayer vs. spheroid generated tumors can be compared to each other in terms of formation time and growth pace. Moving the highest-confidence nodes (e.g., EZH2±PARP; miR-548ah-3p mimic with modifications) into xenograft or patient-derived spheroid implantation models, focusing on time to relapse and platinum/PARPi resensitization.

Immune axis clarity. Repeat mimic experiments with 2′-O-methyl/LNA-modified duplexes and endotoxin-free prep; include RIG-I/TLR7-8 reporter assays to rule in/out innate activation.

Secretome/immune axis (optional). Assess whether mimic or epigenetic perturbations alter cytokine/chemokine output that could influence immune interactions in vivo.

Final synthesis

Stepping back, our data support a conservative but actionable model: ovarian CSCs integrate DDR (ATM/BRCA1), polycomb-guided chromatin repression (EZH2/SUZ12), and post-transcriptional plasticity (miRNAs, APA) to occupy a slow-cycling, repair-competent state that endures chemotherapy. Intervening at single nodes may be insufficient; rather, network-level perturbations—for example, miRNA restoration in tandem with epigenetic/DDR modulation—may push CSCs out of quiescence and unmask drug sensitivity. Our observations do not "prove" this architecture in a formal sense, but they align with—and extend—evidence that APA programs and polycomb/DDR circuits co-operate during stress, quiescence, and therapy tolerance.

As a practical matter, we also show that carefully constrained APA analysis using bulk RNA-seq—anchored to known 3′UTR ends (QAPA-style) and validated visually in IGV—is a defensible approach to hypothesis-generation when specialized 3′-end protocols are not feasible. Many studies, including QAPA itself and DaPars, have advanced the field using standard RNA-seq, provided that site annotation and bias control are explicit.

Finally, clinical context matters. PARP benefit in BRCA-mutant disease is robust, whereas BRCA-WT tumors remain the larger challenge—precisely where CSC plasticity, polycomb/DDR dependencies, and post-transcriptional control could open new therapeutic angles. Our work points to several tractable experiments to test this hypothesis and, in doing so, lays groundwork for rational combinations that constrain CSC state transitions rather than chasing them (H. Y. Jin et al., 2015).

BIBLIOGRAPHY

Abubaker, K., Latifi, A., Luwor, R., Nazaretian, S., Zhu, H., Quinn, M. A., Thompson, E. W., Findlay, J. K., & Ahmed, N. (2013). Short-term single treatment of chemotherapy results in the enrichment of ovarian cancer stem cell-like cells leading to an increased tumor burden. *Molecular Cancer*, *12*(1), 1. https://doi.org/10.1186/1476-4598-12-24

Acland, M., Mittal, P., Lokman, N. A., Klingler-hoffmann, M., Oehler, M. K., & Hoffmann, P. (2018). *Mass Spectrometry Analyses of Multicellular Tumor Spheroids*. *1700124*. https://doi.org/10.1002/prca.201700124

Al-Dimassi, S., Abou-Antoun, T., & El-Sibai, M. (2014). Cancer cell resistance mechanisms: A mini review. *Clinical and Translational Oncology*, *16*(6), 511–516. https://doi.org/10.1007/s12094-014-1162-1

Atun, R., Bhakta, N., Denburg, A., Frazier, A. L., Friedrich, P., Gupta, S., Lam, C. G., Ward, Z. J., Yeh, J. M., Allemani, C., Coleman, M. P., Di Carlo, V., Loucaides, E., Fitchett, E., Girardi, F., Horton, S. E., Bray, F., Steliarova-Foucher, E., Sullivan, R., … Rodriguez-Galindo, C. (2020). Sustainable care for children with cancer: a Lancet Oncology Commission. *The Lancet Oncology*, *21*(4), e185–e224. https://doi.org/10.1016/S1470-2045(20)30022-X

Baba, T., Convery, P. A., Matsumura, N., Whitaker, R. S., Kondoh, E., Perry, T., Huang, Z., Bentley, R. C., Mori, S., Fujii, S., Marks, J. R., Berchuck, A., & Murphy, S. K. (2009). Epigenetic regulation of CD133 and tumorigenicity of CD133+ ovarian cancer cells. *Oncogene*, *28*(2), 209–218. https://doi.org/10.1038/onc.2008.374

Barbieri, I., & Kouzarides, T. (2020). Role of RNA modifications in cancer. *Nature Reviews Cancer*, *20*(6), 303–322. https://doi.org/10.1038/s41568-020-0253-2

Batlle, E., & Clevers, H. (2017). Cancer stem cells revisited. *Nature Medicine*, *23*(10), 1124–1134. https://doi.org/10.1038/nm.4409

Beg, M. S., Brenner, A. J., Sachdev, J., Borad, M., Kang, Y. K., Stoudemire, J., Smith, S., Bader, A. G., Kim, S., & Hong, D. S. (2017). Phase I study of MRX34, a liposomal miR-34a mimic, administered twice weekly in patients with advanced solid tumors. *Investigational New Drugs*, *35*(2), 180–188. https://doi.org/10.1007/s10637-016-0407-y

Bell, D., Berchuck, A., Birrer, M., Chien, J., Cramer, D. W., Dao, F., Dhir, R., Disaia, P., Gabra, H., Glenn, P., Godwin, A. K., Gross, J., Hartmann, L., Huang, M., Huntsman, D. G., Iacocca, M., Imielinski, M., Kalloger, S., Karlan, B. Y., … Thomson, E. (2011). Integrated genomic analyses of ovarian carcinoma. *Nature*, *474*(7353), 609–615. https://doi.org/10.1038/nature10166

Bendoraite, A., Knouf, E. C., Garg, K. S., Parkin, R. K., Kroh, E. M., O'Briant, K. C., Ventura, A. P., Godwin, A. K., Karlan, B. Y., Drescher, C. W., Urban, N., Knudsen, B. S., & Tewari, M. (2010). Regulation of miR-200 family microRNAs and ZEB transcription factors in ovarian cancer: Evidence supporting a mesothelial-to-epithelial transition. *Gynecologic Oncology*, *116*(1), 117–125. https://doi.org/10.1016/j.ygyno.2009.08.009

Bharti, R., Dey, G., Khan, D., Myers, A., Huffman, O. G., Saygin, C., Braley, C., Richards, E., Sangwan, N., Willard, B., Lathia, J. D., Fox, P. L., Lin, F., Jha, B. K., Brown, J. M., Yu, J. S., Dwidar, M., Joehlin-Price, A., Vargas, R., … Reizes, O. (2024). Cell surface CD55 traffics to the nucleus leading to cisplatin resistance and stemness by inducing PRC2 and H3K27 trimethylation on chromatin in ovarian cancer. *Molecular Cancer*, *23*(1), 1–23. https://doi.org/10.1186/s12943-024-02028-5

Bley, N., Schott, A., Müller, S., Misiak, D., Lederer, M., Fuchs, T., Aßmann, C., Glaß, M., Ihling, C., Sinz, A., Pazaitis, N., Wickenhauser, C., Vetter, M., Ungurs, O., Strauss, H. G., Thomssen, C., & Hüttelmaier, S. (2021). IGF2BP1 is a targetable SRC/MAPK-dependent driver of invasive growth in ovarian cancer. *RNA Biology*, *18*(3), 391–403. https://doi.org/10.1080/15476286.2020.1812894

Bonnet, D., & Dick, J. E. (1997). Human acute myeloid leukemia is organized as a

hierarchy that originates from a primitive hematopoietic cell. *Nature Medicine*, *3*(7), 730–737. https://doi.org/10.1038/nm0797-730

Bradbury, A., O'Donnell, R., Drew, Y., Curtin, N. ., & Saha, S. (2020). Characterisation of Ovarian Cancer Cell Line Damage Response Biomarkers for Therapeutic Targeting. *Cancers*, *i*, 1–17.

Bray, F., Laversanne, M., Sung, H., Ferlay, J., Siegel, R. L., Soerjomataram, I., & Jemal, A. (2024). Global cancer statistics 2022: GLOBOCAN estimates of incidence and mortality worldwide for 36 cancers in 185 countries. *CA: A Cancer Journal for Clinicians*, *74*(3), 229–263. https://doi.org/10.3322/caac.21834

Cai, H., Zheng, D., Yao, Y., Yang, L., Huang, X., & Wang, L. (2022). Roles of Embryonic Lethal Abnormal Vision-Like RNA Binding Proteins in Cancer and Beyond. *Frontiers in Cell and Developmental Biology*, *10*(April), 1–15. https://doi.org/10.3389/fcell.2022.847761

Chang, C. J., & Hung, M. C. (2012). The role of EZH2 in tumour progression. *British Journal of Cancer*, *106*(2), 243–247. https://doi.org/10.1038/bjc.2011.551

Chang, L. L., Xu, X. Q., Liu, X. L., Guo, Q. Q., Fan, Y. N., He, B. X., & Zhang, W. Z. (2021). Emerging role of m6A methylation modification in ovarian cancer. *Cancer Cell International*, *21*(1), 1–16. https://doi.org/10.1186/s12935-021-02371-3

Chi, P., Allis, C. D., & Wang, G. G. (2010). Covalent histone modifications-miswritten, misinterpreted and mis-erased in human cancers. *Nature Reviews Cancer*, *10*(7), 457–469. https://doi.org/10.1038/nrc2876

Chirshev, E., Suzuki, T., Wang, H., Nguyen, A., Hojo, N., Sanderman, L., Mirshahidi, S., Ioffe, Y. J., & Unternaehrer, J. J. (2021). Let-7i reduces aggressive phenotype and induces BRCAness in ovarian cancer cells. *Cancers*, *13*(18), 1–15. https://doi.org/10.3390/cancers13184617

Choi, Y. E., Meghani, K., Brault, M., Leclerc, L., He, Y. J., Day, T. A., Elias, K. M., Drapkin, R., Weinstock, D. M., Dao, F., Karin, K., Matulonis, U., Levine, D. A., &

Konstantinopoulos, P. A. (2016). of microRNA-622 in BRCA1-mutant ovarian cancer. *Cell Reports*, *14*(3), 429–439. https://doi.org/10.1016/j.celrep.2015.12.046.Platinum

Cress, R. D., Chen, Y. S., Morris, C. R., Petersen, M., & Leiserowitz, G. S. (2015). Characteristics of long-term survivors of epithelial ovarian cancer. *Obstetrics and Gynecology*, *126*(3), 491–497. https://doi.org/10.1097/AOG.0000000000000981

Croce, C. M. (2009). Causes and consequences of microRNA dysregulation in cancer. *Nature Reviews Genetics*, *10*(10), 704–714. https://doi.org/10.1038/nrg2634

Dagogo-Jack, I., & Shaw, A. T. (2018). Tumour heterogeneity and resistance to cancer therapies. *Nature Reviews Clinical Oncology*, *15*(2), 81–94. https://doi.org/10.1038/nrclinonc.2017.166

Dawson, M. A., & Kouzarides, T. (2012). Cancer epigenetics: From mechanism to therapy. *Cell*, *150*(1), 12–27. https://doi.org/10.1016/j.cell.2012.06.013

Ding, L., Gu, H., Xiong, X., Ao, H., Cao, J., Lin, W., Yu, M., Lin, J., & Cui, Q. (2019). Micrornas involved in carcinogenesis, prognosis, therapeutic resistance and applications in human triple-negative breast cancer. *Cells*, *8*(12), 1–35. https://doi.org/10.3390/cells8121492

Ding, Y., Huang, X., Ji, T., Qi, C., Gao, X., & Wei, R. (2024). The emerging roles of miRNA-mediated autophagy in ovarian cancer. *Cell Death and Disease*, *15*(5), 1–15. https://doi.org/10.1038/s41419-024-06677-8

Easwaran, H., Tsai, H. C., & Baylin, S. B. (2014). Cancer Epigenetics: Tumor Heterogeneity, Plasticity of Stem-like States, and Drug Resistance. *Molecular Cell*, *54*(5), 716–727. https://doi.org/10.1016/j.molcel.2014.05.015

Edmondson, R., Broglie, J. J., Adcock, A. F., & Yang, L. (2014). Three-dimensional cell culture systems and their applications in drug discovery and cell-based biosensors. *Assay and Drug Development Technologies*, *12*(4), 207–218. https://doi.org/10.1089/adt.2014.573

Erson-Bensan, A. E. (2016). Alternative polyadenylation and RNA-binding proteins. *Journal of Molecular Endocrinology*, *57*(2), F29–F34. https://doi.org/10.1530/JME-16-0070

Erson-Bensan, A. E., & Can, T. (2016). Alternative polyadenylation: Another foe in cancer. *Molecular Cancer Research*, *14*(6), 507–517. https://doi.org/10.1158/1541-7786.MCR-15-0489

Fader, A. N., Java, J., Krivak, T. C., Bristow, R. E., Tergas, A. I., Bookman, M. A., Armstrong, D. K., Tanner, E. J., & Gershenson, D. M. (2014). The prognostic significance of pre- and post-treatment CA-125 in grade 1 serous ovarian carcinoma: A Gynecologic Oncology Group study. *Gynecologic Oncology*, *132*(3), 560–565. https://doi.org/10.1016/j.ygyno.2013.11.016

Fahmi, N. A., Ahmed, K. T., Chang, J. W., Nassereddeen, H., Fan, D., Yong, J., & Zhang, W. (2022). APA-Scan: detection and visualization of 3′-UTR alternative polyadenylation with RNA-seq and 3′-end-seq data. *BMC Bioinformatics*, *23*, 1–13. https://doi.org/10.1186/s12859-022-04939-w

Fang, G., Liu, J., Wang, Q., Huang, X., Yang, R., Pang, Y., & Yang, M. (2017). MicroRNA-223-3p regulates ovarian cancer cell proliferation and invasion by targeting SOX11 expression. *International Journal of Molecular Sciences*, *18*(6). https://doi.org/10.3390/ijms18061208

Feinberg, A. P., Koldobskiy, M. A., & Göndör, A. (2016). Epigenetic modulators, modifiers and mediators in cancer aetiology and progression. *Nature Reviews Genetics*, *17*(5), 284–299. https://doi.org/10.1038/nrg.2016.13

Flavahan, W. A., Gaskell, E., & Bernstein, B. E. (2017). Epigenetic plasticity and the hallmarks of cancer. *Science*, *357*(6348). https://doi.org/10.1126/science.aal2380

Flores, C. P., Garcia-Vázquez, R., Rincón, D. G., Ruiz-Garcia, E., De La Vega, H. A., Marchat, L. A., Salinas Vera, Y. M., & López-Camarillo, C. (2017). MicroRNAs driving invasion and metastasis in ovarian cancer: Opportunities for translational

medicine (Review). *International Journal of Oncology*, *50*(5), 1461–1476. https://doi.org/10.3892/ijo.2017.3948

Ghosh, S., Ataman, M., Bak, M., Börsch, A., Schmidt, A., Buczak, K., Martin, G., Dimitriades, B., Herrmann, C. J., Kanitz, A., & Zavolan, M. (2022). CFIm-mediated alternative polyadenylation remodels cellular signaling and miRNA biogenesis. *Nucleic Acids Research*, *50*(6), 3096–3114. https://doi.org/10.1093/nar/gkac114

Greaves, M., & Maley, C. C. (2012). Clonal evolution in cancer. *Nature*, *481*(7381), 306–313. https://doi.org/10.1038/nature10762

Gruber, A. J., & Zavolan, M. (2019). Alternative cleavage and polyadenylation in health and disease. *Nature Reviews Genetics*, *20*(10), 599–614. https://doi.org/10.1038/s41576-019-0145-z

Guan, Y., Yao, H., Zheng, Z., Qiu, G., & Sun, K. (2011). MiR-125b targets BCL3 and suppresses ovarian cancer proliferation. *International Journal of Cancer*, *128*(10), 2274–2283. https://doi.org/10.1002/ijc.25575

Ha, K. C. H., Blencowe, B. J., & Morris, Q. (2018). QAPA: A new method for the systematic analysis of alternative polyadenylation from RNA-seq data. *Genome Biology*, *19*(1), 1–18. https://doi.org/10.1186/s13059-018-1414-4

Haberland, M., Montgomery, R. L., & Olson, E. N. (2009). The many roles of histone deacetylases in development and physiology: Implications for disease and therapy. *Nature Reviews Genetics*, *10*(1), 32–42. https://doi.org/10.1038/nrg2485

Hanahan, D. (2022). Hallmarks of Cancer: New Dimensions. *Cancer Discovery*, *12*(1), 31–46. https://doi.org/10.1158/2159-8290.CD-21-1059

Hanahan, D., & Weinberg, R. A. (2000). The Hallmarks of Cancer Review Douglas. *Cell*, *100*(7), 57–70.

Hanahan, D., & Weinberg, R. A. (2011). Hallmarks of cancer: The next generation. *Cell*, *144*(5), 646–674. https://doi.org/10.1016/j.cell.2011.02.013

Hao, L., Zhang, J., Liu, Z., Lin, X., & Guo, J. (2023). Epitranscriptomics in the development, functions, and disorders of cancer stem cells. *Frontiers in Oncology*, *13*(March), 1–16. https://doi.org/10.3389/fonc.2023.1145766

Hong, D. S., Kang, Y. K., Borad, M., Sachdev, J., Ejadi, S., Lim, H. Y., Brenner, A. J., Park, K., Lee, J. L., Kim, T. Y., Shin, S., Becerra, C. R., Falchook, G., Stoudemire, J., Martin, D., Kelnar, K., Peltier, H., Bonato, V., Bader, A. G., … Beg, M. S. (2020). Phase 1 study of MRX34, a liposomal miR-34a mimic, in patients with advanced solid tumours. *British Journal of Cancer*, *122*(11), 1630–1637. https://doi.org/10.1038/s41416-020-0802-1

Hua, W., Zhao, Y., Jin, X., Yu, D., He, J., Xie, D., & Duan, P. (2018). METTL3 promotes ovarian carcinoma growth and invasion through the regulation of AXL translation and epithelial to mesenchymal transition. *Gynecologic Oncology*, *151*(2), 356–365. https://doi.org/10.1016/j.ygyno.2018.09.015

Huang, H., Weng, H., Sun, W., Qin, X., Shi, H., Wu, H., Zhao, B. S., Mesquita, A., Liu, C., Yuan, C. L., Hu, Y. C., Hüttelmaier, S., Skibbe, J. R., Su, R., Deng, X., Dong, L., Sun, M., Li, C., Nachtergaele, S., … Chen, J. (2018). Recognition of RNA N 6 - methyladenosine by IGF2BP proteins enhances mRNA stability and translation. *Nature Cell Biology*, *20*(3), 285–295. https://doi.org/10.1038/s41556-018-0045-z

Jafari, N., Abediankenari, S., & Hossein-Nataj, H. (2021). miR-34a mimic or pre-mir-34a, which is the better option for cancer therapy? KatoIII as a model to study miRNA action in human gastric cancer cells. *Cancer Cell International*, *21*(1), 1–15. https://doi.org/10.1186/s12935-021-01872-5

Janssen, H. L. A., Reesink, H. W., Lawitz, E. J., Zeuzem, S., Rodriguez-Torres, M., Patel, K., van der Meer, A. J., Patick, A. K., Chen, A., Zhou, Y., Persson, R., King, B. D., Kauppinen, S., Levin, A. A., & Hodges, M. R. (2013). Treatment of HCV Infection by Targeting MicroRNA. *New England Journal of Medicine*, *368*(18), 1685–1694. https://doi.org/10.1056/nejmoa1209026

Jiang, N. J., Yin, Y. N., Lin, J., Li, W. Y., Long, D. R., & Mei, L. (2023). MicroRNA-21 in

gynecological cancers: From molecular pathogenesis to clinical significance. *Pathology Research and Practice*, *248*(June), 154630. https://doi.org/10.1016/j.prp.2023.154630

Jin, B., & Robertson, K. D. (2013). DNA Methyltransferases, DNA Damage Repair, and Cancer. In A. R. Karpf (Ed.), *Epigenetic Alterations in Oncogenesis* (pp. 3–29). Springer New York. https://doi.org/10.1007/978-1-4419-9967-2_1

Jin, H. Y., Gonzalez-Martin, A., Miletic, A. V., Lai, M., Knight, S., Sabouri-Ghomi, M., Head, S. R., Macauley, M. S., Rickert, R. C., & Xiao, C. (2015). Transfection of microRNA mimics should be used with caution. *Frontiers in Genetics*, *6*(DEC), 1–23. https://doi.org/10.3389/fgene.2015.00340

Jones, P. A., & Baylin, S. B. (2007). The Epigenomics of Cancer. *Cell*, *128*(4), 683–692. https://doi.org/10.1016/j.cell.2007.01.029

Jones, R. J. (2009). Cancer stem cells-clinical relevance. *Journal of Molecular Medicine*, *87*(11), 1105–1110. https://doi.org/10.1007/s00109-009-0534-4

Kan, R. L., Chen, J., & Sallam, T. (2022). Crosstalk between epitranscriptomic and epigenetic mechanisms in gene regulation. *Trends in Genetics*, *38*(2), 182–193. https://doi.org/10.1016/j.tig.2021.06.014

Kenny, H. A., Lal-Nag, M., White, E. A., Shen, M., Chiang, C. Y., Mitra, A. K., Zhang, Y., Curtis, M., Schryver, E. M., Bettis, S., Jadhav, A., Boxer, M. B., Li, Z., Ferrer, M., & Lengyel, E. (2015). Quantitative high throughput screening using a primary human three-dimensional organotypic culture predicts in vivo efficacy. *Nature Communications*, *6*. https://doi.org/10.1038/ncomms7220

Kim, K. H., & Roberts, C. W. M. (2016). Targeting EZH2 in cancer. *Nature Medicine*, *22*(2), 128–134. https://doi.org/10.1038/nm.4036

Koutsaki, M., Libra, M., Spandidos, D. A., & Zaravinos, A. (2017). The miR-200 family in ovarian cancer. *Oncotarget*, *8*(39), 66629–66640. https://doi.org/10.18632/oncotarget.18343

Kreso, A., & Dick, J. E. (2014). Evolution of the cancer stem cell model. *Cell Stem Cell*, *14*(3), 275–291. https://doi.org/10.1016/j.stem.2014.02.006

Kumar, V., Vashishta, M., Kong, L., Wu, X., Lu, J. J., Guha, C., & Dwarakanath, B. S. (2021). The Role of Notch, Hedgehog, and Wnt Signaling Pathways in the Resistance of Tumors to Anticancer Therapies. *Frontiers in Cell and Developmental Biology*, *9*(April), 1–24. https://doi.org/10.3389/fcell.2021.650772

Kurman, R. J., & Shih, I. M. (2016). The dualistic model of ovarian carcinogenesis revisited, revised, and expanded. *American Journal of Pathology*, *186*(4), 733–747. https://doi.org/10.1016/j.ajpath.2015.11.011

Laks, D. R., Visnyei, K., & Kornblum, H. I. (2010). Brain tumor stem cells as therapeutic targets in models of glioma. *Yonsei Medical Journal*, *51*(5), 633–640. https://doi.org/10.3349/ymj.2010.51.5.633

Latifi, A., Abubaker, K., Castrechini, N., Ward, A. C., Liongue, C., Dobill, F., Kumar, J., Thompson, E. W., Quinn, M. A., Findlay, J. K., & Ahmed, N. (2011). Cisplatin treatment of primary and metastatic epithelial ovarian carcinomas generates residual cells with mesenchymal stem cell-like profile. *Journal of Cellular Biochemistry*, *112*(10), 2850–2864. https://doi.org/10.1002/jcb.23199

Lheureux, S., Gourley, C., Vergote, I., & Oza, A. M. (2019). Epithelial ovarian cancer. *The Lancet*, *393*(10177), 1240–1253. https://doi.org/10.1016/S0140-6736(18)32552-2

Liang, G., & Weisenberger, D. J. (2017). DNA methylation aberrancies as a guide for surveillance and treatment of human cancers. *Epigenetics*, *12*(6), 416–432. https://doi.org/10.1080/15592294.2017.1311434

Liao, J., Qian, F., Tchabo, N., Mhawech-Fauceglia, P., Beck, A., Qian, Z., Wang, X., Huss, W. J., Lele, S. B., Morrison, C. D., & Odunsi, K. (2014). Ovarian cancer spheroid cells with stem cell-like properties contribute to tumor generation, metastasis and chemotherapy resistance through hypoxia-resistant metabolism. *PLoS ONE*, *9*(1), 1–13. https://doi.org/10.1371/journal.pone.0084941

Liu, C., Kelnar, K., Liu, B., Chen, X., Calhoun-Davis, T., Li, H., Patrawala, L., Yan, H., Jeter, C., Honorio, S., Wiggins, J. F., Bader, A. G., Fagin, R., Brown, D., & Tang, D. G. (2011). The microRNA miR-34a inhibits prostate cancer stem cells and metastasis by directly repressing CD44. *Nature Medicine*, *17*(2), 211–216. https://doi.org/10.1038/nm.2284

Liu, T., Wei, Q., Jin, J., Luo, Q., Liu, Y., Yang, Y., Cheng, C., Li, L., Pi, J., Si, Y., Xiao, H., Li, L., Rao, S., Wang, F., Yu, J., Yu, J., Zou, D., & Yi, P. (2021). The m6A reader YTHDF1 promotes ovarian cancer progression via augmenting EIF3C translation. *Nucleic Acids Research*, *48*(7), 3816–3831. https://doi.org/10.1093/NAR/GKAA048

Liu, X., Wei, Q., Yang, C., Zhao, H., Xu, J., Mobet, Y., Luo, Q., Yang, D., Zuo, X., Chen, N., Yang, Y., Li, L., Wang, W., Yu, J., Xu, J., Liu, T., & Yi, P. (2024). RNA m5C modification upregulates E2F1 expression in a manner dependent on YBX1 phase separation and promotes tumor progression in ovarian cancer. *Experimental and Molecular Medicine*, *56*(3), 600–615. https://doi.org/10.1038/s12276-024-01184-4

Ma, Y., Shen, N., Wicha, M. S., & Luo, M. (2021). The roles of the let-7 family of microrna s in the regulation of cancer stemness. *Cells*, *10*(9), 1–20. https://doi.org/10.3390/cells10092415

Mansoori, B., Mohammadi, A., Davudian, S., Shirjang, S., & Baradaran, B. (2017). The Different Mechanisms of Cancer Drug Resistance: A Brief Review. *Advanced Pharmaceutical Bulletin*, *7*(3), 339–348. https://doi.org/10.15171/apb.2017.041

Mao, Z., Tian, Y., Wu, L., & Zhang, Y. (2025). Epitranscriptomic mechanisms and implications of RNA m^5C modification in cancer. *Theranostics*, *15*, 8404–8428. https://doi.org/10.7150/thno.112332

Margueron, R., & Reinberg, D. (2011). The Polycomb complex PRC2 and its mark in life. *Nature*, *469*(7330), 343–349. https://doi.org/10.1038/nature09784

Mariotto, A. B., Enewold, L., Zhao, J., Zeruto, C. A., & Robin Yabroff, K. (2020). Medical care costs associated with cancer survivorship in the United States. *Cancer*

Epidemiology Biomarkers and Prevention, *29*(7), 1304–1312. https://doi.org/10.1158/1055-9965.EPI-19-1534

Matanes, E., López-Ozuna, V. M., Octeau, D., Baloch, T., Racovitan, F., Dhillon, A. K., Kessous, R., Raban, O., Kogan, L., Salvador, S., Lau, S., Gotlieb, W. H., & Yasmeen, A. (2021). Inhibition of Poly ADP-Ribose Glycohydrolase Sensitizes Ovarian Cancer Cells to Poly ADP-Ribose Polymerase Inhibitors and Platinum Agents. *Frontiers in Oncology*, *11*(October), 1–12. https://doi.org/10.3389/fonc.2021.745981

Mattick, J. S., Amaral, P. P., Carninci, P., Carpenter, S., Chang, H. Y., Chen, L. L., Chen, R., Dean, C., Dinger, M. E., Fitzgerald, K. A., Gingeras, T. R., Guttman, M., Hirose, T., Huarte, M., Johnson, R., Kanduri, C., Kapranov, P., Lawrence, J. B., Lee, J. T., … Wu, M. (2023). Long non-coding RNAs: definitions, functions, challenges and recommendations. *Nature Reviews Molecular Cell Biology*, *24*(6), 430–447. https://doi.org/10.1038/s41580-022-00566-8

Matulonis, U. A., Sood, A. K., Fallowfield, L., Howitt, B. E., Sehouli, J., & Karlan, B. Y. (2016). Ovarian cancer. *Nature Reviews. Disease Primers*, *2*, 16061. https://doi.org/10.1038/nrdp.2016.61

Mitra, A. K., Davis, D. A., Tomar, S., Roy, L., Gurler, H., Xie, J., Lantvit, D. D., Cardenas, H., Fang, F., Liu, Y., Loughran, E., Yang, J., Sharon Stack, M., Emerson, R. E., Cowden Dahl, K. D., Barbolina, M. V., Nephew, K. P., Matei, D., & Burdette, J. E. (2015). In vivo tumor growth of high-grade serous ovarian cancer cell lines. *Gynecologic Oncology*, *138*(2), 372–377. https://doi.org/10.1016/j.ygyno.2015.05.040

Mitschka, S., & Mayr, C. (2022). Context-specific regulation and function of mRNA alternative polyadenylation. *Nature Reviews Molecular Cell Biology*, *23*(12), 779–796. https://doi.org/10.1038/s41580-022-00507-5

Miyamoto, M., Sawada, K., Nakamura, K., Yoshimura, A., Ishida, K., Kobayashi, M., Shimizu, A., Yamamoto, M., Kodama, M., Hashimoto, K., & Kimura, T. (2020). Paclitaxel exposure downregulates miR-522 expression and its downregulation induces paclitaxel resistance in ovarian cancer cells. *Scientific Reports*, *10*(1), 1–13.

https://doi.org/10.1038/s41598-020-73785-8

Moore, K., Colombo, N., Scambia, G., Kim, B.-G., Oaknin, A., Friedlander, M., Lisyanskaya, A., Floquet, A., Leary, A., Sonke, G. S., Gourley, C., Banerjee, S., Oza, A., González-Martín, A., Aghajanian, C., Bradley, W., Mathews, C., Liu, J., Lowe, E. S., … DiSilvestro, P. (2018). Maintenance Olaparib in Patients with Newly Diagnosed Advanced Ovarian Cancer. *New England Journal of Medicine*, *379*(26), 2495–2505. https://doi.org/10.1056/nejmoa1810858

Muñoz, P., Iliou, M. S., & Esteller, M. (2012). Epigenetic alterations involved in cancer stem cell reprogramming. *Molecular Oncology*, *6*(6), 620–636. https://doi.org/10.1016/j.molonc.2012.10.006

Nath, S., & Devi, G. R. (2016). Three-dimensional culture systems in cancer research: Focus on tumor spheroid model. *Pharmacology and Therapeutics*, *163*, 94–108. https://doi.org/10.1016/j.pharmthera.2016.03.013

Nayak, R., Pandey, S., Kumar, D., Kumar, S., & Pai, K. S. R. (2025). Signaling networks and MiRNA crosstalk in ovarian cancer chemoresistance. *Journal of Ovarian Research* , *18*(1). https://doi.org/10.1186/s13048-025-01770-8

Nowell, P. C. (1976). Linked references are available on JSTOR for this article : The Clonal Evolution of Tumor Cell Populations. *Science*, *194*(4260), 23–28.

Parikh, A., Lee, C., Joseph, P., Marchini, S., Baccarini, A., Kolev, V., Romualdi, C., Fruscio, R., Shah, H., Wang, F., Mullokandov, G., Fishman, D., D'Incalci, M., Rahaman, J., Kalir, T., Redline, R. W., Brown, B. D., Narla, G., & Difeo, A. (2014). MicroRNA-181a has a critical role in ovarian cancer progression through the regulation of the epithelial-mesenchymal transition. *Nature Communications*, *5*. https://doi.org/10.1038/ncomms3977

Parreno, V., Martinez, A. M., & Cavalli, G. (2022). Mechanisms of Polycomb group protein function in cancer. *Cell Research*, *32*(3), 231–253. https://doi.org/10.1038/s41422-021-00606-6

Poetz, F., Lebedeva, S., Schott, J., Lindner, D., Ohler, U., & Stoecklin, G. (2022). Control of immediate early gene expression by CPEB4-repressor complex-mediated mRNA degradation. *Genome Biology*, *23*(1), 1–35. https://doi.org/10.1186/s13059-022-02760-5

Pomel, C., Jeyarajah, A., Oram, D., Shepherd, J., Milliken, D., Dauplat, J., & Reynolds, K. (2007). Cytoreductive surgery in ovarian cancer. *Cancer Imaging : The Official Publication of the International Cancer Imaging Society*, *7*(1), 210–215. https://doi.org/10.1102/1470-7330.2007.0030

Prieto-Vila, M., Takahashi, R. U., Usuba, W., Kohama, I., & Ochiya, T. (2017). Drug resistance driven by cancer stem cells and their niche. *International Journal of Molecular Sciences*, *18*(12). https://doi.org/10.3390/ijms18122574

Pujade-Lauraine, E., Ledermann, J. A., Selle, F., Gebski, V., Penson, R. T., Oza, A. M., Korach, J., Huzarski, T., Poveda, A., Pignata, S., Friedlander, M., Colombo, N., Harter, P., Fujiwara, K., Ray-Coquard, I. L., Banerjee, S., Liu, J., Lowe, E. S., Bloomfield, R., … Vergote, I. (2017). Olaparib tablets as maintenance therapy in patients with platinum-sensitive, relapsed ovarian cancer and a BRCA1/2 mutation (SOLO2/ENGOT-Ov21): a double-blind, randomised, placebo-controlled, phase 3 trial. *The Lancet Oncology*, *18*(9), 1274–1284. https://doi.org/10.1016/S1470-2045(17)30469-2

Rehwinkel, J., & Mehdipour, P. (2025). ADAR1: from basic mechanisms to inhibitors. *Trends in Cell Biology*, *35*(1), 59–73. https://doi.org/10.1016/j.tcb.2024.06.006

Reid, B. M., Permuth, J. B., & Sellers, T. A. (2017). Epidemiology of ovarian cancer: a review. *Cancer Biology and Medicine*, *14*(1), 9–32. https://doi.org/10.20892/j.issn.2095-3941.2016.0084

Reya, T., Morrison, S. J., Clarke, M. F., & Weissman, I. L. (2001). Stem cells, cancer, and cancer stem cells. *Nature*, *414*(6859), 105–111. https://doi.org/10.1038/35102167

Roundtree, I. A., Evans, M. E., Pan, T., & He, C. (2017). Dynamic RNA Modifications in

Gene Expression Regulation. *Cell*, *169*(7), 1187–1200. https://doi.org/10.1016/j.cell.2017.05.045

Rupaimoole, R., & Slack, F. J. (2017). MicroRNA therapeutics: Towards a new era for the management of cancer and other diseases. *Nature Reviews Drug Discovery*, *16*(3), 203–221. https://doi.org/10.1038/nrd.2016.246

Saburi, A., Kahrizi, M. S., Naghsh, N., Etemadi, H., İlhan, A., Adili, A., Ghoreishizadeh, S., Tamjidifar, R., Akbari, M., & Ercan, G. (2022). A comprehensive survey into the role of microRNAs in ovarian cancer chemoresistance; an updated overview. *Journal of Ovarian Research*, *15*(1), 1–14. https://doi.org/10.1186/s13048-022-01012-1

Sandberg, R., Neilson, J. R., Sarma, A., Sharp, P. A., & Burge, C. B. (2008). Proliferating cells express mRNAs with shortened 3′ untranslated regions and fewer microRNA target sites. *Science*, *320*(5883), 1643–1647. https://doi.org/10.1126/science.1155390

Senrung, A., Lalwani, S., Janjua, D., Tripathi, T., Kaur, J., & Ghuratia, N. (2023). 3D tumor spheroids : morphological alterations a yardstick to anti - cancer drug response. *In Vitro Models*, *2*(6), 219–248. https://doi.org/10.1007/s44164-023-00059-8

Shalem, O., Sanjana, N. E., Hartenian, E., Shi, X., Scott, D. A., Heckl, D., Ebert, B. L., Root, D. E., & Doench, J. G. (2014). Genome-Scale CRISPR-Cas9 Knockout Screening in Human Cells. *Science*, *343*(6166), 84–87. https://doi.org/10.1126/science.1247005.Genome-Scale

Shen, C., Sheng, Y., Zhu, A. C., Robinson, S., Jiang, X., Dong, L., Chen, H., Su, R., Yin, Z., Li, W., Deng, X., Chen, Y., Hu, Y. C., Weng, H., Huang, H., Prince, E., Cogle, C. R., Sun, M., Zhang, B., … Chen, J. (2020). RNA Demethylase ALKBH5 Selectively Promotes Tumorigenesis and Cancer Stem Cell Self-Renewal in Acute Myeloid Leukemia. *Cell Stem Cell*, *27*(1), 64-80.e9. https://doi.org/10.1016/j.stem.2020.04.009

Shi, J., Wang, E., Milazzo, J. P., Wang, Z., Kinney, J. B., & Vakoc, C. R. (2015). Discovery of cancer drug targets by CRISPR-Cas9 screening of protein domains. *Nature Biotechnology*, *33*(6), 661–667. https://doi.org/10.1038/nbt.3235

Shibue, T., & Weinberg, R. A. (2017). EMT, CSCs, and drug resistance: The mechanistic link and clinical implications. *Nature Reviews Clinical Oncology*, *14*(10), 611–629. https://doi.org/10.1038/nrclinonc.2017.44

Shield, K., Ackland, M. L., Ahmed, N., & Rice, G. E. (2009). Multicellular spheroids in ovarian cancer metastases: Biology and pathology. *Gynecologic Oncology*, *113*(1), 143–148. https://doi.org/10.1016/j.ygyno.2008.11.032

Shimono, Y., Zabala, M., Cho, R. W., Lobo, N., Dalerba, P., Qian, D., Diehn, M., Liu, H., Panula, S. P., Chiao, E., Dirbas, F. M., Somlo, G., Pera, R. A. R., Lao, K., & Clarke, M. F. (2009). Downregulation of miRNA-200c Links Breast Cancer Stem Cells with Normal Stem Cells. *Cell*, *138*(3), 592–603. https://doi.org/10.1016/j.cell.2009.07.011

Society, A. C. (2025). *Cancer Facts & Figures 2025*. ACS.

Sommerkamp, P., Cabezas-Wallscheid, N., & Trumpp, A. (2021). Alternative Polyadenylation in Stem Cell Self-Renewal and Differentiation. *Trends in Molecular Medicine*, *27*(7), 660–672. https://doi.org/10.1016/j.molmed.2021.04.006

Steg, A. D., Bevis, K. S., Katre, A. A., Ziebarth, A., Dobbin, Z. C., Alvarez, R. D., Zhang, K., Conner, M., & Landen, C. N. (2012). Stem cell pathways contribute to clinical chemoresistance in ovarian cancer. *Clinical Cancer Research*, *18*(3), 869–881. https://doi.org/10.1158/1078-0432.CCR-11-2188

Svoronos, A. A., Engelman, D. M., & Slack, F. J. (2016). OncomiR or tumor suppressor? The duplicity of MicroRNAs in cancer. *Cancer Research*, *76*(13), 3666–3670. https://doi.org/10.1158/0008-5472.CAN-16-0359

Takai, N., & Narahara, H. (2010). Histone Deacetylase Inhibitor Therapy in Epithelial Ovarian Cancer. *Journal of Oncology*, *2010*, 1–6. https://doi.org/10.1155/2010/458431

Thoma, C. R., Zimmermann, M., Agarkova, I., Kelm, J. M., & Krek, W. (2014). 3D cell culture systems modeling tumor growth determinants in cancer target discovery. *Advanced Drug Delivery Reviews*, *69–70*, 29–41. https://doi.org/10.1016/j.addr.2014.03.001

Tian, B., & Manley, J. L. (2016). Alternative polyadenylation of mRNA precursors. *Nature Reviews Molecular Cell Biology*, *18*(1), 18–30. https://doi.org/10.1038/nrm.2016.116

Toledo, C. M., Ding, Y., Hoellerbauer, P., Davis, R. J., Basom, R., Girard, E. J., Lee, E., Corrin, P., Hart, T., Bolouri, H., Davison, J., Zhang, Q., Hardcastle, J., Aronow, B. J., Plaisier, C. L., Baliga, N. S., Moffat, J., Lin, Q., Li, X. N., … Paddison, P. J. (2015). Genome-wide CRISPR-Cas9 Screens Reveal Loss of Redundancy between PKMYT1 and WEE1 in Glioblastoma Stem-like Cells. *Cell Reports*, *13*(11), 2425–2439. https://doi.org/10.1016/j.celrep.2015.11.021

Torre, L. A., Trabert, B., DeSantis, C. E., Miller, K. D., Samimi, G., Runowicz, C. D., Gaudet, M. M., Jemal, A., & Siegel, R. L. (2018). Ovarian cancer statistics, 2018. *CA: A Cancer Journal for Clinicians*, *68*(4), 284–296. https://doi.org/10.3322/caac.21456

Vaughan, S., Coward, J. I., Bast, R. C., Berchuck, A., Berek, J. S., Brenton, J. D., Coukos, G., Crum, C. C., Drapkin, R., Etemadmoghadam, D., Friedlander, M., Gabra, H., Kaye, S. B., Lord, C. J., Lengyel, E., Levine, D. A., McNeish, I. A., Menon, U., Mills, G. B., … Balkwill, F. R. (2011). Rethinking ovarian cancer: Recommendations for improving outcomes. *Nature Reviews Cancer*, *11*(10), 719–725. https://doi.org/10.1038/nrc3144

Verschraegen, C., Lounsbury, K., Howe, A., & Greenblatt, M. (2015). Therapeutic implications for ovarian cancer emerging from the tumor Cancer Genome Atlas. *Translational Cancer Research*, *4*(1), 40–59. https://doi.org/10.3978/j.issn.2218-676X.2015.02.01

Wainwright, E. N., & Scaffidi, P. (2017). Epigenetics and Cancer Stem Cells: Unleashing, Hijacking, and Restricting Cellular Plasticity. *Trends in Cancer*, *3*(5), 372–386. https://doi.org/10.1016/j.trecan.2017.04.004

Wang, B., Wang, M., Zhang, W., Xiao, T., Chen, C., Wu, A., Wu, F., Traugh, N., Wang, X., Li, Z., Mei, S., Cui, Y., Shi, S., Lipp, J. J., Hinterndorfer, M., Zuber, J., Brown, M., Li, W., & Liu, X. S. (2019). MAGeCK Flute. *Nature Protocols*, *14*(March), 756–780.

Wang, J., & Wu, Y. (2024). MicroRNA-486-3p affects cisplatin resistance in high-grade serous ovarian cancer by regulating TMIGD2: An experimental study. *Heliyon*, *10*(15), e34978. https://doi.org/10.1016/j.heliyon.2024.e34978

Wang, Q., Zheng, Y., Wang, P., Zhang, J., Liu, H., Li, Q., Yin, R., Bian, C., Peng, H., & Peng, Z. (2021). The prognostic factor for recurrence in advanced-stage high-grade serous ovarian cancer after complete clinical remission: a nested case-control study. *Journal of Ovarian Research*, *14*(1), 1–7. https://doi.org/10.1186/s13048-021-00908-8

Wang, S., Lv, W., Li, T., Zhang, S., Wang, H., Li, X., Wang, L., Ma, D., Zang, Y., Shen, J., Xu, Y., & Wei, W. (2022). Dynamic regulation and functions of mRNA m6A modification. *Cancer Cell International*, *22*(1), 1–12. https://doi.org/10.1186/s12935-022-02452-x

Wang, T., Wei, J. J., Sabatini, D. M., & Lander, E. S. (2014). Genetic screens in human cells using the CRISPR-Cas9 system. *Science*, *343*(6166), 80–84. https://doi.org/10.1126/science.1246981

Wang, Y., Wu, J., Zhao, J., Xu, T., Zhang, M., Liu, J., Wang, Y., Wang, Q., & Song, X. (2024). Global characterization of RNA editing in genetic regulation of multiple ovarian cancer subtypes. *Molecular Therapy Nucleic Acids*, *35*(1), 102127. https://doi.org/10.1016/j.omtn.2024.102127

Wei, S. H., Brown, R., & Huang, T. H.-M. (2003). Aberrant DNA methylation in ovarian cancer: is there an epigenetic predisposition to drug response? *Annals of the New York Academy of Sciences*, *983*, 243–250. https://doi.org/10.1111/j.1749-6632.2003.tb05979.x

Wen, Y., Cai, J., Hou, Y., Huang, Z., & Wang, Z. (2017). Oncotarget 37974 www.impactjournals.com/oncotarget Role of EZH2 in cancer stem cells: from biological insight to a therapeutic target. *Oncotarget*, *8*(23), 37974–37990. www.impactjournals.com/oncotarget/

Wen, Y., Hou, Y., Yi, X., Sun, S., Guo, J., He, X., Li, T., Cai, J., & Wang, Z. (2021). EZH2

activates CHK1 signaling to promote ovarian cancer chemoresistance by maintaining the properties of cancer stem cells. *Theranostics*, *11*(4), 1795–1813. https://doi.org/10.7150/thno.48101

Widschwendter, M., Siegmund, K. D., Müller, H. M., Fiegl, H., Marth, C., Müller-Holzner, E., Jones, P. A., & Laird, P. W. (2004). Association of breast cancer DNA methylation profiles with hormone receptor status and response to tamoxifen. *Cancer Research*, *64*(11), 3807–3813. https://doi.org/10.1158/0008-5472.CAN-03-3852

Wilson, B. G., & Roberts, C. W. M. (2011). SWI/SNF nucleosome remodellers and cancer. *Nature Reviews Cancer*, *11*(7), 481–492. https://doi.org/10.1038/nrc3068

Wu, H., Chen, S., Li, X., Li, Y., Shi, H., Qing, Y., Shi, B., Tang, Y., Yan, Z., Hao, Y., Wang, D., & Liu, W. (2025). RNA modifications in cancer. *MedComm*, *6*(1), 1–38. https://doi.org/10.1002/mco2.70042

Xia, Z., Donehower, L. A., Cooper, T. A., Neilson, J. R., Wheeler, D. A., Wagner, E. J., & Li, W. (2014). Dynamic analyses of alternative polyadenylation from RNA-seq reveal a 3’2-UTR landscape across seven tumour types. *Nature Communications*, *5*. https://doi.org/10.1038/ncomms6274

Xie, W., Sun, H., Li, X., Lin, F., Wang, Z., & Wang, X. (2021). Ovarian cancer : epigenetics , drug resistance , and progression. *Cancer Cell International*, 1–16. https://doi.org/10.1186/s12935-021-02136-y

Xu, C., & Zhang, J. (2020). A different perspective on alternative cleavage and polyadenylation. *Nature Reviews Genetics*, *21*(1), 63. https://doi.org/10.1038/s41576-019-0198-z

Yang, D., Peng, M., Hou, Y., Qin, Y., Wan, X., Zhu, P., Liu, S., Yang, L., Zeng, H., Jin, T., Qiu, Y., Li, Q., & Liu, M. (2020). Oxidized ATM promotes breast cancer stem cell enrichment through energy metabolism reprogram-mediated acetyl-CoA accumulation. *Cell Death and Disease*, *11*(7). https://doi.org/10.1038/s41419-020-2714-7

Yang, L., Liu, J., Jin, Y., Xing, J., Zhang, J., Chen, X., & Yu, A. (2024). Synchronous

profiling of mRNA N6-methyladenosine modifications and mRNA expression in high-grade serous ovarian cancer: a pilot study. *Scientific Reports*, *14*(1), 1–18. https://doi.org/10.1038/s41598-024-60975-x

Yedier-Bayram, O., Gokbayrak, B., Kayabolen, A., Aksu, A. C., Cavga, A. D., Cingöz, A., Kala, E. Y., Karabiyik, G., Günsay, R., Esin, B., Morova, T., Uyulur, F., Syed, H., Philpott, M., Cribbs, A. P., Kung, S. H. Y., Lack, N. A., Onder, T. T., & Bagci-Onder, T. (2022). EPIKOL, a chromatin-focused CRISPR/Cas9-based screening platform, to identify cancer-specific epigenetic vulnerabilities. *Cell Death and Disease*, *13*(8). https://doi.org/10.1038/s41419-022-05146-4

Yi, X., Guo, J., Guo, J., Sun, S., Yang, P., Wang, J., Li, Y., Xie, L., Cai, J., & Wang, Z. (2017). EZH2-mediated epigenetic silencing of TIMP2 promotes ovarian cancer migration and invasion. *Scientific Reports*, *7*(1), 1–16. https://doi.org/10.1038/s41598-017-03362-z

Zhang, J., Guo, X., Chang, D. Y., Rosen, D. G., Mercado-Uribe, I., & Liu, J. (2012). CD133 expression associated with poor prognosis in ovarian cancer. *Modern Pathology*, *25*(3), 456–464. https://doi.org/10.1038/modpathol.2011.170

Zhang, S., Balch, C., Chan, M. W., Lai, H. C., Matei, D., Schilder, J. M., Yan, P. S., Huang, T. H. M., & Nephew, K. P. (2008). Identification and characterization of ovarian cancer-initiating cells from primary human tumors. *Cancer Research*, *68*(11), 4311–4320. https://doi.org/10.1158/0008-5472.CAN-08-0364

Zhang, Z., Liu, X., Chu, C., Zhang, Y., Li, W., Yu, X., Han, Q., Sun, H., Zhang, Y., Zhu, X., Chen, L., Wei, R., Fan, N., Zhou, M., & Li, X. (2024). MIR937 amplification potentiates ovarian cancer progression by attenuating FBXO16 inhibition on ULK1-mediated autophagy. *Cell Death and Disease*, *15*(10), 1–13. https://doi.org/10.1038/s41419-024-07120-8

Zhao, B. S., & He, C. (2015). Pseudouridine in a new era of RNA modifications. *Cell Research*, *25*(2), 153–154. https://doi.org/10.1038/cr.2014.143

Zheng, D., Wang, R., Ding, Q., Wang, T., Xie, B., Wei, L., Zhong, Z., & Tian, B. (2018). Cellular stress alters 3′UTR landscape through alternative polyadenylation and isoform-specific degradation. *Nature Communications*, *9*(1), 1–14. https://doi.org/10.1038/s41467-018-04730-7

Zhou, B., Xu, H., Xia, M., Sun, C., Li, N., Guo, E., Guo, L., Shan, W., Lu, H., Wu, Y., Li, Y., Yang, D., Weng, D., Meng, L., Hu, J., Ma, D., Chen, G., & Li, K. (2017). Overexpressed miR-9 promotes tumor metastasis via targeting E-cadherin in serous ovarian cancer. *Frontiers of Medicine*, *11*(2), 214–222. https://doi.org/10.1007/s11684-017-0518-7

Zhu, J. W., Charkhchi, P., & Akbari, M. R. (2022). Potential clinical utility of liquid biopsies in ovarian cancer. *Molecular Cancer*, *21*(1), 1–24. https://doi.org/10.1186/s12943-022-01588-8